UNITED NATIONS EDUCATIONAL, SCIENTIFIC AND CULTURAL ORGANIZATION
INTERNATIONAL ATOMIC ENERGY AGENCY
INTERNATIONAL CENTRE FOR THEORETICAL PHYSICS
I.C.T.P., P.O. BOX 586, 34100 TRIESTE, ITALY, CABLE: CENTRATOM TRIESTE

SMR.998c - 8

Research Workshop on Condensed Matter Physics
30 June - 22 August 1997
MINIWORKSHOP ON
PATTERN FORMATION AND SPATIO-TEMPORAL CHAOS
28 JULY - 8 AUGUST 1997

"Clustering and pattern formation in 2-D Hindmarsh-Rose neural networks"

H. A. CERDEIRA
International Centre for Theoretical Physics
P.O. Box 586
Miramare
34100 Trieste
Italy

These are preliminary lecture notes, intended only for distribution to participants.

Physica D 63 (1993) 341–349
North-Holland

PHYSICA D

Order in the turbulent phase of globally coupled maps

Gabriel Perez, Sudeshna Sinha[1] and Hilda A. Cerdeira[2,3]
ICTP, P.O. Box 586, 34100 Trieste, Italy

Received 14 June 1991
Revised manuscript received 18 July 1992
Accepted 23 July 1992
Communicated by E. Jen

The broad peaks seen in the power spectra of the mean field in a globally coupled map system indicate a subtle coherence between the elements, even in the "turbulent" phase. These peaks are investigated in detail with respect to the number of elements coupled, nonlinearity and global coupling strengths. We find that this roughly periodic behavior also appears in the probability distribution of the mapping, which is therefore not invariant. We also find that these peaks are determined by two distinct components: effective renormalization of the nonlinearity parameter in the local mappings, and the strength of the mean field interaction term. Finally, we demonstrate the influence of background noise on the peaks, which is quite counterintuitive, as they become *sharper* with increase in strength of the noise, up to a certain critical noise strength.

1. Introduction

Globally coupling in dynamical systems yields a host of very novel features. This class of complex systems is of considerable importance in modeling phenomena as diverse as Josephson junction arrays, vortex dynamics in fluids, and even evolutionary dynamics, biological information processing and neurodynamics. The ubiquity of globally coupled phenomena has thus made it a focus of much recent research activity [1–4].

In this paper we study the globally coupled map (GCM) introduced by Kaneko [2]. It is a dynamical system of N elements consisting of local mappings as well as an additive average-type interaction term, through which the global information influences the individual elements. It is thus analogous to a mean field version of coupled map lattices. The explicit form of the GCM we use is

$$x_{n+1}(i) = (1-\epsilon) f(x_n(i)) + \frac{\epsilon}{N} \sum_{j=1}^{N} f(x_n(j)) , \qquad (1)$$

where n is a discrete time step and i is the index of the elements ($i = 1, 2, \ldots, N$). The function $f(x)$ was chosen to be the well known dissipative chaotic logistic map

$$f(x) = 1 - ax^2 . \qquad (2)$$

This choice helps us to make contact with previous results.

The above GCM model has two conflicting trends: destruction of coherence due to the chaotic dynamics of the individual elements, and a kind of synchronization through the global av-

[1]Now at the Theoretical Physics Division, Central Complex, Bhabha Atomic Research Centre, Bombay 400 085, India.

[2]Also at Universidade Estadual de Campinas, Instituto de Fisica, 13081 Campinas, SP, Brazil.

[3]Associate member of the Istituto Nazionale di Fisica Nucleare (INFN).

eraging. For large global coupling, this synchronization may be complete (all elements moving coherently), and appears even in the fully chaotic (in time) regime. On the other hand, for a nonlinearity parameter a such that the local dynamics is strongly chaotic, and in the presence of a small coupling, the behavior of the system is "turbulent". This means that all elements of the lattice behave chaotically in time (all Lyapunov exponents are positive [3]), and that there is no clustering (partial "entrainment" or synchronization). In fact, the distance between any two different elements of the lattice that have at some moment close values grows exponentially with time. (For $\epsilon = 0.1$ and $a = 1.99$ this exponent is ≈ 0.4). So, in practice, the elements of the lattice seem to behave like independent quasirandom variables.

This has led to the following "simplicity" hypothesis: if in this turbulent regime the different elements of the lattice behave in fact as independent quasirandom numbers, then in the $N \to \infty$ limit the mean field h_n, defined by

$$h_n \equiv \frac{1}{N} \sum_{j=1}^{N} f(x_n(j)) , \tag{3}$$

should converge to a fixed value, uncoupling the system. In fact, a similar idea has been used by Kuramoto and others [4] in order to analyze the $N \to \infty$ limit of a globally coupled system of limit cycle oscillators, and its coherent–incoherent transition. This "simplicity" hypothesis can also be cast in the following terms: consider for a moment a system similar to eq. (1), with some fixed a and ϵ, but where we substitute the time dependent mean field h_n by some constant h_{in}. This gives us a lattice of uncoupled logistic maps, which in the $N \to \infty$ has an invariant probability distribution. From this distribution we can evaluate h_{out}, defined as the average value of $f(x)$. Then two questions come immediately to mind: is there a solution for the self-consistency equation $h_{out}(h_{in}; a, \epsilon) = h_{in}$? And if so, is that solution stable under small fluctuations of h_{in}, in the fully coupled model?

Coming back to a finite lattice, we would expect the fluctuations that appear in the system to behave statistically, if this limiting value for h does exist. In particular, we should expect a decay in the mean square deviation (MSD) of the mean field $(\equiv \langle h^2 \rangle - \langle h \rangle^2)$ as $1/N$ (law of large numbers), and its distribution to be Gaussian (central limit theorem). These two questions were explored by Kaneko [3] and the results found were that the system in eq. (1) *violated the law of large numbers but not the central limit theorem* (this last affirmation has been reevaluated in ref. [5], where it was found that the tails of the distribution diverged from those of a Gaussian). Even in the fully "turbulent" phase, where there is absolutely no synchronization among the elements, a subtle coherence emerged. This was reflected in the saturation of the MSD, that stopped decaying after some critical lattice size N_c, in the broad peaks that appear in the power spectrum of the mean field h_n, and in the fact that the mutual information of the system remained non-zero for all lattice sizes.

It should be noted that these results are not universal, since there are related systems that show proper statistical behavior. In particular, it has been found [5] that a globally coupled lattice of tent maps (eq. (1) with $f(x) = 1 - a|x|$), behaves as expected in its turbulent regime. The MSD of the mean field dies away as $1/N$ and the Fourier transform of h_n does not develop any peaks.

In section 2 of this paper we examine, through numerical experiments, the transition between the power spectrum of a single $x_n(i)$ (which is only mildly humped) to the spectrum of the collective quantity h_n which displays broad peaks, indicating collective "beats" in its dynamics. Then, in section 3 we examine the behavior of another global quantity, namely the probability distribution of the mapping, for possible similar behaviour. Here too we find evidence of non-statistical behavior, with the emergence of a kind of collective "beating", and a saturation in the fluctuations of the probability

values. This clearly means that the probability distribution of the mapping is not invariant. In section 4 we attempt an analysis of this emergence of order in terms of two distinct effects, one due to an effective renormalization of the local nonlinear parameter of the map, and another due to the synchronization induced by the mean field acting over the individual elements. Finally we investigate the influence of noise in the system. The surprising result here is that the peaks in the power spectrum of the mean field get *sharper* as the strength of noise increases, up to a certain critical noise strength. This counterintuitive phenomena are demonstrated through numerical experiments in section 5.

2. Emergence of peaks in the power spectrum

In this section we want to trace the development of the peaks in the power spectrum of the mean field. Clearly, when $N = 1$, i.e., when there is a single logistic map, we have a very flat (aperiodic) spectrum. But even as we put in another element ($N = 2$) we find a "ghost" of the peaks making its presence felt. So, the appearance of one broad peak in the spectrum is almost immediate, as is evident from the power spectra for very low lattice sizes in fig. 1. It takes larger lattices to resolve this peak into its various components. For these spectra we have evaluated the autocorrelation function, which is defined by

$$C = \frac{1}{M}\sum_{i=1}^{M}\frac{\Sigma_{j=1}^{M} P(j+i \bmod M)P(J)}{\Sigma_{j=1}^{M} P(j)\,P(j)}\,, \qquad (4)$$

where $P(j)$ is the value of the power at the jth frequency index, and M is the number of discrete points in the spectrum. This provides a good measure of the "flatness" of a spectrum, with C taking the value 1 when the spectrum is completely flat, and 0 when there are just δ-peaks. A better indicator of the sharpness of the peaks is given by

$$S = -\log_{10} C\,, \qquad (5)$$

where $S = 0$ is the signature of a completely flat spectrum and $S \to \infty$ is the signature of (very sharp) δ-peaks. We find that S increases very fast with increasing lattice size N (size fig. 2), indicating that the peaks emerge rapidly, on

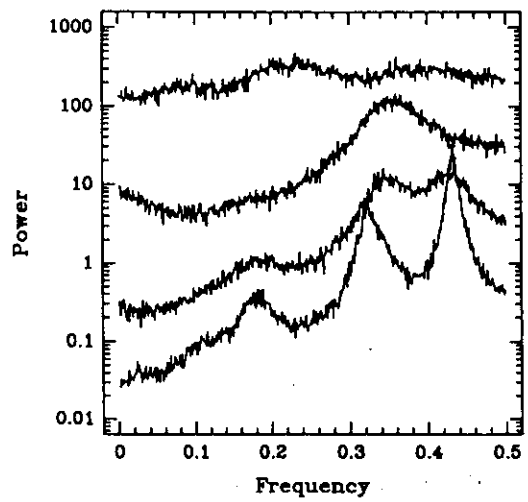

Fig. 1. Power spectra of the mean field for lattice sizes $N = 1, 8, 64$ and 512 (from top to bottom). Here $a = 1.99$, $\epsilon = 0.1$ and we average over 100 runs of 1024 iterations each.

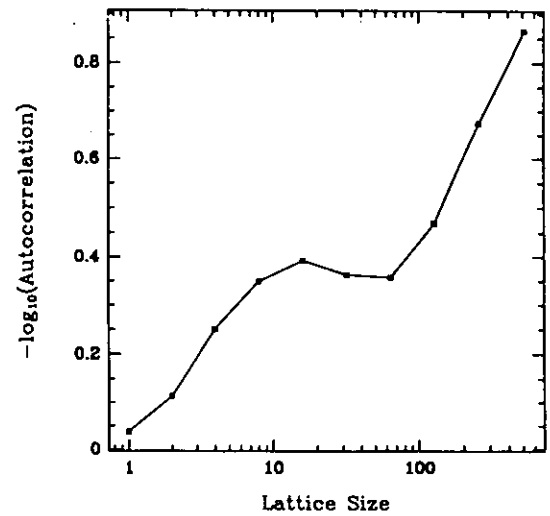

Fig. 2. Measure of the sharpness of the peaks in the power spectra, as defined in the text, vs. lattice size N ($a = 1.99$, $\epsilon = 0.1$).

addition of elements, from the flat spectrum corresponding to a system with a single element.

We also investigate the power spectra of partial sums, given as

$$S_m(n) = \frac{1}{m} \sum_{i=1}^{m} f(x_n(i)) , \tag{6}$$

where the $x_n(i)$ evolve under the effect of the full mean field h_n, as given by eq. (1). The power spectrum for a single element under the influence of the full mean field ($S_1(n)$) shows some influence of the roughly periodic behavior of h_n (see fig. 3). It contains, in any case, much more periodic modulation that the single isolated logistic map, as can be seen by comparing to the topmost spectrum in fig. 1. It is interesting to notice that this behavior remains unchanged for small partial sums, so much so that the different spectra look like parallel displacements of each other, except for the intrusions of the two main frequencies. This suggests that under the influence of the full mean field the partial sums behave as h_n plus some amount of white noise, where the intensity of this noise decays initially as $1/N$. This behavior is quite different from that of the mean field for small lattices, shown in fig. 1.

3. Probability distributions

We now investigate the dynamics of the probability distributions, defined as

$$P_\delta(y; n) = \frac{1}{2\delta N} \sum_{i=1}^{N} \Theta[\delta - |x_n(i) - y|] , \tag{7}$$

for small δ and large N. For a logistic map in the chaotic regime this quantity is invariant in the $N \to \infty$ limit. Here the individual local maps are well inside the chaotic regime (nonlinearity parameter $a = 1.99$). However, the "beating" behavior observed in the mean field should be reflected in the dynamics of the probability distributions, and there is a good possibility that the finite lattice fluctuations in this distribution will not die out with growing N. What numerical experiments show is that indeed this happens, as can be seen in fig. 4, where the MSD of $P(y)$ as

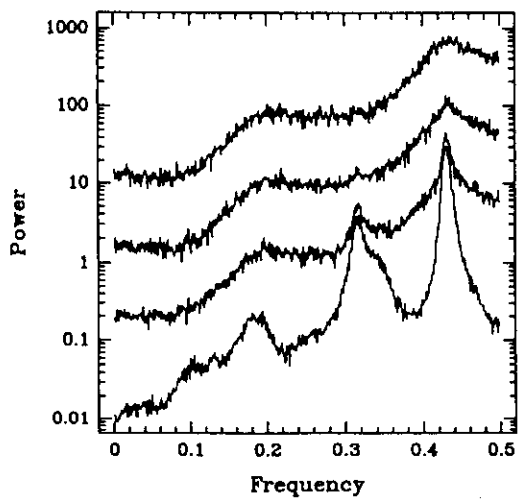

Fig. 3. Power spectra of partial sums S_m, as defined in the text, for $m = 1, 8, 64$ and the full lattice (from top to bottom). Here $a = 1.99$, $\epsilon = 0.1$, $N = 10\,000$ and we average over 100 runs of 1024 iterations each.

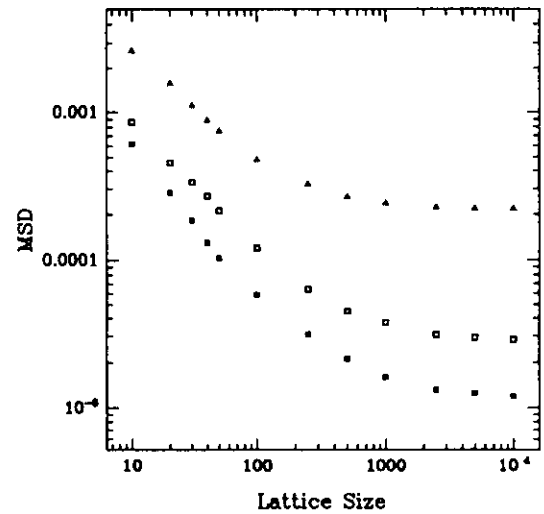

Fig. 4. Mean square deviation of $P_\delta(y; n)$, ($\delta = 0.01$), vs. lattice size N, at three different values of y; $y = 0.0$ (■), $y = 0.5$ (□), and $y = 0.9$ (▲) ($a = 1.99$, $\epsilon = 0.1$, $N = 10\,000$ and the number of iterations is 10 000).

a function of N is plotted for three different values of y. (It should be noted that we are considering well populated bins here). It is clear from the plot that, after a critical N, the MSD does not fall as $1/N$ but saturates instead. Therefore, this distribution *does not converge to an invariant distribution* as N grows.

Further, we have noticed that the power spectrum of $P(y; n)$ shows the same broad peaks as the mean field h_n. This can be seen by taking the first few moments of the distribution and doing a spectral analysis. We have done this for the first four moments, and the resulting spectra are almost identical to that of the mean field. On the other hand, we can also follow the time evolution of the probability at a given value of y. Fig. 5 shows the power spectrum of a representative bin, where the peaks are clearly discernible. (There are, however, other bins where the peaks are less pronounced or almost non-existing). Although these spectral curves are not equal to that of the mean field, the peaks on the "beating" bins match with those of h_n, which is not surprising, since these are just different manifestations of the same underlying collective effect.

4. Dependence on the global coupling parameter

It is instructive to study the functional dependence of the MSD on the global coupling parameter ϵ, since it gives the strength of the global averaging, and is in this sense the source of the synchronization effect. Thus, we have checked the value of the MSD of the mean field as a function of ϵ. At first viewing this functional dependence seems very erratic. (see fig. 6a). Moreover, in the explored range of ϵ (0.0–0.2), the maximum value of the MSD was found to be one order of magnitude larger than the value at $\epsilon = 0.1$, where most of the work has been concentrated up to now [3].

We now attempt an explanation of this non-systematic behavior, and in particular of the surprisingly large values of the MSD found in certain small ranges of ϵ. This can partially be accounted for if we consider the effects of the coupling as divided roughly in two components. One is the renormalization of the nonlinear parameter a by the introduction of the multiplicative $1 - \epsilon$ term in the individual maps. The other

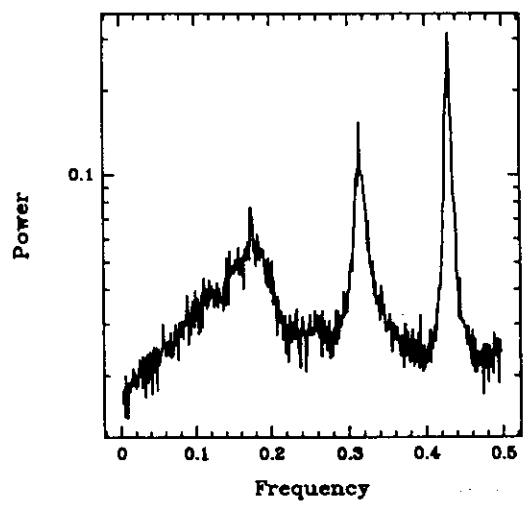

Fig. 5. Power spectrum of $P_\delta(y; n)$ ($\delta = 0.01$) at $y = 0.9$. Here we average over 100 runs of 1024 iterations each ($a = 1.99$, $\epsilon = 0.1$ and $N = 10\,000$).

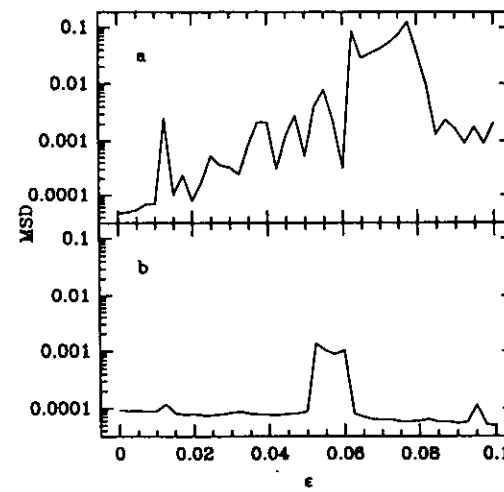

Fig. 6. Mean square deviation vs. global coupling parameter ϵ for (a) the full map, as given in eq. (1) in the text, and (b) a set of uncoupled logistic maps with $a_{eff} = a(1 - \epsilon)^2$ ($a = 1.99$, $N = 10\,000$).

is the action of the mean field, whose effective strength in the dynamics of the individual elements is determined by ϵ. (Notice, however, that the nonlinear parameter a used to construct the mean field remains unaffected by the global coupling ϵ). To check this hypothesis we have explored, as a function of ϵ, the behavior of a set of uncoupled logistic maps with the local nonlinear parameter set to the renormalized value, which is given by

$$a_{\text{eff}} = a(1-\epsilon)^2 . \tag{8}$$

We have computed the MSD for such a system, and find that its profile is similar to that of the fully coupled maps (see fig. 6b). What is striking here is the appearance of a plateau of large values for the MSD close to a similar plateau in the fully coupled problem. This plateau occurs around $a_{\text{eff}} \approx 1.75$ and corresponds to the 3-window of the logistic map [6]. The width of the plateau is related to the width of the periodic window. Furthermore, a second smaller and narrower sharp peak appears at $a_{\text{eff}} \approx 1.94$, which corresponds to a very narrow 4-window. This shows that there is an influence of the periodic windows of the logistic map in the value of the MSD for the fully coupled problem, through the ϵ-dependent renormalization of the nonlinearity parameter in the local mappings. This hypothesis is further sustained by the fact that the power spectrum of h_n in the fully coupled map, for values of ϵ corresponding to the largest plateau, shows a clearly dominant $\frac{1}{3}$ frequency (see fig. 7), and the power spectrum for ϵ corresponding to the smaller peak shows a clear $\frac{1}{4}$ frequency (see fig. 8).

So the skeleton of the functional dependence of the MSD on coupling comes from the effects of renormalizing the nonlinear parameter in the local maps, which may push them into periodic windows, leading to some synchronization. This synchronization is not complete, because the mean field is still being evaluated at the bare value of a, where the dynamics is strongly chaotic. It is, however, strong enough to produce the narrow ranges of ϵ where the deviation is an order of magnitude larger than elsewhere. But this is clearly not a full explanation of the almost periodic fluctuations of h_n. The MSD for the uncoupled case is much too small compared to that of the fully coupled case, and accounts for only the gross features of the MSD vs. ϵ curve.

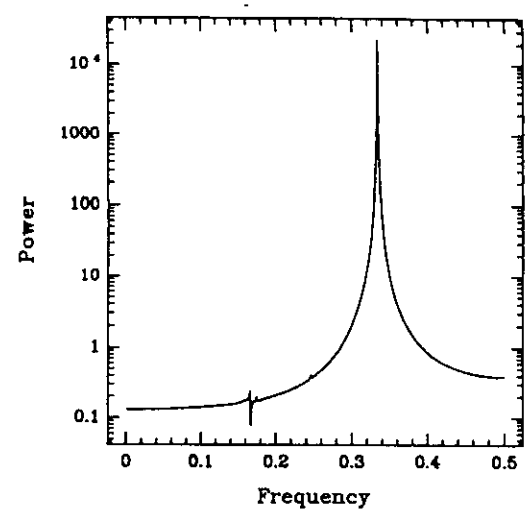

Fig. 7. Power spectrum of h_n at $\epsilon = 0.075$ ($a = 1.99$, $N = 10\,000$). Here we average over 100 runs of 1024 iterations each.

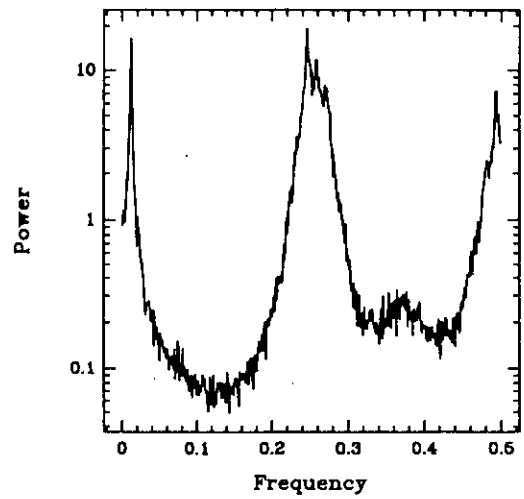

Fig. 8. Power spectrum of h_n at $\epsilon = 0.0125$ ($a = 1.99$, $N = 10\,000$). Here we average over 100 runs of 1024 iterations each.

So, the "flesh" of the MSD comes from the effects of the mean field which lead to synchronization by global averaging. For a full characterization of the broad collective motion of the system one must then take into account both effects. As an extra verification, have also computed the MSD for a system analogous to eq. (1), but where the local maps are not multiplied by the $1-\epsilon$ term, and so there is no renormalization of the nonlinearity parameter. For such a system the effects come solely from the interaction with the mean field, and we find that the MSD, as expected, increases monotonically with ϵ. We have investigated also a realistic physical system that displays the same kind of phenomena, with similar results [7].

5. Effects of noise

We now examine the effects of additive noise in the dynamics of the mean field. For this simulate the system

$$x_{n+1}(i) = (1-\epsilon) f(x_n(i)) + \frac{\epsilon}{N}\sum_{j=1}^{N} f(x_n(j)) + \sigma\eta_n^i , \qquad (9)$$

where η_n^i is a random number uniformly distributed in the interval $[-0.5, 0.5]$. As described in ref. [3], adding noise to the system impedes the saturation of the MSD, but does not restore the normal $1/N$ behavior. Instead, the fluctuations now decay as $1/N^{\alpha}$, with $\alpha < 1$ for σ not too large. This effect appears only for noise strength above some threshold σ_c. We have found that this anomalous decay of the MSD does not mean that the mean field h_n stops being almost periodic. On the contrary, it is found that for values of the added noise up to a value roughly equal to σ_c the sharpness of the power spectrum increases. This counterintuitive behavior can be clearly seen in figs. 9a, b and c, where we have plotted the power spectra for three values of σ, and in fig. 10, which shows the value of S, the measure of sharpness defined in eqs. (4) and (5), vs. σ. Clearly the sharpness increases with increasing noise, up to $\sigma = 0.009$, and decreases from there on. We do not have an explanation of this very surprising phenomenon as yet.

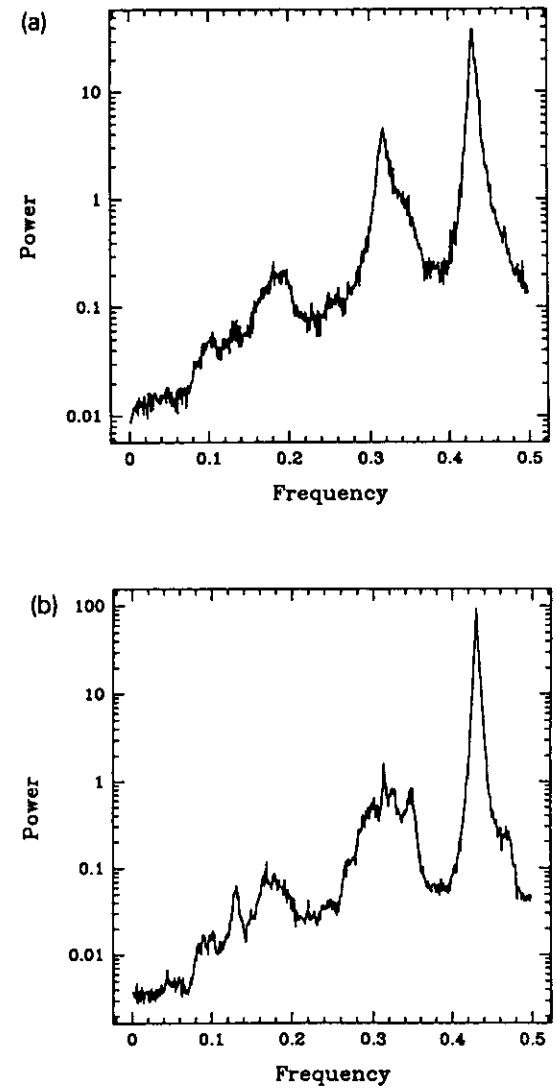

Fig. 9. Power spectra of the mean field in the presence of noise of strength σ = (a) 0.0, (b) 0.004, (c) 0.009 ($a = 1.99$, $\epsilon = 0.1$, $N = 10\,000$). Here we average over 100 runs of 1024 iterations each.

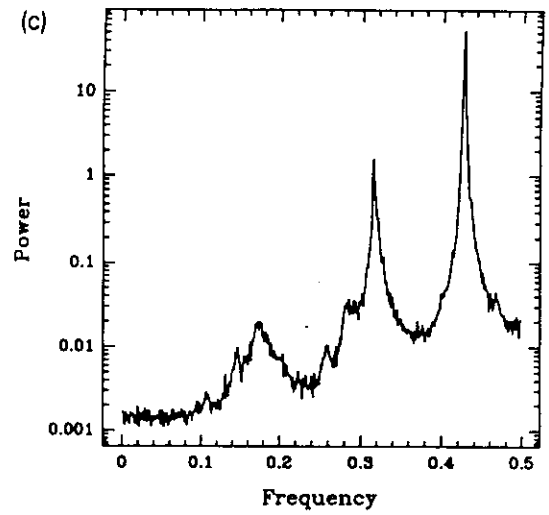

Fig. 9. (cont.).

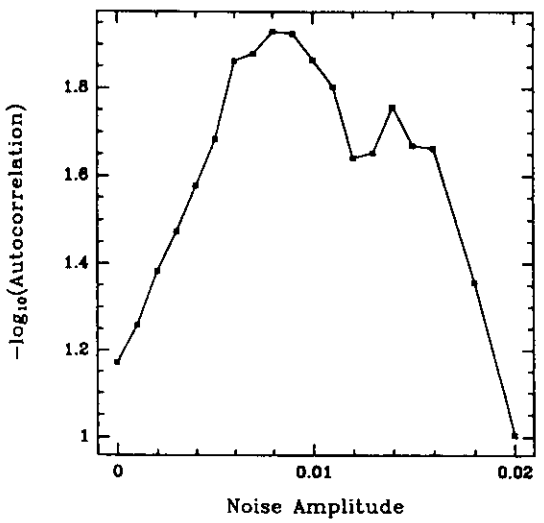

Fig. 10. Measure of the sharpness of peaks in the power spectra, as defined in the text, vs. noise strength σ ($a = 1.99$, $\epsilon = 0.1$, $N = 10\,000$).

6. Conclusions and comments

Here we have investigated various aspects of the dynamics of the mean field in a globally coupled chaotic system. The mean field shows evidence of a rough periodicity as is suggested through the broad, significant peaks in its power spectrum. We trace the development of these peaks with respect to the number of elements coupled, and study their presence in partial averages. Further, we examine another important global quantity, namely the probability distribution, and find that it is *not invariant*, and like the mean field, does not obey the law of large numbers. Moreover, there is evidence of a similar "beating" pattern in its power spectra, with frequencies of this roughly-periodic behavior matching those of the mean field.

Next we find the functional dependence of the mean square deviation of the mean field on the global coupling parameter. We then attempt to decompose the effect we observe as coming from two distinct sources: one, the renormalization of the nonlinearity parameter in the local maps, and second, the contribution from the mean field, which introduces a degree of synchronization. This way of looking at the system helps us account for the extremely large deviations found in certain ranges of the coupling parameter. We can in fact identify the largest plateau in the MSD vs. ϵ graph with the period-3 window, into which the local maps are pushed due to the effective renormalization of a.

Lastly, we explore the effects of noise on the rough periodicities observed in the mean field. We find that the periodicities do in fact persist up to a reasonably large strength of noise. Furthermore, the peaks actually get sharper with increase of the noise strength, up to a critical value. This strange effect is another instance of stabilization of periodic motion through small noise, resembling in a way the phenomenon of stochastic resonance [8]. However, it is not evident that there exists any direct connection between our observations and this other problem.

Acknowledgements

We are grateful for the hospitality of the Condensed Matter Group at the International Center of Theoretical Physics. We would also like to thank A. Erzan for valuable comments.

References

[1] J. Crutchfield and K. Kaneko, in: Directions in Chaos, ed. B.-L. Hao (World Scientific, Singapore, 1987);
T. Hwa, Ph.D. thesis (MIT);
P. Alstrom and R.K. Ritala, Phys. Rev. A 35 (1987) 300;
P. Hadley and K. Wiesenfeld, Phys. Rev. Lett. 62 (1989) 1335;
R.V. Sole and J. Valls, Phys. Lett. A 153 (1991) 330;
K. Kaneko, Physica D 54 (1991) 5.

[2] K. Kaneko, Phys. Rev. Lett. 63 (1989) 219; Physica D 41 (1990) 137.

[3] K. Kaneko, Phys. Rev. Lett. 65 (1990) 1391.

[4] Y. Kuramoto and I. Nishikawa, J. Stat. Phys. 49 (1987) 569;
H. Daido, J. Stat. Phys. 60 (1990) 753;
S.H. Strogatz and R.E. Mirollo, J. Stat. Phys. 63 (1991) 613.

[5] K. Kaneko, University of Tokyo preprint (1991).

[6] P. Collet and J.P. Eckmann, Iterated Maps on the Interval as Dynamical Systems (Birkhauser, Basel, 1980).

[7] G. Perez et al., Phys. Rev. A 45 (1992) 5469.

[8] L. Gammaitoni et al., Phys. Rev. Lett. 62 (1989) 349; Phys. Lett. A 142 (1989) 59;
for a comprehensive review, see F. Moss, in: Some Problems in Statistical Physics, ed. G.H. Weiss, Frontiers in Applied Mathematics (SIAM, Philadelphia, 1992).

Dynamical behavior of the firings in a coupled neuronal system

Wei Wang
The International Center for Theoretical Physics, P.O. Box 586, 34100 Trieste, Italy
and Physics Department, Nanjing University, Nanjing 210008, People's Republic of China

G. Perez
The International Center for Theoretical Physics, P.O. Box 586, 34100 Trieste, Italy

Hilda A. Cerdeira
The International Center for Theoretical Physics, P.O. Box 586, 34100 Trieste, Italy
and Universidade Estadual de Campinas, Instituto de Fisica, 13081 Campinas, São Paulo, Brazil
(Received 27 October 1992)

The time-interval sequences and the spatiotemporal patterns of the firings of a coupled neuronal network are investigated in this paper. For a single neuron stimulated by an external stimulus I, the time-interval sequences show a low-frequency firing of bursts of spikes and a reversed period-doubling cascade to a high-frequency repetitive firing state as the stimulus I is increased. For two neurons coupled to each other through the firing of the spikes, the complexity of the time-interval sequences becomes simple as the coupling strength increases. A network with a large number of neurons shows a complex spatiotemporal pattern structure. As the coupling strength increases, the number of phase-locked neurons increases and the time-interval diagram shows temporal chaos and a bifurcation in the space. The dynamical behavior is also verified by the behavior of the Lyapunov exponent.

PACS number(s): 87.10.+e, 05.45.+b

I. INTRODUCTION

Aspects of the dynamical behavior of a coupled neuronal system, such as the synchronized patterns of neural activity which result from the cooperative dynamical properties, have attracted considerable interest over recent years [1–4]. Some experimental results have been obtained in the olfactory system, the visual cortex, and other brain areas. Local groups of neurons responding to a common stimulus display synchronized activity, and neurons responding to separate stimuli are also phase locked [5,6]. It has been suggested that the selective synchronization of neural activity serves as a mechanism for binding spatially distributed features into a coherent object [5,7]. It has also been well known for decades that a major component of sensory information is transmitted to the brain using a code based on the time intervals between firings of neurons, that is, action potentials or spikes [8–11]. Moreover, statistical analyses of experimentally obtained spike trains have concluded that the time intervals contain a significant irregular component [12]. It is thus important to investigate how the sensory information is encoded and how this process is affected by the irregular firings.

Recently an investigation of synchronized chaos in a network model of bursting neurons responding to an inhomogeneous stimulus has been made by Hansel and Sompolinsky [13]. They found that there are three types of phases for the network: an asynchronous stationary state, synchronized oscillations, and synchronized chaos. They concluded that the mechanism for generating the synchronized chaotic state in their network model is the long-range positive interactions in a population of neurons with a distribution of local driving currents.

In this paper, we are interested in the dynamical properties of the time-interval sequences and the spatiotemporal patterns of firings in a coupled neuronal system which presents a complex dynamical behavior of the neural activity. The outline of this paper is as follows. In Sec. II we describe the models of the coupled network. In Sec. III we present and discuss the results. In Sec. IV a summary is given.

II. A COUPLED NEURONAL NETWORK

A network of coupled Hindmarsh-Rose neurons [14] is represented by the following equations [13]:

$$\frac{dX_i}{dt}=f_1(X_i,Y_i,Z_i)+I_i+\sum_{\substack{j=1\\ j\neq i}}^{N}J_{ij}S_j(t)$$

$$=Y_i-aX_i^3+bX_i^2-Z_i+I_i+\sum_{\substack{j=1\\ j\neq i}}^{N}J_{ij}S_j(t)\,, \quad (1)$$

$$\frac{dY_i}{dt}=f_2(X_i,Y_i,Z_i)=c-dX_i^2-Y_i\,, \quad (2)$$

$$\frac{dZ_i}{dt}=f_3(X_i,Y_i,Z_i)=r[s(X_i-X_0)-Z_i]\,. \quad (3)$$

The Hindmarsh-Rose neuron of the three-variable model is a modification of Fitzhugh's Bonhoeffer–van der Pol model [15,16], with the property that each action potential is separated by a long interspike interval typical of real neurons. That is, each neuron is characterized by

three time-dependent variables: the membrane potential X_i, the recovery variable Y_i, and a slow adaptation current Z_i. The external inputs are given by I_i. In the coupled neuronal network, the effect of the firing activity of the jth neuron on the ith neuron is modeled in Eq. (1) by an impulse current to the ith neuron, proportional to the synaptic strength J_{ij}, generated when the jth neuron is active. The neuron is active whenever its membrane potential exceeds a threshold value X^*,

$$S_j(t)=\Theta(X_j(t)-X^*)\ , \tag{4}$$

where $\Theta(x)=1$ if $x\geq 0$ and $\Theta(x)=0$ if $x<0$.

We first consider a network consisting of only two neurons that respond to a common external stimulus I:

$$\frac{dX_i}{dt}=f_1(X_i,Y_i,Z_i)+I+JS_j(t)\ , \tag{5}$$

$$\frac{dY_i}{dt}=f_2(X_i,Y_i,Z_i)\ , \tag{6}$$

$$\frac{dZ_i}{dt}=f_3(X_i,Y_i,Z_i)\ , \tag{7}$$

where $i=1,2$ and $j=2,1$, respectively.

To characterize the dynamical behavior of the time-interval sequences we record the successive times when the variable X crosses the $X=0$ line from above. That is, we define T_n by $X(T_n)=0$ and $X(T_n^-)>0$. After this, the time intervals $\delta_n=T_{n+1}-T_n$ can be obtained for all firings. From these δ_n values we can know that if the firing pattern is a train of bursts of one spike (period-1), the δ_n will have an unique value. For a train of bursts of n spikes (period-n), we get n different values for δ_n. For a train of bursts of undetermined number of spikes (chaotic), the δ_n will show a spread of values. In this paper we have also studied the spatiotemporal patterns of the firings for coupled neuronal network, Eqs. (1)–(3), with the numbers of neurons $N=800$. We used a uniform distribution for the stimulus I_i, with $1\leq I_i\leq 5$ (i.e., $I_i=1+4i/N$). This distribution is the same as that used in Ref. [13]. The spatiotemporal patterns of the firings are obtained by plotting the neural activity, i.e., the firing time $t=T_n$, as defined before, with a point in the time axis against the space, i.e., the location of the ith neuron.

All the numerical calculations are done by using a modified fourth-order Runge-Kutta method. In the study of the time-interval sequences of the firings for a single and two coupled neurons, the time steps were chosen as $\Delta t=0.0125$. We first run the program to $t=2300$ to discard the transient and then followed the time to $t=3800$ or longer. To get the spatiotemporal patterns of a network with a large number of neurons, the time step was chosen to be $\Delta t=0.1$. We have also done some calculations with smaller steps, finding that the patterns do not change. All parameters are held constant at $a=1.0$, $b=3.0$, $c=1.0$, $d=5.0$, $s=4.0$, $r=0.006$, and $X_0=-1.6$, which are the values used in Ref. [14].

III. RESULTS AND DISCUSSION

A. The firing of a single neuron

First, in this section, we present results for the time-interval sequences for firing when there is no coupling between the neurons in the network. In this case, we only need to study one set of equations, Eqs. (5)–(7), with $J=0$. In Fig. 1, we plot the time interval δ_n against the stimulus I. From Fig. 1, we can see that when $I<1.32$, there is no spike since the stimulus I is too small to stimulate the neuron from its stable quiescent state with $X=X_0<0$. As I increases there is a train of regularly spaced spikes, the period-1 state. There is only one δ_n value for each I value when $1.32<I<1.57$. When $1.57<I<2.13$, there are periodic bursts of two spikes per burst, i.e., a period-2 state. For this case, in Fig. 1 there are two values of δ_n. Then it follows period-3 and period-4. At $I=2.83$, there is an intermittency transition to chaos. Finally, there follows a reversed period doubling cascade to a period-1 state again. This is due to the fact that for a large stimulus I, the system is in high-frequency repetitive firing state. The code for the information process is different for the differing firing states.

B. The firing of two coupled neurons

When the neurons in a network are completely synchronized and phase locked, we can use a simplified model of two coupling neurons to study the network since from Eqs. (1)–(3) all the states of neurons are equivalent and all the neurons are fired at the same time.

In Figs. 2(a)–2(c) we show the time intervals of the firings δ_n against the stimulus I for the coupling strengths $J=0.5$, 1.0, and 3.5, repetitive. From these plots we can see that as the coupling increases, the complexity of the time-interval sequences becomes simple. That is, as the coupling increases, the bifurcation region

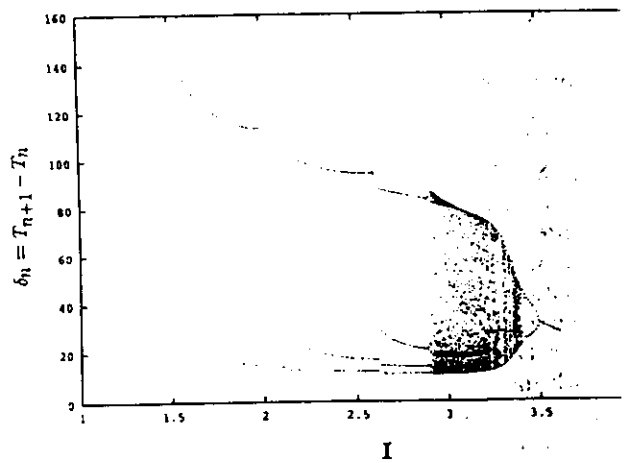

FIG. 1. $\delta_n=T_{n+1}-T_n$, the time-interval sequences of the firing for a single neuron vs the external stimulus I. Results from simulations of one set of equations, Eqs. (5)–(7), with $J=0$, and the time step $\Delta t=0.0125$ were used. For each value, the time is followed to $t=5000$ and the first $t=2300$ are eliminated for transient.

:come narrower. When the coupling is low, for exam-
e, in the case of $J=0.5$, the firing of the system keeps
ost of the features of the single neuron, the case of
=0. There is a bifurcation to a low-frequency repetitive
ing state consisting of a train of regular spaced spikes,

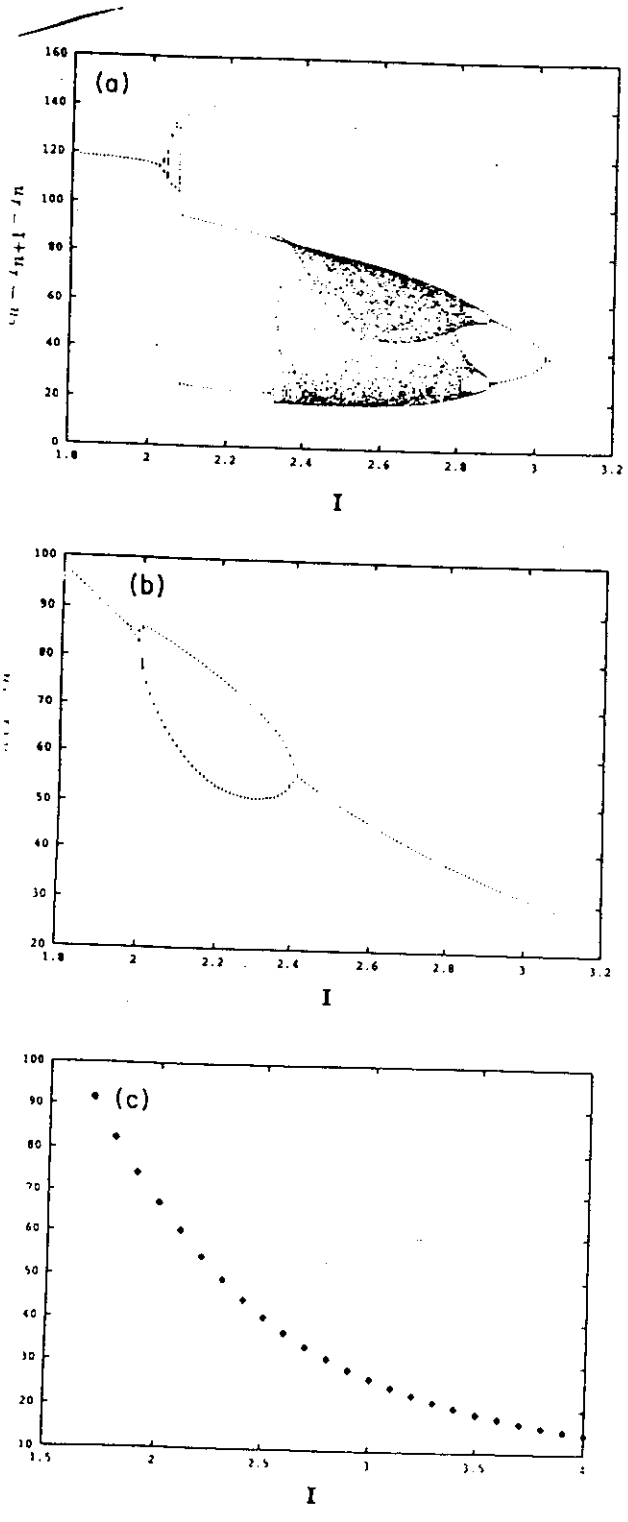

FIG. 2. $\delta_n = T_{n+1} - T_n$, the time-interval sequences of the ng for two coupled neurons with the coupling strength J vs external stimulus I. (a) $J=0.5$; (b) $J=1.5$; (c) $J=3.5$. The e step $\Delta t=0.0125$ was used. For each value of I, the time is owed to $t=5000$ with the first $t=2300$ eliminated.

and a region of chaotic firing, as well as a reversed period-doubling cascades to a period-1 state [see Fig. 2(a)]. However, when $J=1.0$, the bifurcation region is small [see (Fig. 2(b)] and there are almost only period-1 and period-2 firing states. Finally, when $J=3.5$, the bifurcation region disappears and there is only a period-1 repetitive firing state [see Fig. 2(c)]. Actually as the coupling increases, the effective stimulus $I'=I+JS_j(t)$ is increased, which enables the neuron to be stimulated with a repetitive firing. If the coupling is larger than a certain value, there is no more chaotic firing.

C. Spatiotemporal patterns of a coupled network

Now we consider a network consisting of N neurons with different values of I_i coupled globally by excitatory interactions, $J_{ij}=J/N$. Here we are using I_i distributed uniformly between 1 and 5, as before. Simulations of the network with $0<J<6.0$ revealed three phases [13]: an asynchronous stationary state, synchronized oscillations, and synchronized chaos. Here in this paper we are interested in the spatiotemporal patterns and the time intervals of the firings of the network as shown in Fig. 3 for the coupling strengths $J=0.5$, 3.0, and 6.0, respectively. From these plots we can see that there are some structures of the firing state. For the lower stimulated region (the smaller i region) the firing period is longer, and for the higher stimulated region the period is shorter and the points become dense since for the high stimulus I, the neuron is repetitively fired. In addition, for some small groups, or clusters, of neurons, the activities have a synchronized behavior as they have the same frequency of firings, phase locked. Notice, however, that the actual time of firing within one of these clusters is widely distributed. When the coupling increases, the synchronization is expanded to a larger group of neurons, and finally to the whole network of neurons.

When $J=0.5$, we can see from Fig. 3(a) that the pattern of firings can be divided into four regions: (1) nonfiring region for $(i<60)$—there is no firings since the local effective stimulus $I'=I+\sum_j J_{ij}S_j(t)$ is too small and is not enough to stimulate the neurons from its quiescent state; (2) periodic firing region for $(60<i<370)$—the firing is period-1 to period-4 but the time widths of these period-n bursts are different; (3) chaotic firing region for $(370<i<500)$—the firing is chaotic, the time interval is irregular and with no structure in the pattern. The total numbers of chaotic neurons is about $n=130$, which takes about $n/N\simeq 16\%$ for the network; (4) the repetitive high-frequency firing region for $(500<i<800)$—for this region, the pattern is regular. In Fig. 3(b), we have constructed a time-interval sequence versus the local neurons from the spatiotemporal pattern showed in Fig. 3(a). From this figure we can see that the time interval property is similar to Fig. 2(a). There is a bifurcation of a train burst consisting of one, two, three, and four spikes, and an intermittency to chaotic state, as well as a reversed bifurcation to a period-1 firing state. The difference is that this bifurcation is in the neuronal space and not in J as seen before.

As the coupling strength J increases, the number of n

of neurons being chaotic also increases. For example, when $J=1.5$, the number n is about $n=700$, which takes about $n/N \simeq 90\%$ of the neurons in the network. For $J=2.0$ this factor is almost 1, which means that all the neurons are chaotic. In Fig. 3(c) we have shown the case for $J=3.0$, an intermediate coupling. We can see that the nonfiring region has disappeared and there is a spatially correlated oscillation for the neurons. However, the oscillation is not phase locked in the whole network and only in some very small regions there is a ph... locked activity. The synaptic current $I_s(t)$ is periodic ... and very noisy. The activity of most of the neurons te... to synchronize with this periodic current $I_s(t)$. We c... this a quasisynchronization. From the time-inter... figure shown in Fig. 3(d), the bifurcation region is exte... ed to the whole network and many points are distribut... irregularly near the two main values of δ_n for each ne... ron. As our conclusion, such an irregular spatiotempor...

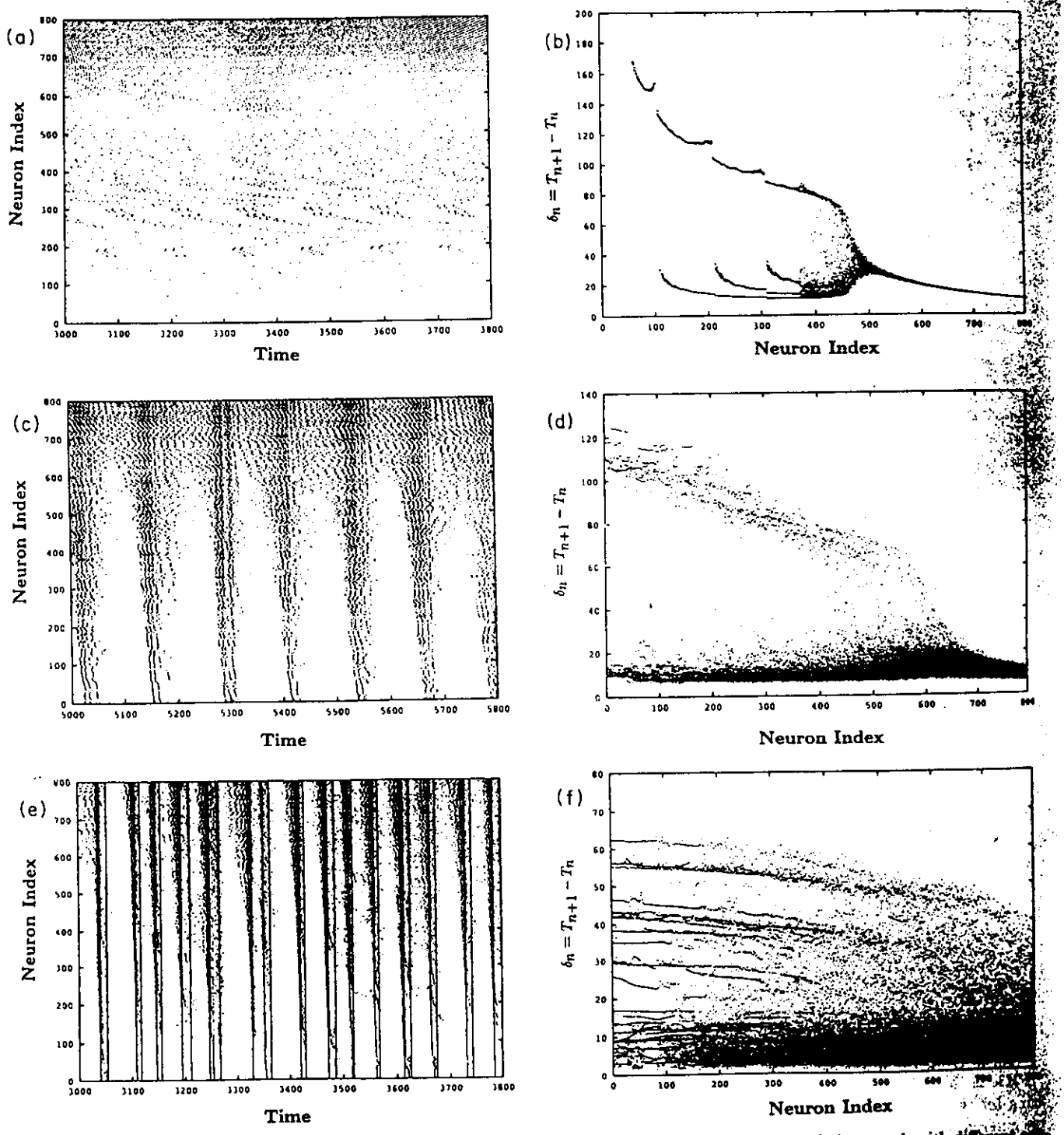

FIG. 3. The spatiotemporal patterns: neuron i vs the time intervals of the firing of spike for a coupled network with differ... pling strength J: (a) and (b) $J=0.5$; (c) and (d) $J=3.0$; (e) and (f) $J=6.0$. The time step $\Delta t=0.1$ and the number of the ne... $N=800$ were used.

behavior is definitely chaotic since the time-interval sequences against the local neurons can be recognized as an attractor for the network.

In Figs. 3(e) and 3(f) we presented the results for $J=6.0$. From the spatiotemporal pattern of the activity, we can see that the spatial structure is more ordered, i.e., all the neurons are phase locked together. But for the temporal behavior, the activity of the neurons is chaotic.

It should be noticed that for very small values of J (and even for $J=0$), the synaptic current I_{syn} is not given by a constant plus noise. In fact, we have found that a periodic component, albeit of very small amplitude, appears for large values of N. This periodic component simply represents the effects of the oscillatory behavior of the independent neurons for most of the values of I included in the interval $1 \le I \le 5$. An average over some set of periodically evolving variables will have in general at least quasiperiodic behavior and is only in special cases that the periodic components balance perfectly and the average becomes a constant. There is of course a noisy component, coming from the chaotic neurons, but this component decays for large N. In addition, the introduction of the coupling acts as a positive feedback and tend to increase the periodic component. In Fig. 4 we plotted the periodicity of the synaptic current for (a) $J=0$ and (b) $J=0.5$, in a network of 10^4 neurons. It is clearly seen that the synaptic current is periodic even for $J=0$. In Fig. 5 we show the corresponding power spectra of the

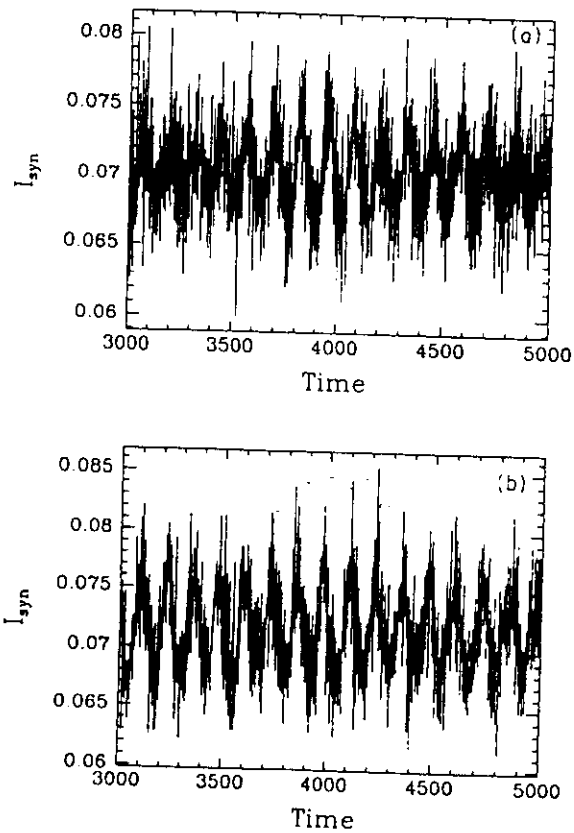

FIG. 4. The synaptic current I_{syn} vs time for a coupled network with the number of the neurons $N=10000$ and the coupling strengths (a) $J=0$; (b) $J=0.5$.

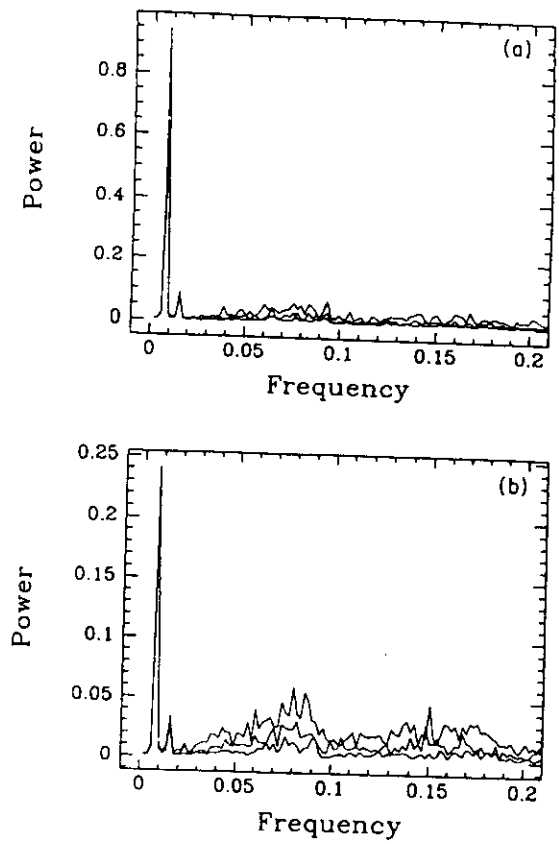

FIG. 5. Power spectra of the synaptic current I_{syn} for a coupled neuronal network with the number of the neurons $N=2400, 4800, 10000$ (from the top curve to the bottom one) and the coupling strengths (a) $J=0$; (b) $J=0.5$.

synaptic current $I_{syn}(t)$. As the number of neurons is increased, the noisy part decreases, but there still exists a peak of very low frequency which represents the periodicity of the synaptic current. However, in the case of large values of J, the synaptic current $I_{syn}(t)$ is impulselike. The neurons are synchronized to this impulselike current. The fronts of the activity of the neuron encode the information at the same time (except for the high-I region there are some dilute activities).

Finally, in order to verify the chaotic behavior, we have also calculated the local maximum Lyapunov exponent λ_i against the neuron i as shown in Figs. 6(a) and 6(b), respectively. From these two figures, we can see that there are positive value of λ_i for the chaotic region and negative ones for periodic behavior. At the transitions between one phase-locking region and another, there are some small factors with positive λ_i.

IV. SUMMARY

Neuronal activity is well known to be noisy. This stochasticity is observed both during information transmission and spontaneously. One of the most obvious features of such stochasticity is in the uncertainty arising in the interspike interval (the time-interval sequences

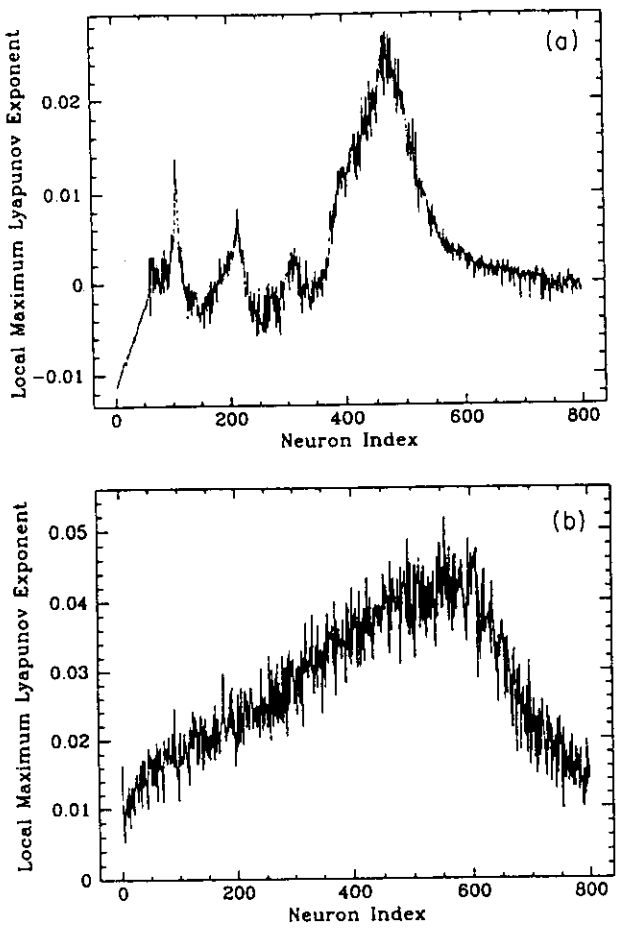

FIG. 6. The local maximum Lyapunov exponent λ_i vs the neuron i. The time is followed to $t=9000$ and the first $t=4000$ are eliminated for transient. (a) $J=0.5$; (b) $J=3.0$.

studied in this paper), for example, in the interspike interval distribution for a neuron in the spinal chord of a decerebrate cat, where they may be a variance of the order of 20% of the mean interval [17]. In this paper, we started from a model of coupled neuronal network[s] with any noise and studied the time-interval sequences [and] spatiotemporal patterns of the activities of the neu[rons]. We found that (1) for a single neuron, or a network [with] zero coupling, the chaotic activities can exist for a [wide] range of the external stimulus [16]; (2) for a coupled two-neuron model, the chaotic activity is dominated by the coupling strength. For large coupling, the bifurcation region can disappear totally; (3) for a coupled network with an uniform distribution of the external stimulus, the activity of the neurons can be regular or irregular (chaotic). From the spatiotemporal patterns, the strong coupling results in a spatio-order phase, or synchronized firing state of the neurons, while the temporal behavior of the neurons is chaotic. The whole chaotic behavior cannot be accounted for by the finite-size noise. The three phases for this coupled neuronal network are (a) an asynchronous stationary state ($0<J<0.8$); (b) quasisynchronized chaos ($0.9<J<3.2$); (c) synchronized chaos ($J>3.2$). However, for more strong coupling, we can also expect to have a nonchaotic activity of neurons, the fronts of activity appear in a regular time interval, since (a) the strong coupling increases the spatiocorrelation which can have a complete synchronization of the neurons and (b) the effect of this very high coupling or the synaptic current is shifted to the local neurons, and it can result in a high-frequency repetitive firing of the neuron.

It is worth noting that for modeling more realistic neuronal network, one must consider the structure of the network. This can be done assuming the local coupling and stimulus are a function of the number of neuron i.e., differently in the space. However, the qualitative results for the nonlinear behavior are the same as for the simple model.

ACKNOWLEDGMENTS

H.A.C. acknowledges support from the Instituto Nazionale de Fisica Nucleare (INFN). W.W. would also like to thank E. Canessa for valuable discussions.

[1] C. Skarda and W. J. Freeman, Behav. Brain Sci. **10**, 161 (1987).
[2] O. Sporns, G. Tononi, and G. M. Edelman, Proc. Natl. Acad. Sci. U.S.A. **88**, 129 (1991).
[3] H. G. Schuster and P. Wagner, Biol. Cybern. **64**, 77 (1990); **64**, 83 (1990).
[4] H. Sompolinsky, D. Golomb, and D. Kleifeld, Proc. Natl. Acad. Sci. U.S.A. **87**, 7200 (1990); Phys. Rev. A **43**, 6990 (1991).
[5] C. M. Gray, P. Konig, A. K. Engel, and W. Singer, Nature (London) **338**, 334 (1989).
[6] R. Eckhorn *et al.*, Biol. Cybern. **60**, 121 (1988).
[7] Ch. von der Malburg and W. Schneider, Biol. Cybern. **54**, 29 (1986).
[8] J. C. Eccles, *The Understanding of the Brain* (McGraw-Hill, New York, 1973).
[9] S. W. Kuffler, R. Fitzhugh, and H. B. Barlow, J. Gen. Physiol. **40**, 683 (1957).
[10] R. M. Siegel, Physica (Amsterdam) D **42**, 385 (1990).
[11] A. Longtin, A. Bulsara, and F. Moss, Phys. Rev. Lett. 656 (1991).
[12] H. C. Tuchwell, *Stochastic Processes in the Neuroscie* (SIAM, Philadelphia, 1989); A. V. Holden, *Models of Stochastic Activity of Neurons*, Lecture Notes Biomathematics Vol. 12 (Springer, Berlin, 1976); G. S path and S. K. Srinivasan, *Stochastic Models for S Trains of Single Neurons*, Lecture Notes in Biomathe ics Vol. 16 (Springer, Berlin, 1977).
[13] D. Hansel and H. Sompolinsky, Phys. Rev. Lett. **68**, (1992).
[14] J. L. Hindmarsh and R. M. Rose, Proc. R. Soc. Lor Ser. B **221**, 87 (1984).
[15] R. Fitzhugh, Biophys. J. **1**, 445 (1961).
[16] Wei Wang, J. Phys. A **22**, L627 (1989).
[17] J. G. Taylor, in *Neurodynamics*, edited by F. Pasem and H.-D. Doebner (World Scientific, Singapore, 1991)

Instabilities and nonstatistical behavior in globally coupled systems

Gabriel Perez
International Centre for Theoretical Physics, P. O. Box 586, 34100 Trieste, Italy

Hilda A. Cerdeira
International Centre for Theoretical Physics, P. O. Box 586, 34100 Trieste, Italy
and Universidade Estadual de Campinas, Instituto de Fisica, 13081 Campinas, São Paulo, Brazil
(Received 17 August 1992)

The mean field in a globally coupled system of chaotic logistic maps does not obey the standard rules of statistics, even for systems of very large sizes. This indicates the existence of intrinsic instabilities in its evolution. Here these instabilities are related to the very nonsmooth behavior of mean values in a single logistic map, as a function of its parameter. Problems of this kind do not affect a similar system of coupled tent maps, where good statistical behavior has been found. We also explore the transition between these two regimes.

PACS number(s): 05.45.+b, 05.90.+m

I. INTRODUCTION

In recent times there has been a number of efforts to analyze the interplay between temporal chaos and space synchronization in globally coupled systems. These are systems of considerable importance in modeling phenomena as diverse as Josephson-junction arrays, multimode lasers, vortex dynamics in fluids, and even evolutionary dynamics, biological information processing, and neurodynamics [1]. There is a great wealth of phenomena in these systems, originating in the presence of two conflicting trends in their dynamics. On one side, the presence of a common driving factor, coming from some type of average over the system, introduces a partial synchronization in the evolution of its elements. On the other, the chaotic divergence between the evolution of any two different elements tends to destroy this coherence. There are, therefore, two limiting behaviors, one in which a large coupling forces the synchronization of a set of weakly chaotic elements, and another in which strongly chaotic but weakly coupled systems display incoherent behavior. This last situation is characterized as having exponential divergence of trajectories not only in time —positive Lyapunov exponents—but also in space, in the sense that if at any given time two different elements of the system have very close magnitudes, those magnitudes will diverge from each other exponentially fast. Notice that for strong coupling it is possible to have all the elements of the system converge into a single cluster, and at the same time to have this cluster move chaotically [2].

In fact, at first sight these weakly coupled systems do not look too different from a simple lattice of uncoupled identical chaotic elements, with maybe some shifts in their parameters. A more careful study reveals, however, that there is a detectable and nontrivial influence of the global coupling, which gives rise to some subtle coherent effects, spoiling the statistical properties of the system.

II. GLOBALLY COUPLED LOGISTIC MAPS

Here we consider some of these coherence effects through the particular example of a globally coupled lattice of logistic maps, obeying the equations

$$x_{n+1}(i) = (1-\epsilon) f(x_n(i)) - \frac{\epsilon}{N} \sum_{j=1}^{N} f(x_n(j)), \quad (1)$$

where i is the space index and n is the time index. Here $f(x)$ is the familiar logistic map, $f(x) = 1 - ax^2$, and the mean field h at time n appears in the last term of the equation above,

$$h_n \equiv \frac{1}{N} \sum_{j=1}^{N} f(x_n(j)). \quad (2)$$

This is a simple prototype of globally coupled chaotic systems, and has been exhaustively explored in Refs. [2–4]. For large a and small ϵ the system settles in a "turbulent" regime, where, as mentioned before, all elements $x(i)$ evolve chaotically, without any obvious mutual synchronization.

In this regime, it is reasonable to expect the mean field to obey general statistical rules, since it is an average over quasirandom variables. In particular, it was expected that h should converge to a fixed value h^* as $N \to \infty$, with fluctuations around this limiting value normally distributed (central limit theorem), and with a dispersion that decays as $1/\sqrt{N}$ (law of large numbers). Surprisingly, it was found that this simple system failed to fulfill these expectations [3,4]. This failure has also been verified in similar models [5], which suggests that this is a generic behavior. In particular, it was found that the dispersion of the mean field did not go to zero, as expected, but instead saturated to a fixed positive value for large N; broad peaks indicating a quasiperiodic component were found in the Fourier spectrum of the time

...quence for the mean field: and the mutual information ... the lattice also saturated to a nonzero value for large ...

To understand the relevance of these facts, we should ...ice that, if in effect the mean field converged to a fixed ...e, the system would decouple. Each and every one ...its elements would behave like a single logistic map of ...e form

$$y_{n+1} = 1 - A(a, \epsilon, h^*) y_n^2 \tag{3}$$

...h $A = a(1-\epsilon)(1-\epsilon-\epsilon h^*)$ and $y = x/(1-\epsilon-\epsilon h^*)$, ...here the value of h^* is obtained self-consistently. In fact, ...is assumption of convergence of h to a fixed limit has ...en used successfully in the study of a different globally ...pled nonlinear system [6]. For logistic maps, this re...ction of the dynamics of the (infinite) lattice to that of ...single map does not happen, which clearly implies that ...e self-consistency equation for h^* is unstable around its ...ed points.

III. STATIC MEAN-FIELD MAPPING

A. Definition

Let us consider h, for the time being, not as a dynam... variable but as a fixed input in the system, and call ... h_{in}. Taking the $N \to \infty$ limit on a lattice of the type ...cribed by Eq. (1), we can define a system of equations ...t gives as a final result a static mean field h_{out}, in the ...lowing manner:

$$h_{out} = \lim_{N\to\infty} \frac{1}{N} \sum_{i=1}^{N} \cdots \tag{4}$$

$$\cdots = 1 - \epsilon f(x, \cdots) - \epsilon h_{in}. \tag{5}$$

...s gives us a function $h_{out}(h_{in}; a, \epsilon)$, which we will ...the "static mapping." In this simplified problem we ...check whether or not the self-consistency equation ... = h_{in} has a solution, and explore its stability. Notice ...t h_{out} is invariant because of the existence of an invari... distribution for x and therefore for $f(x)$ [7], when ...e maps are in the chaotic regime. For cases where the ...ps are in some periodic regime (and even when they ...e in chaotic motion inside some periodic window, as ...parts of the 3-windows), the existence of an invariant ...ribution depends on the distribution of initial condi...ns. We will assume that in these cases all different ...ases of the relevant cycle are equally represented, so ...t an invariant distribution can be achieved.

...should be clear that this static mapping is not ...ivalent to the actual evolution of the mean field, ... = $h_n, h_{n-1}, h_{n-2}, \ldots; a, \epsilon$, also defined in the $N \to \infty$ ...it. This "dynamic mapping" depends in principle on ...previous values of h, although this dependence is neg...ible for very old h (i.e., for h_{n-m} when $m \gg 1$). ...exhibits therefore a much richer behavior. What ...important for us here is that they have the same ...ed points. On the stability of these fixed points we ...pose the following hypothesis: *the dynamic mapping* ... = $h_n, h_{n-1}, h_{n-2}, \ldots$ *cannot be stable around its fixed* ...nt $h_i = h^*$, $i = n, n-1, \ldots$, *if the static mapping is not.* Basically, we are assuming that if the process is unstable even in the very simplified form given by the static mapping, the complexities introduced by ... dependence on all previous values of h cannot make its stability anything but worse. The numerical results verify this statement, as we will see next.

B. Numerical results

We have evaluated numerically the static mapping in the range of h_{in} that contains the fixed points $h_{out} = h_{in}$ for the parameters $a = 1.99$ and $\epsilon = 0.1$. The results are shown in Fig. 1. Although this is an extremely non-smooth function, it has to be continuous, since for the different types of bifurcations present in the logist... ap... the average value of x changes continuously [8]. The ...xed points in this graph give $h^* \approx 0.311$, not too different from the actual average of the mean field ($\langle h \rangle \approx 0.3063$) but different enough to imply that $\langle h \rangle$ does not fall on a fixed point. It is clear from the graph that none of these fixed points can be stable, since the absolute slopes $|\Delta h_{out}/\Delta h_{in}|$ obtained numerically are much larger than 1 almost everywhere. We should keep in mind that only 300 points have been calculated to get this figure, and therefore these slopes are defined only in a coarse-grained sense. In fact, the function $h_{out}(h_{in})$ has well-defined derivatives only inside its periodic windows. Therefore even though this function cannot reveal all the complexity of the actual mapping $h_n = h_n(h_{n-1}, h_{n-2}, \ldots)$, its nonsmooth behavior is indicative of why h_n does not converge to an invariant value as $N \to \infty$.

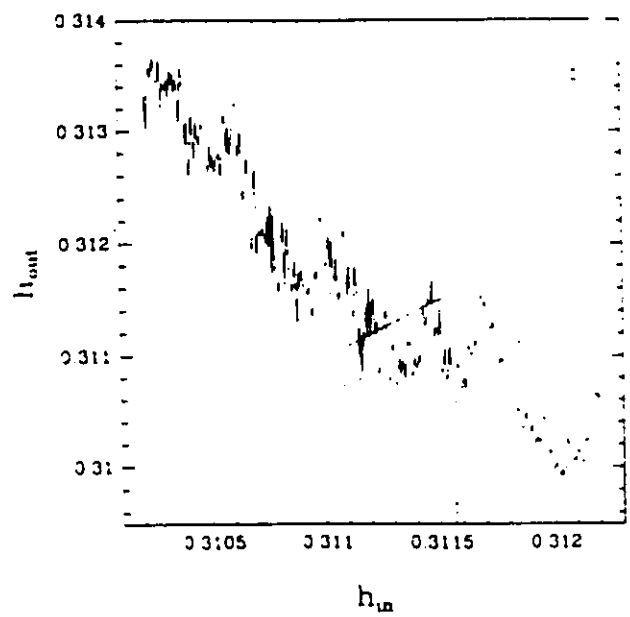

FIG. 1. Static mapping $h_{out}(h_{in})$ from Eq. (1). The line joins 300 points calculated over equally spaced h_{in} values. These points were obtained averaging over 1.5×10^6 iterations, after a transient of 4000 iterations. The straight line is the diagonal $h_{out} = h_{in}$. The typical error level is indicated with the error bar in the upper-right corner. Here $a = 1.99$, $\epsilon = 0.1$, and $f(x)$ is the logistic map.

The presence of the "well" visible in Fig. 1, and of which an enlarged view is given in Fig. 2, deserves some comment. The bottom of the well corresponds to a periodic 14-window that, as is common in the logistic map, begins in a tangent bifurcation and ends in an internal crisis. The infinite slope at the left end of the periodic window is due to the fact that at both sides of a tangent bifurcation in the logistic map the average value of x changes as $\langle x\rangle - \langle x\rangle_c \approx a - a_c|^{1/2}$, where a_c is the critical parameter for the bifurcation. This is also true on the one-band side of an internal crisis [9], where the probability density spreads from the several bands at one side into the one on the other, also as $|a - a_c|^{1/2}$. This explains the infinite slope at the right end. These two facts, together with the continuity of $\langle x\rangle$ in period-doubling bifurcations, sustain our assertion that $h_{out}(h_{in})$ is continuous. These "wells" and their infinite-slope walls should not be isolated instances in the h_{out} versus h_{in} graph, since the periodic windows from where they arise are thought to be dense in the bifurcation diagram of the logistic map [7, 10]. This is what makes it impossible for the map to have a derivative except inside a periodic window.

As pointed out in Ref. [4], all these peculiar phenomena disappear if we change $f(x)$ in the set of equations (1) to a tent map, $f(x) = 1 - a|x|$. For this system, the mean field h_n seems to converge to a limit, with fluctuations that decay as $1/\sqrt{N}$, as expected. A look to the bifurcation diagram for the tent map shows a complete absence of periodic windows, tangent bifurcations, or internal crisis, and suggests a smooth behavior of $\langle x\rangle$ as a function of a, which of course would imply a smooth behavior in $h_{out}(h_{in})$. This has been verified numerically, for $a = 1.99$ and $\epsilon = 0.1$. The results are shown in Fig. 3. The curve h_{out} versus h_{in} obtained here is extremely smooth, within our levels of error, and has a very small slope. The fixed point is $h_{out} = h_{in} = 0.1787$, in perfect agreement with the calculated value of $\langle h\rangle$. Therefore, the simplified

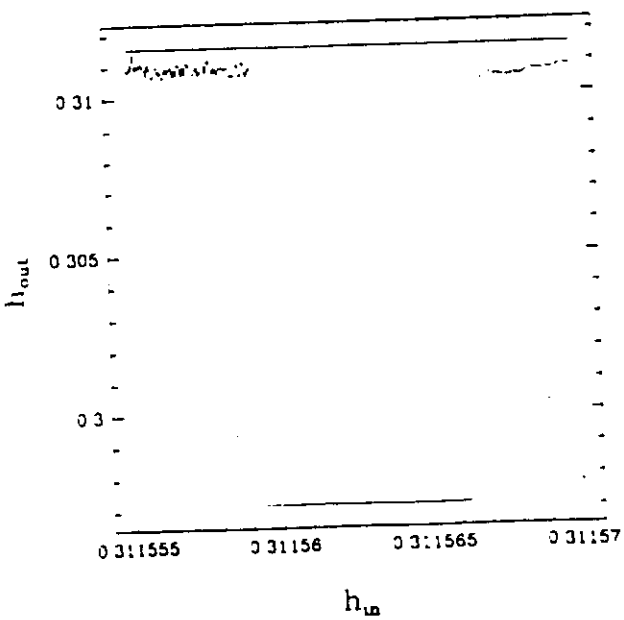

FIG. 2. Enlargement of the "well" visible in Fig. 1. The bottom corresponds to a periodic 14-window, the left wall is a tangent bifurcation, and the right wall is an internal crisis. The line joins 300 points calculated as averages over 7.5×10^7 iterations, after a transient of 4000 iterations. The straight line is the diagonal $h_{out} = h_{in}$. All other parameters are as in Fig. 1. Typical error bars are not significant at the scale of the figure.

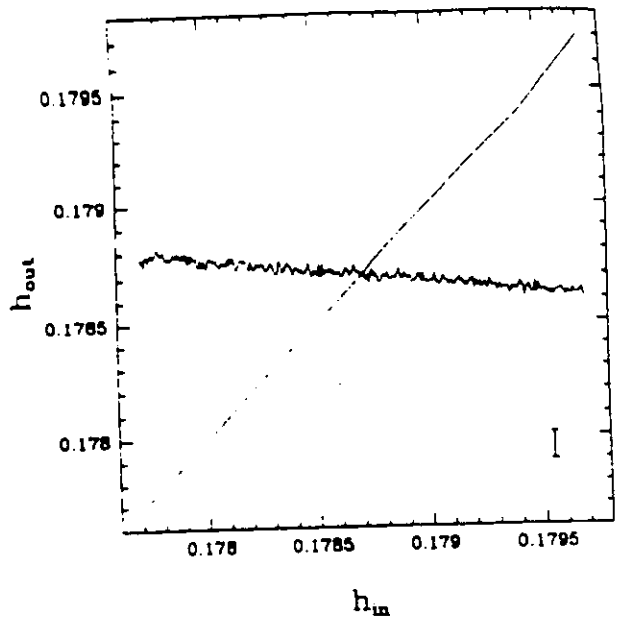

FIG. 3. Static mapping $h_{out}(h_{in})$ for the tent map. The line joins 300 points calculated as in Fig. 1. The straight line is the diagonal $h_{out} = h_{in}$, and a typical error bar is given in the lower-right corner.

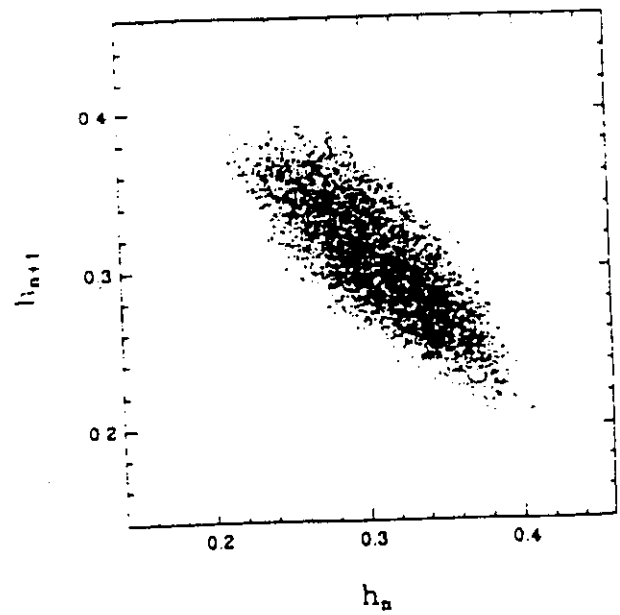

FIG. 4. Distributions of the values of the mean field h_{n+1} vs h_n in the dynamic mapping, where $f(x)$ is the logistic map. These results are for a lattice of size $N = 200\,000$. Here we have plotted 10 000 points, after a transient of 5000 iterations. Other parameters are as in Fig. 1.

static mapping does not suggest instabilities in the more complex dynamic mapping.

In summary, the strong instability of the static mapping $h_{out}(h_{in})$ is a good indicator of the lack of convergence of the mean field h to a fixed value as N grows. The convergence of h towards such a limit in the system with tent maps is accompanied by a smooth and almost flat $h_{out}(h_{in})$. However, we should not forget that this is only a static construction, and cannot represent the full dynamics of the problem. As a matter of fact, the plot of h_{n-1} versus h_n, obtained for a value of N such that the fluctuations have reached their saturation level, shows a very different behavior, as can be seen in Fig. 4. So we have to keep in mind that the static function tells us about the impossibility of achieving a fixed value for h in the $N \to \infty$ limit, but it does not say anything about the actual evolution of this quantity.

IV. INTERMEDIATE CASES: MIXING TENT AND LOGISTIC MAPS

Given the fact that nonstatistical behavior is present in logistic but not in tent maps, it is natural to ask what happens for intermediate situations. For this we have considered a "logistic plus tent" map that interpolates between quadratic and linear behavior. It is given by

$$f_\alpha(x) = 1 - a[\alpha x^2 + (1-\alpha)x]. \quad (6)$$

It has as limits the tent map, when $\alpha = 0$, and the logistic map, when $\alpha = 1$. There are, of course, many other ways of interpolating between these two limits, a simple one using the power map $f_p(x) = 1 - a x^\alpha$, with $1 \le \alpha \le 2$. For concreteness, we will consider here only the function given in Eq. (6).

We have explored numerically the behavior of coupled lattices of these maps. The results for the mean-square deviation (MSD) of the mean field for α close to 1 show clear nonstatistical behavior, which seems to disappear monotonically with decreasing α. See Fig. 5. A very interesting feature here is the slight but consistent recovery of the values of the MSD for values of α less than up to the value of saturation of the MSD. A similar phenomenon was found in Ref. [4], in a coupled lattice of logistic maps subject to the influence of static parametric perturbations.

A much stronger evidence of coherence is found in the power spectrum of the mean field. As mentioned before, one of the signals of nonstatistical behavior in these systems is the appearance of broad peaks in the power spectrum, indicating a quasiperiodic component in the evolution of the system. As can be seen in Fig. 6, this quasiperiodicity is strongly accentuated in the case of maps with a small tent component ($1 - \alpha \approx 0.1$). The quasiperiodic behavior is strong enough as to be visible in the h_{n-1} versus h_n plot, as shown in Figs. 7 and 8. Curiously, as we make α even smaller this trend reverses and the power spectrum becomes almost flat.

This increase in the quasiperiodicity of the mean field has been encountered in two other cases: in the presence of a very small additive noise [11], and when the mean field is not global but includes only the $N/2$ nearest neighbors [12]. These three cases are similar in that all of them point to a connection between small smoothly distributed noise and an increase in quasiperiodicity. In our case, we could roughly consider the tent part of our map as a perturbation over the logistic part (for α close to 1), since one part is added to the other to obtain the total

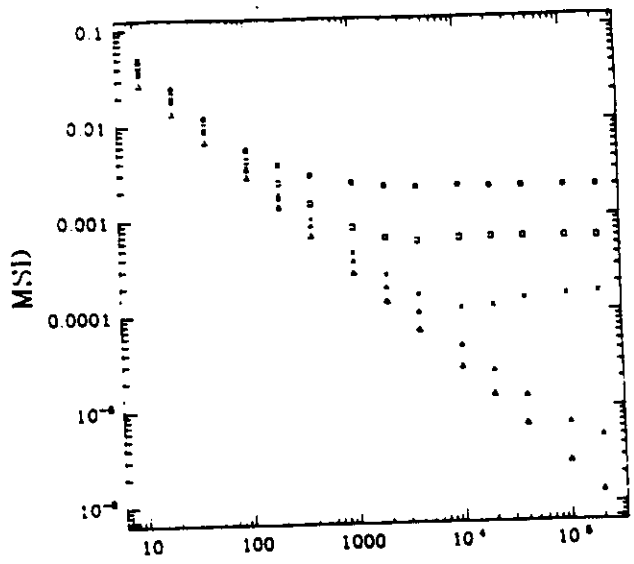

FIG. 5. Mean-square deviation for the mean field vs lattice size for several values of α, in the mixed map. For all points we have used a total of 102 400 iterations, with a transient of 5000 iterations. The values of α are (■) $\alpha = 1.0$ (logistic), (□) $\alpha = 0.95$, (×) $\alpha = 0.9$, (▲) $\alpha = 0.75$, (△) $\alpha = 0.0$ (tent). As before, $a = 1.99$ and $\epsilon = 0.1$.

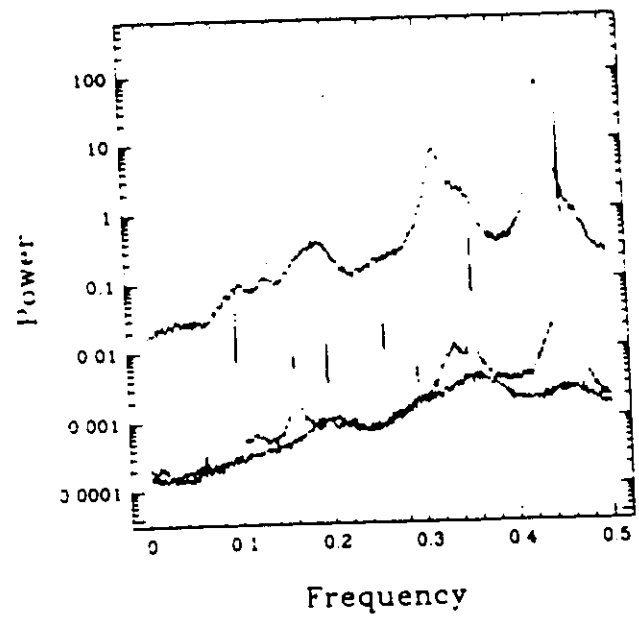

FIG. 6. Power spectra for the mean field for $\alpha = 1$ (upper line), $\alpha = 0.9$ (middle line), and $\alpha = 0.0$ (lower line). Here we are averaging over 100 runs of 1024 iterations each, after a transient of 5000 iterations. The parameters are $a = 1.99$ and $\epsilon = 0.1$.

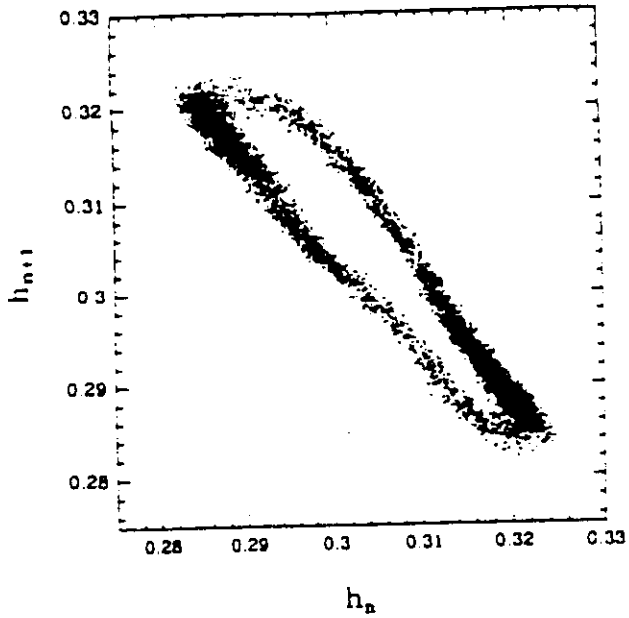

FIG. 7. Distributions of the values of the mean field h_{n+1} vs h_n in the dynamic mapping, where $f(x)$ is the mixed "logistic plus tent" map. Here $\alpha = 0.9$. All other parameters are as in Fig. 4.

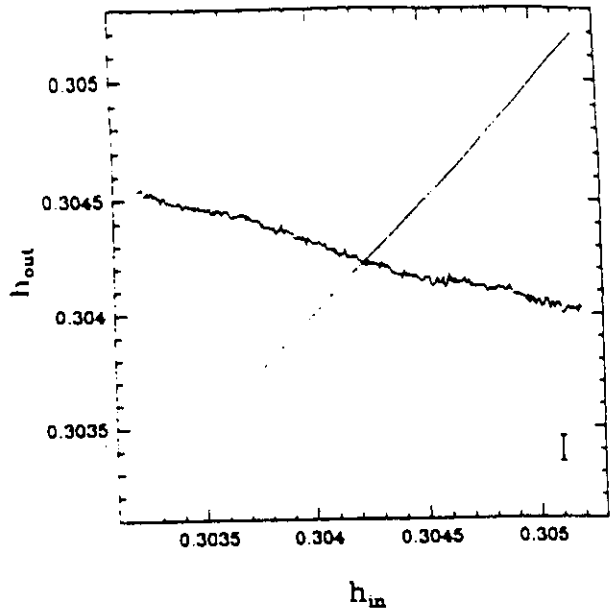

FIG. 9. Static mapping $h_{out}(h_{in})$ for the mixed "logistic plus tent" map. The line joins 300 points calculated as in Fig. 1. The straight line is the diagonal $h_{out} = h_{in}$, and a typical error bar is given in the lower-right corner.

mapping. Obviously, this is a highly correlated perturbation; however, taking into account that the tent map has a behavior closer to white noise (its invariant distributions for $\alpha \lesssim 2.0$ are almost flat) than that of the logistic map, the connection between these two processes is at least plausible. Notice that here we cannot invoke the influence of some periodic window for this increase in quasiperiodicity: first because periodic windows are almost nonexistent in the bifurcation diagram of $f_{lt}(x)$ for $\alpha = 0.9$, and second because this would make it difficult to explain why the total strength of the signal decreases, i.e., why the MSD goes down as we decrease α. A similar argument can be made for the semiglobally coupled map, in the sense that the influence of the elements of the lattice that are not directly affected by the—now local—mean field can be roughly considered as a smoothly distributed small noise.

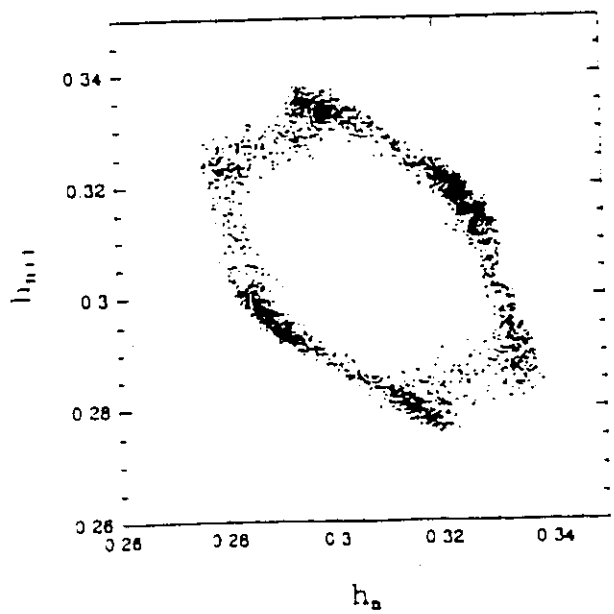

FIG. 8. Distributions of the values of the mean field h_{n+1} vs h_n in the dynamic mapping. Here $f(x)$ is the logistic map, as in Fig. 4, but we have added a uniformly distributed noise of amplitude $\sigma = 0.0045$. All other parameters are as in Fig. 4.

Finally, we have also checked, for these mixed maps, the behavior of the static mapping $h_{out}(h_{in})$. Result for $\alpha = 0.9$ can be seen in Fig. 9. Since the mixed map has a negative Schwarzian derivative except at $x = 0$, where derivatives are not defined, we expect to find only one attractor, and therefore a well-defined $\langle x \rangle$, independent of the initial value x_0. The behavior of the static mapping seems smooth and already (for this value of α) close to that of the tent map. Within our error levels, the curve still shows some structure. A careful look at the bifurcation diagram of this map shows that almost all the periodic windows have disappeared —this is due to the tent-like behavior of the map at its critical point— thus eliminating the multiple points of infinite slope in the h_{out} versus h_{in} graph. The coarse-grained slopes $|\Delta h_{out}/\Delta h_{in}|$ obtained here are much smaller than 1.

Therefore, the results for this case indicate that the stability of the static mapping (at least in the coarse-grained sense we have considered) is not sufficient to insure the stability of the actual dynamics. Our numerical results are of course insufficient to describe the behavior of the actual derivative dh_{out}/dh_{in} (or, equivalently, $d\langle x \rangle/da$) in these maps, and may still allow for differentiability in the tent map and nondifferentiability in the mixed cases.

V. CONCLUSIONS

The behavior of the mean field in globally coupled chaotic systems contains a number of surprises. The nonstatistical behavior of this quantity indicates the existence of an intrinsic instability in the evolution of the system, when we consider its infinite-size limit. Here we have explored the relationship between this instability and the corresponding problem in a simplified mapping for the mean field, which assumes that the dynamics depends only on the last value of this quantity. This is a very crude approximation, since it assumes an infinitely fast relaxation of the probability densities of the process, but it still gives information about its fixed points and some idea about their stability.

The numerical results obtained here indicate that the stability of this static mapping may be a necessary but not sufficient condition for the stability of the actual dynamics, i.e., for a normal statistical behavior of the mean field on the system. This result should be taken only as a first step in the study of the behavior of this kind of problem. In principle, a complete program should be carried out through the analysis of the stability of the eigenmodes of the Perron-Frobenious equation of the system, a point that has been mentioned in Ref. [4].

Under the influence of the previously mentioned instabilities, the mean field develops a dynamics that is weakly quasiperiodic. This is already unexpected, and gives rise to some as yet unresolved questions, as, for instance, what is the mechanism that selects the dominant frequencies? Even more remarkable is the fact that several mechanisms have already been found to strongly increase this quasiperiodicity, and none of them can be considered a form of periodic driving. On the contrary, directly or indirectly all of them can be assimilated into the addition of a small white noise. Also, this increase in quasiperiodicity is accompanied by a reduction of the total strength of the signal.

Finally, we want to mention that there has been recent evidence showing that the phenomena we have explored here also appear in locally coupled systems. Periodicity and quasiperiodicity have been observed in some totalistic cellular automata in 3, 4, and 5 dimensions [13], in medium-range coupled one-dimensional lattice maps [12, 14], and in locally coupled high-dimensional lattice maps [15]. All of this wealth of evidence says that there should be a common and fairly robust mechanism that extracts periodic behavior out of coupled chaos. The precise nature of this mechanism is still unknown.

ACKNOWLEDGMENTS

G.P. wants to thank Professor S.-J. Chang for stimulating discussions and for valuable information. We thank the Istituto Nazionale de Fisica Nucleare (INFN) for computing facilities.

[1] J. Crutchfield and K. Kaneko, in *Directions in Chaos*, edited by B.-L. Hao (World Scientific, Singapore, 1987); P. Alstrom and R. K. Ritala, Phys. Rev. A **35**, 300 (1987); P. Hadley and K. Weisenfeld, Phys. Rev. Lett. **62**, 1335 (1989).
[2] K. Kaneko, Phys. Rev. Lett. **63**, 219 (1989); Physica **41D**, 137 (1990).
[3] K. Kaneko, Phys. Rev. Lett. **65**, 1391 (1990).
[4] K. Kaneko, Physica **55D**, 368 (1992).
[5] K. Kaneko, Physica **54D**, 5 (1991); G. Perez, C. Pando-Lambruschini, S. Sinha and H. A. Cerdeira, Phys. Rev. A **45**, 5469 (1992); S. Sinha, D. Biswas, M. Azam, and S. V. Lawande, *ibid.* **46**, 3193 (1992).
[6] Y. Kuramoto and I. Nishikawa, J. Stat. Phys. **49**, 569 (1987); H. Daido, J. Stat. Phys. **60**, 753 (1990); S. H. Strogatz and R. E. Mirollo, J. Stat. Phys. **63**, 613 (1991).
[7] P. Collet and J. P. Eckmann, *Iterated Maps on the Interval as Dynamical Systems* (Birkhaüser, Boston, 1980).
[8] S.-J. Chang (private communication).
[9] S.-J. Chang and J. Wright, Phys. Rev. A **23**, 1419 (1981).
[10] J. D. Farmer, Phys. Rev. Lett. **55**, 351 (1985).
[11] G. Perez, S. Sinha, and H. Cerdeira, Physica D (to be published).
[12] S. Sinha, D. Biswas, M. Azam, and S. V. Lawande, Phys. Rev. A **46**, 6242 (1992).
[13] H. Chaté and P. Manneville, Europhys. Lett. **14**, 409 (1991); J. Hemmingsson (unpublished); J. A. C. Gallas, P. Grassberger, H. J. Herrmann, and P. Ueberholz, Physica **180A**, 19 (1992); P.-M. Binder, B. Buck, and V. A. Macaulay, J. Stat. Phys. (to be published).
[14] P.-M. Binder and V. Privman (unpublished).
[15] H. Chaté and P. Manneville, Europhys. Lett. **17**, 291 (1992).

Nonsimultaneity effects in globally coupled maps

Gabriel Pérez,[1,3,*] Sudeshna Sinha,[2,3,†] and Hilda A. Cerdeira[3‡]
[1]*Departamento de Física Aplicada, CINVESTAV del IPN, Unidad Mérida, Apartado Postal 73 "Cordemex," 97310 Mérida, Yucatán, Mexico*
[2]*Indian Institute of Astrophysics, Sarjaphi Road, Koramazda, Bangalore 560 034, India*
[3]*International Centre for Theoretical Physics, P.O. Box 586, 34100 Trieste, Italy*
(Received 9 July 1996)

We study the behavior of globally coupled maps when the coupling mean field is either delayed or averaged over several time steps. We find that introducing a delay does not reduce, and in some cases increases, the saturation values for the fluctuations of the mean field. The mean field changes its quasiperiodic behavior by introducing more components in its spectrum, and the distance between main components of this spectrum is reduced in a linear way. On the other hand, averaging the mean field reduces the saturation value for fluctuations, but does not fully restore statistical behavior to the system except in the limit of very large averages. As before, quasiperiodicity is changed by the introduction of more beating frequencies, and the distance between the most important among them decreases linearly. As an extra test, we study the effects that a small periodic driving has over this dynamics, and find that although there is some influence, there are not strong resonances to simple sinusoidal driving. [S1063-651X(96)02412-9]

PACS number(s): 05.45.+b, 47.52.+j

There has been in recent years sustained interest in the dynamics of large lattices of coupled chaotic systems [1]. These models give simple approximations to many interesting physical models, such as coupled Josephson junctions, multimode lasers, arrays of coupled nonlinear circuits, etc. A particular area of interest is that of globally coupled maps (GCMs), where the dynamics is discrete and the coupling is made global.

For these systems, a problem that has attracted some attention is how close to statistical is the behavior of the system when the dynamics of the local maps is chaotic and the coupling is weak. In this case, it is tempting to propose a "simplicity hypothesis," which says that since the chaotic behavior would give for independent maps invariant distributions with compact support, and the influence of the average is moderated by a small parameter, it could happen that in the limit of infinite lattices the average would converge to a fixed point, therefore decoupling the maps; and that for large but finite lattices this mean field would have a Gaussian distribution (central limit theorem), with a variance proportional to $1/N$ (law of large numbers). These hypotheses were originally checked by Kaneko [2], who found that the behavior in most cases was clearly nonstatistical, i.e., that the fluctuations of the mean field saturated at a finite value, as shown by their mean square deviation (MSD), and moreover, that this mean field developed some quasiperiodicity. This phenomenon has been confirmed in several types of coupled systems, and has been shown to survive, and in some cases to be enhanced, under the influence of noise or partial coupling [3].

Global coupling can correspond in some cases to the actual physics of the system [4,5], but in many cases is introduced as a simplifying limit (a mean field approach) to local couplings, which are usually diffusive. One aspect of this use of GCMs that is not satisfactory is the fact that, even though under local dynamics information takes time to travel though the lattice, in the globally coupled limit all effects are always instantaneous. As an approximate way of considering the unavoidable delay effects that appear in locally coupled systems, we have studied the behavior of GCMs under both delay and averaging (in time) of the mean field. Two examples are chosen here. One is Kaneko's original model of a globally coupled lattice of logistic maps [2], a system with the following equations:

$$x_{n+1}(i)=(1-\epsilon)f(x_n(i))+\epsilon h_n,$$
$$h_n\equiv\frac{1}{N}\sum_{j=1}^{N} f(x_n(j)), \quad f(x)=1-ax^2, \tag{1}$$

where $x_n(i)$ is the local variable at location i and iteration n. Here ϵ is the global coupling, and the local map $f(x_n(i))$ is normalized by $1-\epsilon$ so as to avoid getting out of the range $-1\leq x\leq 1$. The other test case is that of a lattice of nonlinear optical elements susceptible of modeling via the Ikeda equations [4,6]

$$E_{n+1}(i)=A+Bf(E_n(i))+\epsilon h_n,$$
$$h_n\equiv\frac{1}{N}\sum_{j=1}^{N} f(E_n(j)), \quad f(E)=E\exp(iE^*E), \tag{2}$$

where now E is complex and represents the amplitude of the slowly varying envelope of the electric field in a nonlinear optical element.

I. DELAY OF THE MEAN FIELD

For both systems, we have studied the effects of delaying the mean field h by changing h_n to h_{n-D} in Eqs. (1) and (2) where D denotes how many iterations h is delayed. We have

*Electronic address: gperez@kin.cieamer.conacyt.mx
†Electronic address: sudeshna@iiap.ernet.in
‡Electronic address: cerdeira@ictp.trieste.it

1063-651X/96/54(6)/6936(4)/$10.00

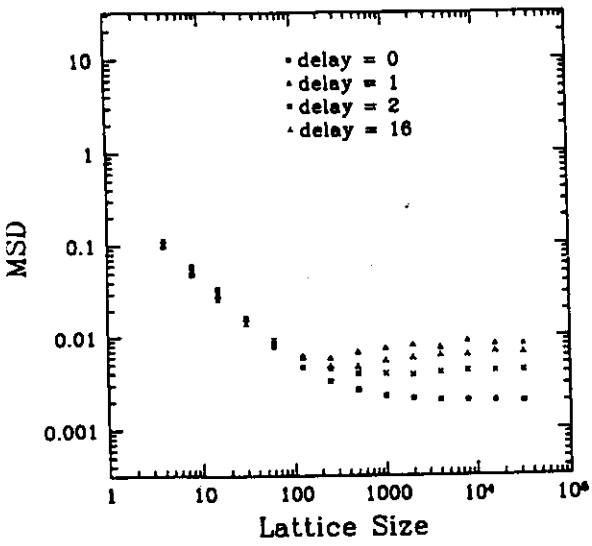

IG. 1. MSD of the mean field vs lattice size for the delayed .tic GCM. Parameters are given in the text. Here we are aver- g over 50 runs of 1024 iterations each, after a transient of 00 iterations. The error levels are of the same size or smaller the markers.

:d values of D from 0 (no delay) up to 17. The param- s used have been $a=1.99$ and $\epsilon=0.1$ for the coupled stic maps of Eqs. (1), and $A=3$, $B=0.3$, and $\epsilon=0.1$ for Ikeda mappings Eqs. (2). (Lattice sizes and running times indicated in the figure captions). The first important find- is that delaying the effects of the mean field does not in case destroy the subtle coherence responsible for the ire of the simplicity hypothesis, and saturation of the D of h as N grows is actually enhanced (see Figs. 1 and This is in itself a nontrivial assertion, since it means that e are memory effects in the dynamics, which allow the ience of past mean fields $h_{n-D}, h_{n-D-1}, h_{n-D-2}, \ldots$,

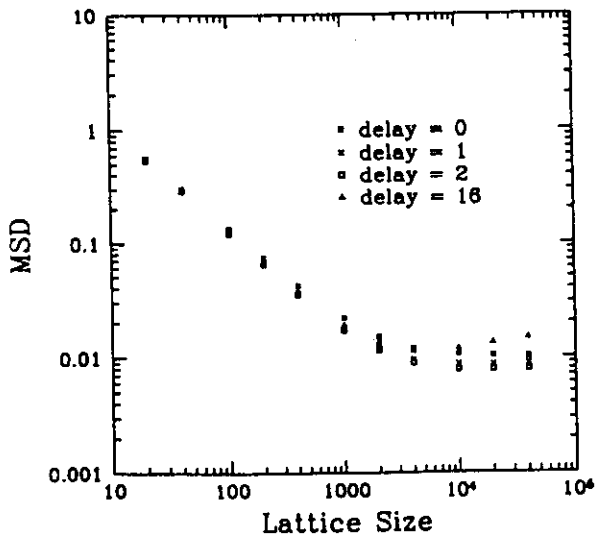

FIG. 2. MSD of the mean field vs lattice size for the delayed la GCM. Parameters are given in the text, and running times are ı Fig. 1. The error levels are of the same size or smaller than the kers.

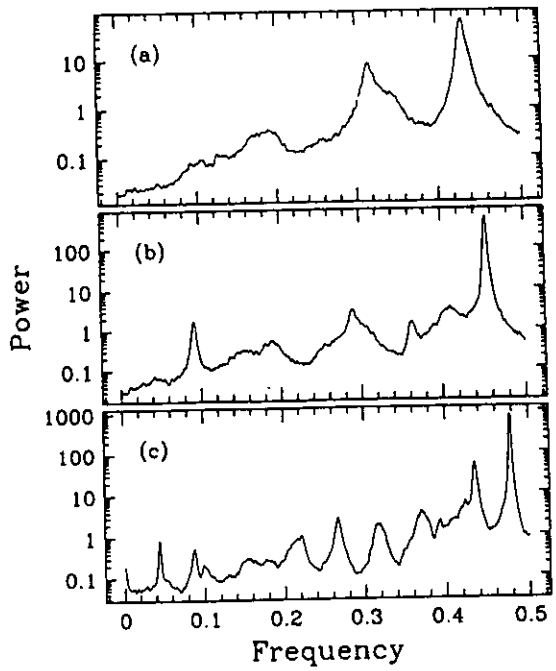

FIG. 3. Power spectra for the mean field of the delayed logistic GCM. The delays are (a) $D=0$ (no delay), (b) $D=4$, and (c) $D=16$. Parameters are given in the text. Here we have performed the Fourier transform over runs of 1024 iterations, and averaged over 50 such runs. The lattice contains 32 000 elements.

to affect the present evolution of the system over a span of D iterations; this for a model where each individual oscillator is losing track of its previous state exponentially fast, due to the existence of positive Lyapunov exponents. In this case, however, the small quasiperiodic fluctuations that affect h for large lattices manage to reproduce themselves even after long delays.

Delaying the mean field does have a clear influence in the form of the quasiperiodicity of the system, as can be seen in the Fourier spectra shown in Figs. 3 and 4. The main effect is an increase in the number of peaks in the spectrum, and a corresponding decrease in their separation. This decrease in separation seems to be linear for the Ikeda mappings [Eqs. (2)], where one can fit the distance between the main peaks in the spectrum (those closest to $\omega=0$) by an approximate formula

$$1/\Delta\omega_D \approx (1/\Delta\omega_0)+\alpha D, \tag{3}$$

where D is the delay, and for the parameters used here, $\Delta\omega_0=0.316\pm0.005$ and $\alpha=1.005\pm0.006$ (i.e., consistent with $\alpha=1$).

For the logistic mappings this particular behavior is not as clear as in the Ikeda system, but estimates made for the largest two peaks in the spectrum (those closest to $\omega=0.5$) show a behavior similar to the one given in Eq. (3), except that we need here to consider odd and even values of D separately. As before, the value found for the constant α is consistent with $\alpha=1$, suggesting an exceedingly simple rule for the accumulation of new peaks in the spectrum: in practice, one gets one new peak for each increase of the delay in one iteration.

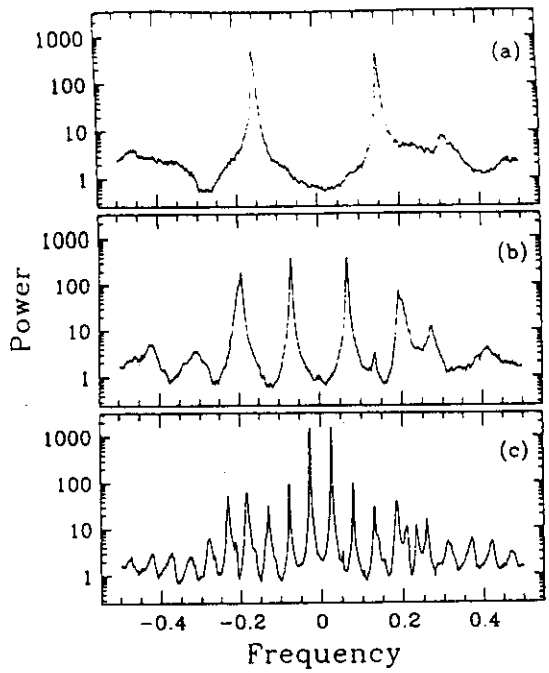

FIG. 4. Power spectra for the mean field of the delayed Ikeda GCM. The delays are (a) $D=0$ (no delay), (b) $D=4$, and (c) $D=16$. Parameters are given in the text. Here we have performed the Fourier transform over runs of 1024 iterations, and averaged over 50 such runs. The lattice contains 40 000 elements.

II. AVERAGING OF THE MEAN FIELD

For both systems, we have studied the averaging of the mean field over a total of P contiguous iterations by changing h_n in Eqs. (1) and (2) to h_n^P where

$$h_n^P \equiv \frac{1}{P}\sum_{j=0}^{P-1} h_{n-j}.$$

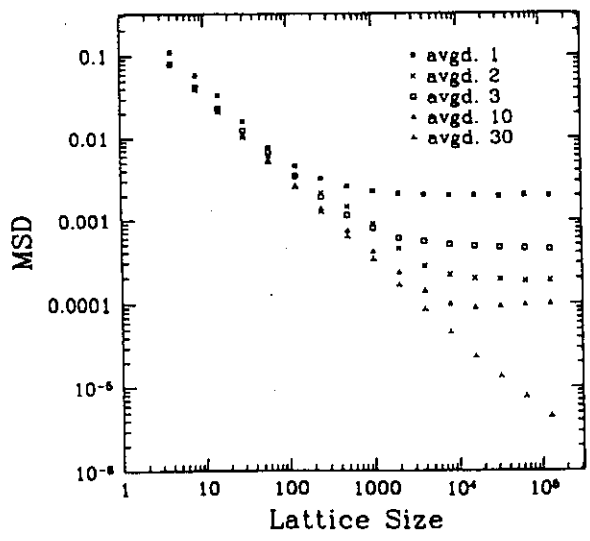

FIG. 5. MSD of the mean field vs lattice size for the averaged logistic GCM. Parameters are given in the text. Here we are averaging over 50 runs of 1024 iterations each, after a transient of 10 000 iterations. The error levels are of the same size or smaller than the markers.

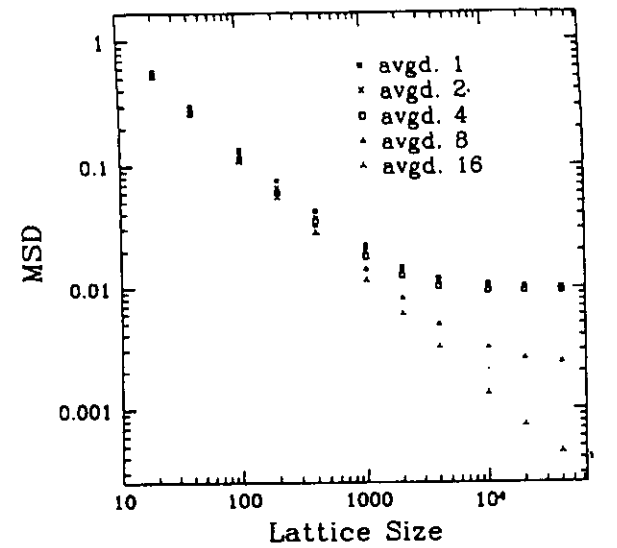

FIG. 6. MSD of the mean field vs lattice size for the averaged Ikeda GCM. Parameters are given in the text, and running times and lattice size are as in Fig. 5. The error levels are of the same size or smaller than the markers.

We have tested values of P up to 30. For this modification of the dynamics one finds, as expected [7], that averaging over several iterations tends to reduce the level of the fluctuations and therefore to render the system closer to statistical. We should notice, however, the following two points: one, the fluctuations in h show robustness, in the sense that, even if it is true that a time average over a few of them reduces the level of saturation of its MSD, it does not restore its statistical behavior. It just increases the value of N where the MSD stops decreasing. Two, the quasiperiodicity of the mean field is still manifest, (see Figs. 5 and 6), and, at least for the case of the Ikeda mappings, show a behavior similar to the one found for delaying: the Fourier spectrum acquires more peaks, and the distance among the two largest of them (the two closest to $\omega=0$) decays linearly, following an approximate rule $1/\Delta\omega_P \approx (1/\Delta\omega_1)+\beta(P-1)$. For the parameters given, we have found $\Delta\omega_1=0.39\pm0.01$ and $\beta=0.554\pm0.008$.

For the logistic mappings, the trend towards multiplicity of peaks and the corresponding decrease in distance between them is visible in the Fourier spectra, but not clearly enough as to be unequivocally quantified.

III. PERIODIC DRIVING

The presence of quasiperiodicity in the mean field for globally coupled maps suggests a test of these systems for possible resonant behavior. For the logistic model, we have done this by changing the action of the mean field h in Eq. (1) to a mixture $\epsilon h_n \rightarrow \alpha h_n + \beta\sin(n\omega)$, with $\epsilon=\alpha+\beta$ (this in order to keep $|x_{n+1}(i)|\leq 1$). We have kept $\epsilon=0.1$, and have checked the behavior of h for two values of α, sweeping over the available ω range. The most important result here is a negative one: we do not find strong resonance in this system, even for the frequencies corresponding to the largest peaks in the nondriven spectrum.

In the first test we have set $\alpha=0.099$ and $\beta=0.001$. Ta

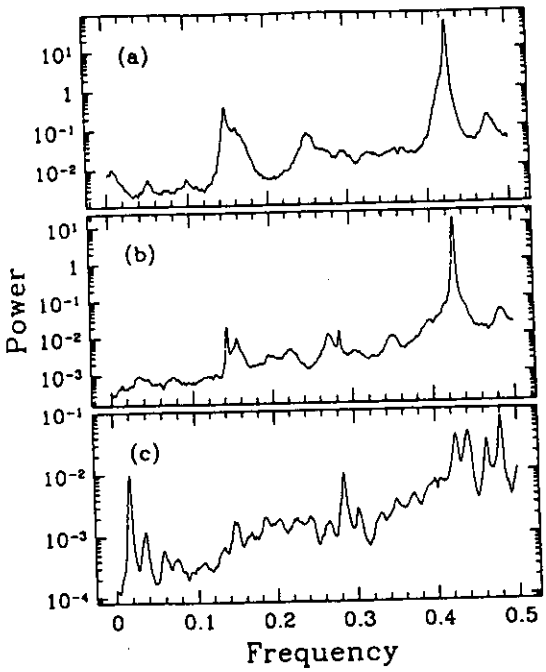

FIG. 7. Power spectra for the mean field of the averaged logistic M. Here we are averaging over (a) $P=3$, (b) $P=10$, and (c) 30 iterations. Parameters are given in the text. We have performed the Fourier transform over runs of 1024 iterations, and averaged over 50 such runs. The lattice contains 128 000 elements.

into account the size of the fluctuations of h for the driven system with the same value of ϵ, we have that in case the autonomous fluctuations should have an amplitude around five times larger than the amplitude of the driving.

For this case, there is essentially no response of the system to the periodic driving. The Fourier spectrum obtained in this case is the same as for the nondriven case, with the addition of an isolated δ spike at the frequency of the driving.

In the second test we have set $\alpha=0.09$ and $\beta=0.01$, which gives an approximated ratio of amplitudes of autonomous to driven fluctuations of 1 to 2, so that in this case the external driving is dominant. In this case we have observed very clear effects of the driving, but not the expected strong resonances at the peak frequencies. Typically, the spectrum shows a somewhat deformed version of the quasiperiodic spectrum from the nondriven case, plus several δ spikes at the frequencies of the driving and its harmonics (including aliased harmonics). In no case have we seen a strong enhancement of the main peaks of the spectrum due to the periodic driving.

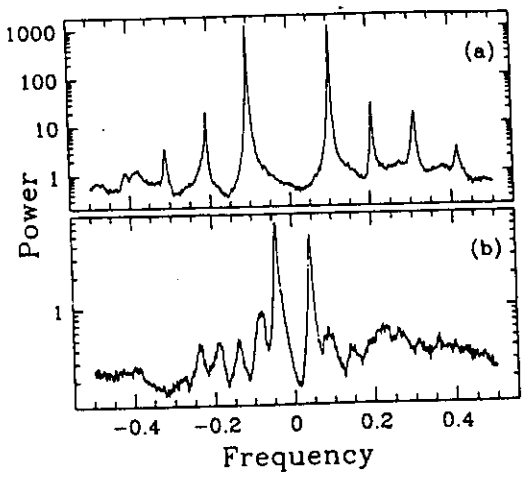

FIG. 8. Power spectra for the mean field of the averaged Ikeda GCM. Here we are averaging over (a) $P=4$ and (b) $P=16$ iterations. Parameters are given in the text. We have performed the Fourier transform over runs of 1024 iterations, and averaged over 50 such runs. The lattice contains 40 000 elements.

Results similar to these were obtained for the Ikeda mappings, showing how the introduction of a very small driving just adds a single spike to the spectrum, with no changes in the quasiperiodic background, and that larger drivings do deform the spectrum and introduce harmonics, but does not create strong resonances. These two results indicate that the quasiperiodicity of the mean field cannot be enhanced by an external driving.

In conclusion, we have found that the use of nonsimultaneous mean fields in globally coupled maps affects the character of their quasiperiodic behavior, increasing linearly the number of peaks in the spectra of their mean fields. The nonstatistical character of these mean fields is preserved, except for the obvious case of time averages over very large spans. Finally, we have not found strong resonance effects in these systems.

G. Perez and S. Sinha thank the ICTP (Trieste), where this work was started, for their hospitality. G. Perez acknowledges support from CONACyT (Mexico), through Grant No. 4178-E9405.

] See, for instance, J. Crutchfield and K. Kaneko, in *Directions in Chaos*, edited by B.-L. Hao (World Scientific, Singapore, 1989); K. Kaneko, Physica D **86**, 158 (1995), and references therein.
] K. Kaneko, Phys. Rev. Lett. **65**, 1391 (1990); Physica D **55**, 368 (1992).
] G. Perez *et al.*, Physica D **63**, 341 (1993); S. Sinha *et al.*, Phys. Rev. A **46**, 6242 (1992); V. Hakim and J. W. Rappel, Europhys. Lett. **27**, 637 (1994).
[4] G. Perez *et al.*, Phys. Rev. A **45**, 5469 (1992).
[5] D. Dominguez and H. A. Cerdeira, Phys. Rev. Lett. **71**, 3359 (1993).
[6] K. Ikeda, Opt. Commun. **30**, 257 (1979); K. Ikeda *et al.*, Phys. Rev. Lett. **45**, 709 (1980); H. Nakatsuoka *et al.*, *ibid.* **50**, 109 (1983).
[7] A. Pikovsky, Phys. Rev. Lett. **71**, 653 (1993).

PHYSICAL REVIEW E VOLUME 49, NUMBER 1 JANUARY 1994

RAPID COMMUNICATIONS

Static parametric fluctuations give nonstatistical behavior in uncoupled chaotic systems

Gabriel Pérez

Departamento de Física Aplicada, Centro de Investigación y de Estudios Avanzados del Instituto Politecnico Nacional, Unidad Mérida, Apartado Postal 73 "Cordemex," 97310 Mérida, Yucatán, Mexico

Hilda A. Cerdeira

International Centre for Theoretical Physics, P. O. Box 586, 34100 Trieste, Italy

(Received 5 October 1993)

We show that an ensemble of logistic maps, with parameters distributed in some range inside a chaotic region, cannot be statistical. This is so because any parameter range for this map includes periodic windows. The effects of this periodicity in the averages of the system can be estimated, and are also apparent in the power spectra of average values. As a counterexample, we show that the behavior for tent maps, where chaotic regions do not include periodic windows, is statistical.

PACS number(s): 05.45.+b, 05.90.+m

I. INTRODUCTION

It was shown in a recent work by Sinha [1] that independent chaotic maps under the influence of global noise behave in a nonstatistical manner. In particular, it was found that when a collection of logistic maps in their chaotic regime has time-dependent but spatially homogeneous fluctuations in its nonlinear parameter, the average value of x shows persistent fluctuations even in the large-N limit. This behavior is similar to that of an ensemble of chaotic maps under weak global coupling, a problem that has been studied in several recent works [2–5].

It was also claimed in that work that when the applied noise is static but space dependent, the behavior of this uncoupled chaotic system is statistical. This means that, for instance, if we have a large collection of logistic maps with their parameters distributed in some narrow range in the chaotic region, the average value of x should converge to some fixed value with fluctuations that die out as $1/\sqrt{N}$. At first sight, this seems quite plausible, since this just reflects the statistical behavior one expects from a collection of independent chaotic oscillators, where each and every one of them is characterized by an invariant probability distribution with finite support. But upon more careful examination one has to realize that there is a failure in this reasoning. This failure lies in the fact that the statistical superposition mentioned before works only if all the mappings included in the parameter region of interest are purely chaotic. By "purely chaotic" we mean here the absence of any periodic behavior, i.e., we exclude cases of the type known as "periodic chaos" [6], where the motion covers in a periodic way a finite collection of distinct chaotic windows.

But it is well known [7] that this is impossible to do with any smooth distribution of parameters in the logistic map, since there is at least a periodic window between any two different points in parameter space where the map is chaotic, and this periodic window (or windows) represents a nonzero fraction of the parameter range. Therefore, as we increase the size of the lattice on which we are working, we will be at the same time maintaining some fraction of the elements moving in a periodic way. And this part of the system will spoil the convergence of the average, by keeping persistent fluctuations whose origin is simply the periodicity of the map in these windows.

In this paper we show that the intrusion of periodic windows does alter the statistical properties of a collection of chaotic maps whose parameters are distributed. We also show that in typical cases this effect is extremely small, thus explaining the results reported in Ref. [1]. We show how this effect depends on the initial configuration of the lattice, and how the effect of periodic windows on the fluctuations of the average can be estimated.

II. UNCOUPLED LOGISTIC MAPS WITH PARAMETRIC NOISE

The model used for this work is

$$x_{n+1}^i = 1 - a^i (x_n^i)^2 , \tag{2.1}$$

where i is the space index and n is the time index. The values of the parameter a are given by

$$a^i = a + \sigma \epsilon^i , \tag{2.2}$$

where ϵ^i is a random number uniformly distributed between -1 and 1, σ is the (small) amplitude of the parameter fluctuations, and a is just the center of the distribution. This is denoted as "case (iii)" in Ref. [1], where a slightly different prescription $a^i = a(1+\sigma'\epsilon^i)$ was used. It is clear that these two prescriptions are identical if one makes $\sigma = a\sigma'$.

In order to test whether or not this system is statistical we calculate the instantaneous mean value h_n of the variable x_n^i, over large size lattices, and study the time evolution of this average. In particular, we check its mean-square deviation (MSD), which is defined by $\langle (\langle h \rangle - h)^2 \rangle$, where the angular brackets are time averages. We also check its power spectrum, which for a su-

1063-651X/94/49(1)/15(4)/$06.00

perposition of purely chaotic systems should be broad.

A comment should be made here about the meaning of these averages. What we want to know here is whether a single lattice, made out of many elements, can be statistical, in the sense that averages over those elements obey the central limit theorem and the law of large numbers. We are not considering the different problem of an ensemble of lattices [8], which depending on the conditions of the problem may or may not be statistical.

Before going over the numerical results, let us try to give an estimate of the size we can expect these effects to have. For this, we can do the following approximation: we can separate the average h_n into two parts. One comes from the points of the lattice where a falls in the purely chaotic region, and another comes from those points with a in a periodic window,

$$h_n = h_n^c + h_n^p \equiv \frac{1}{N} \sum_{a^i \text{ chaotic}} x_n^i + \frac{1}{N} \sum_{a^i \text{ periodic}} x_n^i \,. \tag{2.3}$$

Now, the part that comes from chaotic a will converge towards some fixed value h^* in the infinite lattice limit, with uncorrelated fluctuations ξ_n. These fluctuations will have zero mean and a mean-square deviation that decays as $1/N$ (multiplied by some coefficient of order 1).

For the periodic part we will take into account only the largest periodic window, of periodicity K. At some arbitrarily chosen time $n=0$, after the transients have died, a fraction w_k will have been attracted to the kth point in the cycle, denoted x_k. It is clear that the value x_k changes along the window, and is not even well defined at its end, where the motion is over narrow chaotic strips. However, since for narrow periodic windows these changes are small, we will just approximate the whole interval, including the chaotic strips, by a single representative value of x_k.

With these approximations the value for the periodic part of the average is now

$$h_n^p = \Delta \sum_{k=1}^{K} w_k^n x_k \,, \tag{2.4}$$

where $w_k^n = w_{\langle k-n \rangle \bmod K}$ is the fraction of points in the lattice with value x_k at time n, and Δ is the relative width of the periodic window, assumed to be small. The time average of h is

$$\langle h \rangle = \langle h^c \rangle + \langle h^p \rangle = (1-\Delta) h^* + \frac{\Delta}{K} \sum_{k=1}^{K} x_k \,, \tag{2.5}$$

where the $1/K$ comes from the time average of w_k^n. The mean-square deviation of h becomes

$$\langle (h - \langle h \rangle)^2 \rangle \approx \frac{1}{N} + \Delta^2 \left\langle \left[\sum_{k=1}^{K} \left(w_k - \frac{1}{K} \right) x_k \right]^2 \right\rangle \tag{2.6}$$

$$\approx \frac{1}{N} + \Delta^2 \sum_{i,j=1}^{K} \left(\langle w_i w_j \rangle - \frac{1}{K^2} \right) x_i x_j \,, \tag{2.7}$$

where we are taking $(1-\Delta)^2 \approx 1$. Notice that if one could choose the initial conditions for the lattice so as to cover equally the K basins of attraction of the map f^K, then all the w_k would be equal to $1/K$ and the second term would be zero. Therefore we are considering here an effect that is strongly dependent on the distribution of the initial conditions. In general, if this distribution is homogeneous between some two values—not too close to each other—and covers a good part of the $(-1,1)$ range, there will be small but nonzero deviations from the $1/K$ mean value. This effect is the one that induces persistent fluctuations on the mean values for a lattice of logistic maps.

III. NUMERICAL RESULTS

A. Estimate of nonstatistical effects

To verify what have been said above, we have done a numerical estimate of the size of the effects one may expect in a simulation of a logistic map lattice, in order to see under which conditions we may expect to find them. The first limiting factor here is the relative width of the periodic window, which for typically small cases (say of order 10^{-3}) already makes the possible effects visible only for lattices of 10^6 points or more. Besides this, we also have to check what are the typical values for the fractions w_k for a uniformly distributed set of initial conditions. Our numerical results show that these fractions tend to deviate from the even value $1/K$ by a small amount—of the order of a few percent—for initial conditions with some bias (for instance, x_0^i chosen between 0 and 1), and even for initial conditions distributed homogeneously in the whole $(-1,1)$ range. This adds another factor of 10^{-3}–10^{-4} or smaller to our estimate for the saturation point of the MSD, and means that in typical cases one should not see any nonstatistical effects for lattices of less of 10^9–10^{10} points. This explains the null results found in Ref. [1], where lattices up to 10^4 points were used, and means that in order to see the nonstatistical behavior of these systems in smaller lattices one has to look for some specific conditions, in particular. a parameter range that includes small but still appreciable periodic windows.

In our simulations we have used the parameters $a=1.96$ and $\sigma=0.02$, which gives us a^i in the range 1.94–1.98. This range in parameter space includes a narrow four-window around $a=1.941$, which takes close to $\frac{1}{18}$ of the covered range. We have tested the saturation value given by Eq. (2.7) using an initial distribution with x_0^i between -0.5 and 0.5, which introduces some bias. The results obtained for three different points inside the window—one of them in its chaotic part—were consistent with each other, and the final estimate for the saturation point of the MSD is around 1.5×10^6. The actual values of w_k and x_k for the three tested points are given in Table I.

B. Actual simulation of the lattice

We have simulated the dynamics of this systems on lattices of sizes up to 633 960 points, with the same ranges of a and of initial conditions given above. The first 5000 iterations were discarded as a transient, and the statistics were collected over 50 runs of 1024 iterations each. Since

TABLE I. Values of x for the four cycle, and fractions of initial conditions attracted to them after 5000 iterations. The statistics were compiled over 50 runs, on lattices of 40 000 points. Here we show the results for three different values of a inside the four-window. Errors in the fractions w are all of order 2×10^{-4}.

a	x_1	x_2	x_3	x_4	w_1	w_2	w_3	w_4	Estimated MSD
1.9410	−0.9410	−0.7186	−0.0022	0.9999	0.2506	0.2376	0.2698	0.2420	1.1×10^{-6}
1.9415	−0.9412	−0.7199	−0.0062	0.9999	0.2500	0.2355	0.2740	0.2405	1.6×10^{-6}
1.9425	−0.9425	−0.7255	−0.0225	0.9990	0.2502	0.2315	0.2809	0.2374	2.7×10^{-6}

these effects are sensitive to fluctuations in the distribution of initial conditions, we have repeated the simulation four times, each with a different set of initial conditions. The results of this calculation are given in Fig. 1, which shows the beginning of the saturation of the MSD of h as N grows, and in Fig. 2, which shows the power spectrum of h.

In Fig. 1 we can see that for large n the MSD has deviated strongly for the $1/N$ behavior, and is clearly starting to saturate, with values that approach our previous estimate of 1.5×10^{-6} from above. The bars give the total spread obtained for the four repetitions, i.e., they go from the minimum to the maximum value obtained for the MSD. As a comparison (and control, in order to test that this effect is not just some roundoff effect from the computer), we are including the results from the same calculations performed on lattices of tent maps,

$$x_{n+1}^{i}=1-a^{i}|x_n^{i}|\ , \tag{3.1}$$

using exactly the same parameters and run times as in the logistic case. This system is expected to show perfectly good statistical behavior in this case, because it does not have any periodic windows in the range of a considered; the tent map is purely chaotic for all values of a in the range 1.94–1.98. In the figure we see that the behavior of the MSD for tent map lattices is perfectly statistical, following the $1/N$ law. We have not included spread bars for these points since here the spreads are negligible.

In Fig. 2 we have plotted the power spectrum of h for both the logistic and the tent lattices, for $N=633\,960$. The spikes corresponding to the frequencies $\frac{1}{2}$ and $\frac{1}{4}$ are quite evident in the spectrum for the logistic map. They arise from the periodic part of the mean field, h^p, and include contributions from the purely periodic part (fundamental and subharmonics), and the periodically chaotic [6] final part of the window. The noisy background is formed by the purely chaotic part of the mean field, h^c, which comes from most of the included range in a, with some contribution from the periodically chaotic segment. Notice that periodic chaos contributes to both types of spectrum; in fact, the typical power spectrum of this kind of motion is quite similar to that shown in Fig. 2. The origins of these two are different, however. In "periodic chaos" one single degree of freedom hops periodically from one chaotic window to another. In the present situation, we are thinking about the addition of many degrees of freedom. The average we perform in getting the mean field h reduces the power of the spectrum of h^c for nonzero frequencies, while maintaining the (relatively weak) component h^p.

We should mention that periodic spikes are visible even for much smaller lattices, and appear in power spectra well before saturation of the MSD. For comparison, we also plot the power spectrum for the mean value for a lattice of tent maps. It is evident that there is no periodicity at all in this case.

IV. CONCLUSIONS

We have shown that nonstatistical behavior appears for lattices of uncoupled chaotic maps when these maps are subject to static parametric fluctuations. This effect is due to the intrusion of periodic windows in the chaotic parameter sector, which makes it impossible to say that a given parameter range is purely chaotic. The magnitude

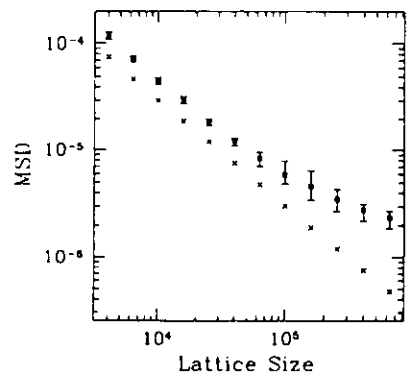

FIG. 1. Mean-square deviation for the lattice average h vs lattice size. The squares correspond to lattices of logistic maps, and the bars show the spread of the MSD. The expected saturation value for the MSD is around 1.5×10^{-6}. The crosses correspond to lattices of tent maps, whose MSD does not saturate.

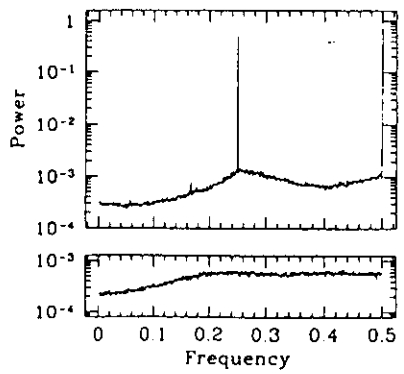

FIG. 2. Power spectrum of the lattice average h for lattices of logistic maps (top), and tent maps (bottom). The vertical scale is the same for both figures.

of this effect can be calculated, and the results from actual simulations agree with other estimates. These effects disappear in cases where it is possible to set a parameter range where the evolution of the maps is purely chaotic, and in the case of the tent map. (Notice that tent maps were used in Ref. [8].)

This nonstatistical behavior is manifested in the saturation of the MSD of the average h as the lattice size N grows, and in the appearance of sharp spikes in the power spectrum of h. However, for most typical cases, the saturation values for the MSD of the average h are so small that they affect only extremely large lattices. Also, the effect is quite sensitive to the distribution one chooses for the initial conditions in the lattice. In principle, it may even be possible to produce a distribution of initial conditions that cancels the effects of at least the largest periodic window, and makes the system behave statistically for even larger sizes of the lattice.

The situation with the power spectrum is different. The spikes that signal periodicity in the lattice appear even for small lattice sizes, even though their behavior becomes consistent only as N grows. For large lattices, one can observe very clearly the effect of the periodic windows on the evolution of the average. The signals coming from the whole window contribute to this periodic effect, including the subharmonics and the periodic chaos. The noisy background comes mainly from the mappings outside the periodic window, with some contributions from the periodic chaos section inside.

This is a very simple model, whose nonstatistical behavior is easy to understand, so much so that it can be estimated beforehand. We believe, however, that there has to be a connection with the more complex but similar phenomena one finds in the case of globally coupled chaotic mappings. (A review is given in Ref. [9].) Both of them show saturation of the MSD, peaks in the power spectrum (broad in the coupled case), and in both cases the nonstatistical effects disappear for the continuously chaotic examples of the tent map. In the uncoupled case the explanation of this fact is simple; with no periodic windows one gets invariant distributions for any values of a, which gives finally simple statistical behavior. For the coupled case the connection between continuous (in parameter space) chaos and statistical behavior has been only postulated and discussed within a static approximation [10], but still the similarity between the two modes seems to imply a deeper connection.

ACKNOWLEDGMENTS

G. P. wants to thank the International Centre for Theoretical Physics, where this work was started, for their hospitality. We thank Daniel Dominguez for many enlightening discussions.

[1] S. Sinha, Phys. Rev. Lett. **69**, 3306 (1992).

[2] K. Kaneko, Phys. Rev. Lett. **65**, 1391 (1990); Physica D **55**, 368 (1992).

[3] G. Perez, S. Sinha, and H. Cerdeira, Physica D **63**, 341 (1993); G. Perez, C. Pando-Lambruschini, S. Sinha, and H. A. Cerdeira, Phys. Rev. A **45**, 5469 (1992).

[4] S. Sinha, D. Biswas, M. Azam, and S. V. Lawande, Phys. Rev. A **46**, 6243 (1992); **46**, 3193 (1992).

[5] H. Chaté and P. Manneville, Europhys. Lett. **14**, 409 (1991); **17**, 291 (1992); J. Hemmingsson, Jülich Report No. HLRZ 85/91, 1991 (unpublished); J. A. C. Gallas, P. Grassberger, H. J. Herrmann, and P. Ueberholz, Physica A **180**, 19 (1992); P.-M. Binder, B. Buck, and V. A. Macaulay, J. Stat. Phys. **68**, (1992); P.-M. Binder and V. Privman, Oxford Report No. OUTP 92-08S, 1992 (unpublished).

[6] S. Thomae and S. Grossmann, J. Stat. Phys. **26**, 485 (1981); S. Grossmann and S. Thomae, Z. Naturforsch. **32a**, 1353 (1977).

[7] P. Collet and J. P. Eckmann, *Iterated Maps on the Interval as Dynamical Systems* (Birkhaüser, Boston, 1980).

[8] A. S. Pikovsky, Phys. Rev. Lett. **71**, 653 (1993).

[9] G. Perez, in *Proceedings of the Adriatico Research Conference "Mesoscopic Systems and Chaos, a Novel Approach"* (World Scientific, Singapore, in press).

[10] G. Perez and H. A. Cerdeira, Phys. Rev. A **46**, 7492 (1992).

PHYSICAL REVIEW E VOLUME 49, NUMBER 1 JANUARY 1994

RAPID COMMUNICATIONS

Static parametric fluctuations give nonstatistical behavior in uncoupled chaotic systems

Gabriel Pérez

Departamento de Física Aplicada, Centro de Investigación y de Estudios Avanzados del Instituto Politecnico Nacional, Unidad Mérida, Apartado Postal 73 "Cordemex," 97310 Mérida, Yucatán, Mexico

Hilda A. Cerdeira

International Centre for Theoretical Physics, P. O. Box 586, 34100 Trieste, Italy

(Received 5 October 1993)

We show that an ensemble of logistic maps, with parameters distributed in some range inside a chaotic region, cannot be statistical. This is so because any parameter range for this map includes periodic windows. The effects of this periodicity in the averages of the system can be estimated, and are also apparent in the power spectra of average values. As a counterexample, we show that the behavior for tent maps, where chaotic regions do not include periodic windows, is statistical.

PACS number(s): 05.45.+b, 05.90.+m

I. INTRODUCTION

It was shown in a recent work by Sinha [1] that independent chaotic maps under the influence of global noise behave in a nonstatistical manner. In particular, it was found that when a collection of logistic maps in their chaotic regime has time-dependent but spatially homogeneous fluctuations in its nonlinear parameter, the average value of x shows persistent fluctuations even in the large-N limit. This behavior is similar to that of an ensemble of chaotic maps under weak global coupling, a problem that has been studied in several recent works [2–5].

It was also claimed in that work that when the applied noise is static but space dependent, the behavior of this uncoupled chaotic system is statistical. This means that, for instance, if we have a large collection of logistic maps with their parameters distributed in some narrow range in the chaotic region, the average value of x should converge to some fixed value with fluctuations that die out as $1/\sqrt{N}$. At first sight, this seems quite plausible, since this just reflects the statistical behavior one expects from a collection of independent chaotic oscillators, where each and every one of them is characterized by an invariant probability distribution with finite support. But upon more careful examination one has to realize that there is a failure in this reasoning. This failure lies in the fact that the statistical superposition mentioned before works only if all the mappings included in the parameter region of interest are purely chaotic. By "purely chaotic" we mean here the absence of any periodic behavior, i.e., we exclude cases of the type known as "periodic chaos" [6], where the motion covers in a periodic way a finite collection of distinct chaotic windows.

But it is well known [7] that this is impossible to do with any smooth distribution of parameters in the logistic map, since there is at least a periodic window between any two different points in parameter space where the map is chaotic, and this periodic window (or windows) represents a nonzero fraction of the parameter range. Therefore, as we increase the size of the lattice on which we are working, we will be at the same time maintaining some fraction of the elements moving in a periodic way. And this part of the system will spoil the convergence of the average, by keeping persistent fluctuations whose origin is simply the periodicity of the map in these windows.

In this paper we show that the intrusion of periodic windows does alter the statistical properties of a collection of chaotic maps whose parameters are distributed. We also show that in typical cases this effect is extremely small, thus explaining the results reported in Ref. [1]. We show how this effect depends on the initial configuration of the lattice, and how the effect of periodic windows on the fluctuations of the average can be estimated.

II. UNCOUPLED LOGISTIC MAPS WITH PARAMETRIC NOISE

The model used for this work is

$$x_{n+1}^i = 1 - a^i (x_n^i)^2 , \tag{2.1}$$

where i is the space index and n is the time index. The values of the parameter a are given by

$$a^i = a + \sigma \epsilon^i , \tag{2.2}$$

where ϵ^i is a random number uniformly distributed between -1 and 1, σ is the (small) amplitude of the parameter fluctuations, and a is just the center of the distribution. This is denoted as "case (iii)" in Ref. [1], where a slightly different prescription $a^i = a(1+\sigma'\epsilon^i)$ was used. It is clear that these two prescriptions are identical if one makes $\sigma = a\sigma'$.

In order to test whether or not this system is statistical we calculate the instantaneous mean value h_n of the variable x_n^i, over large size lattices, and study the time evolution of this average. In particular, we check its mean-square deviation (MSD), which is defined by $\langle (\langle h \rangle - h)^2 \rangle$, where the angular brackets are time averages. We also check its power spectrum, which for a su-

1063-651X/94/49(1)/15(4)/$06.00

perposition of purely chaotic systems should be broad.

A comment should be made here about the meaning of these averages. What we want to know here is whether a single lattice, made out of many elements, can be statistical, in the sense that averages over those elements obey the central limit theorem and the law of large numbers. We are not considering the different problem of an ensemble of lattices [8], which depending on the conditions of the problem may or may not be statistical.

Before going over the numerical results, let us try to give an estimate of the size we can expect these effects to have. For this, we can do the following approximation: we can separate the average h_n into two parts. One comes from the points of the lattice where a falls in the purely chaotic region, and another comes from those points with a in a periodic window,

$$h_n = h_n^c + h_n^p \equiv \frac{1}{N} \sum_{a^i \text{ chaotic}} x_n^i + \frac{1}{N} \sum_{a^i \text{ periodic}} x_n^i \ . \tag{2.3}$$

Now, the part that comes from chaotic a will converge towards some fixed value h^* in the infinite lattice limit, with uncorrelated fluctuations ξ_n. These fluctuations will have zero mean and a mean-square deviation that decays as $1/N$ (multiplied by some coefficient of order 1).

For the periodic part we will take into account only the largest periodic window, of periodicity K. At some arbitrarily chosen time $n=0$, after the transients have died, a fraction w_k will have been attracted to the kth point in the cycle, denoted x_k. It is clear that the value x_k changes along the window, and is not even well defined at its end, where the motion is over narrow chaotic strips. However, since for narrow periodic windows these changes are small, we will just approximate the whole interval, including the chaotic strips, by a single representative value of x_k.

With these approximations the value for the periodic part of the average is now

$$h_n^p = \Delta \sum_{k=1}^{K} w_k^n x_k \ , \tag{2.4}$$

where $w_k^n = w_{(k-n) \bmod K}$ is the fraction of points in the lattice with value x_k at time n, and Δ is the relative width of the periodic window, assumed to be small. The time average of h is

$$\langle h \rangle = \langle h^c \rangle + \langle h^p \rangle = (1-\Delta) h^* + \frac{\Delta}{K} \sum_{k=1}^{K} x_k \ , \tag{2.5}$$

where the $1/K$ comes from the time average of w_k^n. The mean-square deviation of h becomes

$$\langle (h - \langle h \rangle)^2 \rangle \approx \frac{1}{N} + \Delta^2 \left\langle \left[\sum_{k=1}^{K} \left(w_k - \frac{1}{K} \right) x_k \right]^2 \right\rangle \tag{2.6}$$

$$\approx \frac{1}{N} + \Delta^2 \sum_{i,j=1}^{K} \left(\langle w_i w_j \rangle - \frac{1}{K^2} \right) x_i x_j \ , \tag{2.7}$$

where we are taking $(1-\Delta)^2 \approx 1$. Notice that if one could choose the initial conditions for the lattice so as to cover equally the K basins of attraction of the map f^K, then all the w_k would be equal to $1/K$ and the second term would be zero. Therefore we are considering here an effect that is strongly dependent on the distribution of the initial conditions. In general, if this distribution is homogeneous between some two values—not too close to each other—and covers a good part of the $(-1,1)$ range, there will be small but nonzero deviations from the $1/K$ mean value. This effect is the one that induces persistent fluctuations on the mean values for a lattice of logistic maps.

III. NUMERICAL RESULTS

A. Estimate of nonstatistical effects

To verify what have been said above, we have done a numerical estimate of the size of the effects one may expect in a simulation of a logistic map lattice, in order to see under which conditions we may expect to find them. The first limiting factor here is the relative width of the periodic window, which for typically small cases (say of order 10^{-3}) already makes the possible effects visible only for lattices of 10^6 points or more. Besides this, we also have to check what are the typical values for the fractions w_k for a uniformly distributed set of initial conditions. Our numerical results show that these fractions tend to deviate from the even value $1/K$ by a small amount—of the order of a few percent—for initial conditions with some bias (for instance, x_0^i chosen between 0 and 1), and even for initial conditions distributed homogeneously in the whole $(-1,1)$ range. This adds another factor of 10^{-3}–10^{-4} or smaller to our estimate for the saturation point of the MSD, and means that in typical cases one should not see any nonstatistical effects for lattices of less of 10^9–10^{10} points. This explains the null results found in Ref. [1], where lattices up to 10^4 points were used, and means that in order to see the nonstatistical behavior of these systems in smaller lattices one has to look for some specific conditions, in particular, a parameter range that includes small but still appreciable periodic windows.

In our simulations we have used the parameters $a=1.96$ and $\sigma=0.02$, which gives us a^i in the range 1.94–1.98. This range in parameter space includes a narrow four-window around $a=1.941$, which takes close to $\frac{1}{18}$ of the covered range. We have tested the saturation value given by Eq. (2.7) using an initial distribution with x_0^i between -0.5 and 0.5, which introduces some bias. The results obtained for three different points inside the window—one of them in its chaotic part—were consistent with each other, and the final estimate for the saturation point of the MSD is around 1.5×10^6. The actual values of w_k and x_k for the three tested points are given in Table I.

B. Actual simulation of the lattice

We have simulated the dynamics of this systems on lattices of sizes up to 633 960 points, with the same ranges of a and of initial conditions given above. The first 5000 iterations were discarded as a transient, and the statistics were collected over 50 runs of 1024 iterations each. Since

TABLE I. Values of x for the four cycle, and fractions of initial conditions attracted to them after 5000 iterations. The statistics were compiled over 50 runs, on lattices of 40 000 points. Here we show the results for three different values of a inside the four-window. Errors in the fractions w are all of order 2×10^{-4}.

a	x_1	x_2	x_3	x_4	w_1	w_2	w_3	w_4	Estimated MSD
1.9410	−0.9410	−0.7186	−0.0022	0.9999	0.2506	0.2376	0.2698	0.2420	1.1×10^{-6}
1.9415	−0.9412	−0.7199	−0.0062	0.9999	0.2500	0.2355	0.2740	0.2405	1.6×10^{-6}
1.9425	−0.9425	−0.7255	−0.0225	0.9990	0.2502	0.2315	0.2809	0.2374	2.7×10^{-6}

these effects are sensitive to fluctuations in the distribution of initial conditions, we have repeated the simulation four times, each with a different set of initial conditions. The results of this calculation are given in Fig. 1, which shows the beginning of the saturation of the MSD of h as N grows, and in Fig. 2, which shows the power spectrum of h.

In Fig. 1 we can see that for large n the MSD has deviated strongly for the $1/N$ behavior, and is clearly starting to saturate, with values that approach our previous estimate of 1.5×10^{-6} from above. The bars give the total spread obtained for the four repetitions, i.e., they go from the minimum to the maximum value obtained for the MSD. As a comparison (and control, in order to test that this effect is not just some roundoff effect from the computer), we are including the results from the same calculations performed on lattices of tent maps,

$$x^i_{n+1}=1-a^i|x^i_n|\ , \tag{3.1}$$

using exactly the same parameters and run times as in the logistic case. This system is expected to show perfectly good statistical behavior in this case, because it does not have any periodic windows in the range of a considered; the tent map is purely chaotic for all values of a in the range 1.94–1.98. In the figure we see that the behavior of the MSD for tent map lattices is perfectly statistical, following the $1/N$ law. We have not included spread bars for these points since here the spreads are negligible.

In Fig. 2 we have plotted the power spectrum of h for both the logistic and the tent lattices, for $N=633\,960$. The spikes corresponding to the frequencies $\frac{1}{2}$ and $\frac{1}{4}$ are quite evident in the spectrum for the logistic map. They arise from the periodic part of the mean field, h^p, and include contributions from the purely periodic part (fundamental and subharmonics), and the periodically chaotic [6] final part of the window. The noisy background is formed by the purely chaotic part of the mean field, h^c, which comes from most of the included range in a, with some contribution from the periodically chaotic segment. Notice that periodic chaos contributes to both types of spectrum; in fact, the typical power spectrum of this kind of motion is quite similar to that shown in Fig. 2. The origins of these two are different, however. In "periodic chaos" one single degree of freedom hops periodically from one chaotic window to another. In the present situation, we are thinking about the addition of many degrees of freedom. The average we perform in getting the mean field h reduces the power of the spectrum of h^c for nonzero frequencies, while maintaining the (relatively weak) component h^p.

We should mention that periodic spikes are visible even for much smaller lattices, and appear in power spectra well before saturation of the MSD. For comparison, we also plot the power spectrum for the mean value for a lattice of tent maps. It is evident that there is no periodicity at all in this case.

IV. CONCLUSIONS

We have shown that nonstatistical behavior appears for lattices of uncoupled chaotic maps when these maps are subject to static parametric fluctuations. This effect is due to the intrusion of periodic windows in the chaotic parameter sector, which makes it impossible to say that a given parameter range is purely chaotic. The magnitude

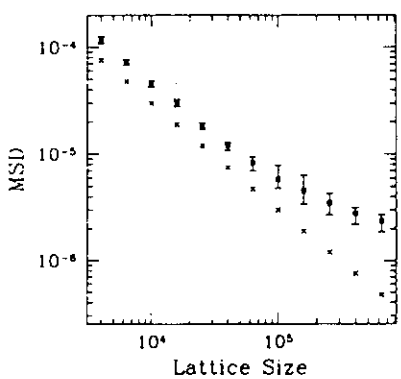

FIG. 1. Mean-square deviation for the lattice average h vs lattice size. The squares correspond to lattices of logistic maps, and the bars show the spread of the MSD. The expected saturation value for the MSD is around 1.5×10^{-6}. The crosses correspond to lattices of tent maps, whose MSD does not saturate.

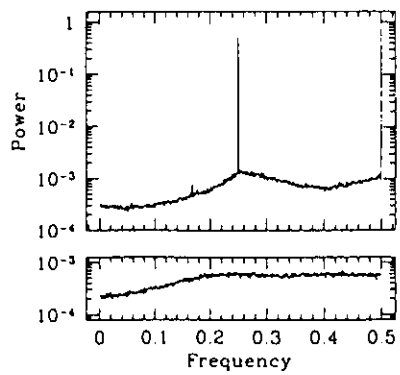

FIG. 2. Power spectrum of the lattice average h for lattices of logistic maps (top), and tent maps (bottom). The vertical scale is the same for both figures.

of this effect can be calculated, and the results from actual simulations agree with other estimates. These effects disappear in cases where it is possible to set a parameter range where the evolution of the maps is purely chaotic, and in the case of the tent map. (Notice that tent maps were used in Ref. [8].)

This nonstatistical behavior is manifested in the saturation of the MSD of the average h as the lattice size N grows, and in the appearance of sharp spikes in the power spectrum of h. However, for most typical cases, the saturation values for the MSD of the average h are so small that they affect only extremely large lattices. Also, the effect is quite sensitive to the distribution one chooses for the initial conditions in the lattice. In principle, it may even be possible to produce a distribution of initial conditions that cancels the effects of at least the largest periodic window, and makes the system behave statistically for even larger sizes of the lattice.

The situation with the power spectrum is different. The spikes that signal periodicity in the lattice appear even for small lattice sizes, even though their behavior becomes consistent only as N grows. For large lattices, one can observe very clearly the effect of the periodic windows on the evolution of the average. The signals coming from the whole window contribute to this periodic effect, including the subharmonics and the periodic chaos. The noisy background comes mainly from the mappings outside the periodic window, with some contributions from the periodic chaos section inside.

This is a very simple model, whose nonstatistical behavior is easy to understand, so much so that it can be estimated beforehand. We believe, however, that there has to be a connection with the more complex but similar phenomena one finds in the case of globally coupled chaotic mappings. (A review is given in Ref. [9].) Both of them show saturation of the MSD, peaks in the power spectrum (broad in the coupled case), and in both cases the nonstatistical effects disappear for the continuously chaotic examples of the tent map. In the uncoupled case the explanation of this fact is simple; with no periodic windows one gets invariant distributions for any values of a, which gives finally simple statistical behavior. For the coupled case the connection between continuous (in parameter space) chaos and statistical behavior has been only postulated and discussed within a static approximation [10], but still the similarity between the two modes seems to imply a deeper connection.

ACKNOWLEDGMENTS

G. P. wants to thank the International Centre for Theoretical Physics, where this work was started, for their hospitality. We thank Daniel Dominguez for many enlightening discussions.

[1] S. Sinha, Phys. Rev. Lett. **69**, 3306 (1992).

[2] K. Kaneko, Phys. Rev. Lett. **65**, 1391 (1990); Physica D **55**, 368 (1992).

[3] G. Perez, S. Sinha, and H. Cerdeira, Physica D **63**, 341 (1993); G. Perez, C. Pando-Lambruschini, S. Sinha, and H. A. Cerdeira, Phys. Rev. A **45**, 5469 (1992).

[4] S. Sinha, D. Biswas, M. Azam, and S. V. Lawande, Phys. Rev. A **46**, 6243 (1992); **46**, 3193 (1992).

[5] H. Chaté and P. Manneville, Europhys. Lett. **14**, 409 (1991); **17**, 291 (1992); J. Hemmingsson, Jülich Report No. HLRZ 85/91, 1991 (unpublished); J. A. C. Gallas, P. Grassberger, H. J. Herrmann, and P. Ueberholz, Physica A **180**, 19 (1992); P.-M. Binder, B. Buck, and V. A. Macaulay, J. Stat. Phys. **68**, (1992); P.-M. Binder and V. Privman, Oxford Report No. OUTP 92-08S, 1992 (unpublished).

[6] S. Thomae and S. Grossmann, J. Stat. Phys. **26**, 485 (1981); S. Grossmann and S. Thomae, Z. Naturforsch. **32a**, 1353 (1977).

[7] P. Collet and J. P. Eckmann, *Iterated Maps on the Interval as Dynamical Systems* (Birkhaüser, Boston, 1980).

[8] A. S. Pikovsky, Phys. Rev. Lett. **71**, 653 (1993).

[9] G. Perez, in *Proceedings of the Adriatico Research Conference "Mesoscopic Systems and Chaos, a Novel Approach"* (World Scientific, Singapore, in press).

[10] G. Perez and H. A. Cerdeira, Phys. Rev. A **46**, 7492 (1992).

Order and Turbulence in rf-Driven Josephson Junction Series Arrays

Daniel Domínguez and Hilda A. Cerdeira*
International Centre for Theoretical Physics, P.O. Box 586, Miramare, 34100 Trieste, Italy
(Received 20 May 1993)

We study underdamped Josephson junction series arrays that are globally coupled through a resistive shunting load and driven by an rf bias current. We find coherent, ordered, partially ordered, and turbulent regimes in the I-V characteristics. The ordered regime corresponds to giant Shapiro steps. In the turbulent regime there is a saturation of the broadband noise for a large number of junctions. This corresponds to a breaking of the law of large numbers already seen in globally coupled maps. Coexisting with this, we find an emergence of novel pseudosteps in the I-V characteristics.

PACS numbers: 74.50.+r, 05.45.+b, 74.40.+k, 85.25.Cp

The dynamics of rf-driven Josephson junction arrays has been of great interest in recent years, both experimentally [1] and theoretically [2]. Much of the interest has concentrated in the study of giant Shapiro steps in two-dimensional arrays [1,2]. Also one-dimensional series arrays, but with a dc current drive, have been extensively studied when the junctions are globally coupled through an external shunting load [3,4]. Some investigations of chaos and turbulence on two-dimensional Josephson junction arrays, but where there is a locally coupled dynamics, have also been done recently [5]. Apart from being a realization of nonlinear dynamical systems with many degrees of freedom, Josephson junction arrays are devices that have potential applications as high frequency coherent power sources [6,7], parametric amplifiers, and voltage standards [6].

Here we study one-dimensional Josephson junction series arrays (JJSA) when they are driven by an *rf bias current*. It has been shown that underdamped, rf-driven, single Josephson junctions show chaotic behavior [8,9]. When these junctions are globally coupled in a JJSA, two conflicting trends will be present: destruction of coherence due to the chaotic divergences of the individual junctions, and synchronization through the global averaging of the common shunting load. This interplay between temporal chaos and space synchronization has been studied recently in globally coupled logistic maps (GCM) [10–13]. These systems exhibit coherent, ordered, partially ordered, and turbulent phases [10]. In particular, a surprising result was found by Kaneko [11]: in the turbulent phase, where spatial coherence is completely destroyed, a subtle collective behavior emerges. This was seen as a violation of the law of large numbers as a function of the number of logistic maps. In this paper, we show that the same kinds of phenomena exist in rf-driven underdamped JJSA. Moreover, we find that whenever the JJSA shows a breaking of the law of large numbers, novel pseudo-Shapiro steps emerge in the I-V characteristics of the JJSA. This last effect is a new result which does not result directly from the previously known phenomena in GCM.

We consider an underdamped JJSA shunted by a resistive load, and subjected to an rf bias current $I_B(t) = I_{dc} + I_{rf}\sin(\omega_{rf}t)$ [14]. The dynamical behavior of Josephson junctions is commonly described with the resistively shunted junction model [15]. With this model, the governing equations of the JJSA [3] are

$$\ddot{\phi}_k + g\dot{\phi}_k + \sin\phi_k + i_L = i_{dc} + i_{rf}\sin(\Omega_{rf}\tau)\,, \qquad (1)$$

$$i_L = \sigma v(\tau) = \frac{\sigma}{N}\sum_{j=1}^{N} g\dot{\phi}_j\,, \qquad (2)$$

where ϕ_k is the superconducting phase difference across the junction k, and $k = 1,\ldots,N$. We use reduced units, with currents normalized by the critical current, $i = I/I_c$; time normalized by the plasma frequency $\omega_p t = \tau$, with $\omega_p = \sqrt{2eI_c/\hbar C}$ and C the capacitance of the junctions; and voltages by rI_c, with r the shunt resistance of the junctions. Here, i_L is the current flowing through the resistive load; $g = (\frac{\hbar}{2eCr^2I_c})^{1/2} = 1/\beta_c^{1/2}$, with β_c the McCumber parameter [15]; $v = V_{total}/N$ is the total voltage across the array per junction; $\sigma = \frac{rN}{R}$, with R the resistance of the shunting load, represents the strength of the global coupling in the array; and the normalized rf frequency is $\Omega_{rf} = \omega_{rf}/\omega_p$. Equation (1) represents current conservation, and Eq. (2) comes from requiring the total voltage across the array equal to the voltage across the load.

The simplest attractor of the system is the coherent state for which $\phi_k(\tau) = \phi_j(\tau) = \phi_0(\tau)$. In this case the equations reduce to

$$\ddot{\phi}_0 + \tilde{g}\dot{\phi}_0 + \sin\phi_0 = i_{dc} + i_{rf}\sin(\Omega_{rf}\tau)\,, \qquad (3)$$

with $\tilde{g} = g(1+\sigma)$. This corresponds to the dynamics of one single Josephson junction. It is known that it can have chaotic behavior in the underdamped regime, i.e., for $\tilde{g} < 2$, and below the plasma frequency, $\Omega_{rf} < 1$ [9]. In this paper we choose $\tilde{g} = 0.2$, $\Omega_{rf} = 0.8$, and $i_{rf} = 0.61$, and we analyze the behavior of the JJSA as a function of i_{dc}, the coupling σ, and the number of junctions, N. We work with fixed $\tilde{g}$, instead of g, in order to have the same coherent attractor in all the cases . We integrate the dynamical equations using a fourth order Runge-Kutta method with fixed step $\Delta\tau = T/160$, with $T = 2\pi/\Omega_{rf}$ the period of the rf drive, and we iterate the dynamics for times as long as $1024T$, after discarding the first 256 periods. For some particular cases, we have checked our

0031-9007/93/71(20)/3359(4)$06.00

results with $\Delta\tau = T/320$ and integration time $2048T$. For each run we used different sets of random initial conditions $\{\phi_k(0), \dot{\phi}_k(0)\}$.

One of the responses that can be measured experimentally is the I-V characteristics of the JJSA, which is the time average voltage per junction $\langle v(\tau)\rangle = \bar{v}$ as a function of i_{dc}. When the junctions are rf biased, they show Shapiro steps [8,9,16]. These are regions for which the average voltage is constant and $\bar{v} = \frac{n}{m} g\Omega_{rf}$. They correspond to phase locked states, which are periodic solutions in resonance with the rf current, either harmonic ($m = 1$) or subharmonic ($m > 1$). In other parts of the I-V it is possible to have chaotic solutions, in which the junction switches pseudorandomly between unstable, overlapping Shapiro steps [8,9]. We study the chaotic nature of the solutions by computing the maximum Liapunov exponent λ of the JJSA. Experimentally, most chaotic modes can be observed as broadband noise in the power spectrum of the voltage [8,9]. The power spectrum is computed as $S(\omega) = \frac{2}{T_m}\left|\int_0^{T_m} v(\tau)e^{i\omega\tau}d\tau\right|^2$. In the presence of broadband noise, the low frequency part of the spectrum approaches a constant, $S_0 = \lim_{\omega\to 0} S(\omega)$.

We first analyze the dynamics of one single Josephson junction with the parameters specified above. In Figs. 1(a) and 1(b) we show the I-V characteristics and Liapunov exponent, respectively. We have also computed S_0 (not shown), which essentially correlates with the behavior of λ in this case. We distinguish four different regimes as a function of i_{dc}. (i) There are periodic solutions, with $\lambda < 0$ and $S_0 \to 0$. They appear either below the critical current ($i_{dc} < i_c = 0.036$), where there is no average dissipation $\bar{v} = 0$, or at the Shapiro steps, which in this case are at voltages $\frac{1}{2}g\Omega_{rf}$ ($0.256 < i_{dc} < 0.428$) and $3g\Omega_{rf}$ ($0.476 < i_{dc} < 0.508$). (ii) There are chaotic solutions in the region between i_c and the step at $\frac{1}{2}g\Omega_{rf}$ ($0.036 < i_{dc} < 0.256$), for which $\lambda > 0$, S_0 finite. In this region some periodic "windows" are also seen (notably for voltages $\frac{1}{2}g\Omega_{rf}$ and $\frac{1}{3}g\Omega_{rf}$). (iii) For high currents ($i_{dc} > 0.508$), where there is a linear resistive behavior in the I-V, we find quasiperiodic solutions (also subharmonics with high m are possible here), for which $\lambda \approx 0$, $S_0 \to 0$. (iv) Finally, between the two steps, there is a region ($0.428 < i_{dc} < 0.476$) where either periodic solutions with $\bar{v} = \frac{1}{2}g\Omega_{rf}$, quasiperiodic solutions, or chaotic solutions can exist, depending on the initial conditions. In this region the I-V shows hysteresis. Note that we have deliberately chosen a case with few stable Shapiro steps. For this set of parameters, most of the Shapiro steps are unstable and overlapping, giving place to a wide region of chaotic states.

Now we study the spatiotemporal behavior of JJSA. Also in Figs. 1(a) and 1(b) we show the I-V curve and maximum Liapunov exponent for an array with 128 junctions and coupling $\sigma = 0.2$. With regard to the temporal behavior, we see two main differences with respect to the single junction. The chaotic region (ii) above $i_c = 0.03$ is narrower ($0.03 < i_{dc} < 0.2$), leaving place to periodic solutions corresponding to the Shapiro step at $\bar{v} = \frac{1}{2}g\Omega_{rf}$ ($0.2 < i_{dc} < 0.364$). On the other hand, the region (iv) with hysteresis is wider ($0.364 < i_{dc} < 0.514$), and shows more chaotic solutions than in the single junction case. This region has grown at the expense of part of the $\bar{v} = \frac{1}{2}g\Omega_{rf}$ Shapiro step and the $\bar{v} = 3g\Omega_{rf}$ Shapiro step. We find that this tendency is increased as a function of increasing σ, with the chaotic region (ii) narrowing and the region (iv) expanding in their respective ranges in i_{dc}.

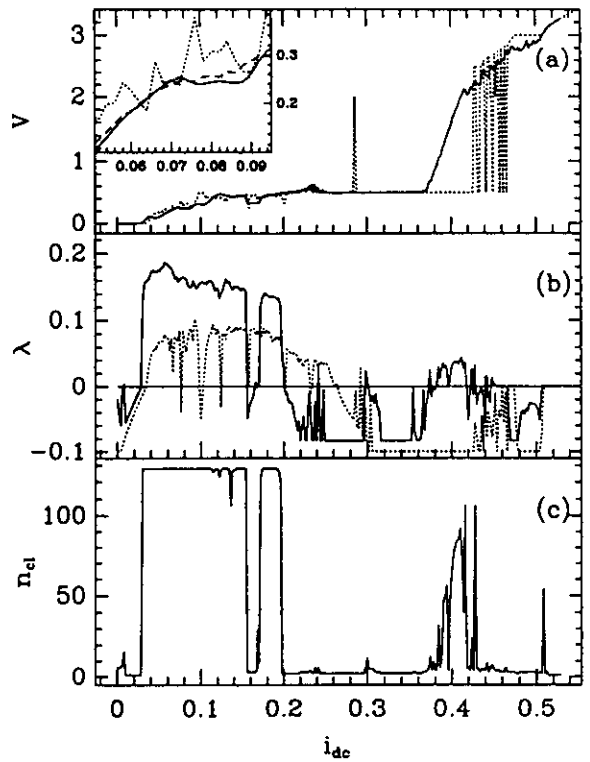

FIG. 1. (a) I-V characteristics for one single Josephson junction with $g = 0.2$, $\Omega_{rf} = 0.8$, $i_{rf} = 0.61$ (dotted line); and for a series array with the same parameters and $N = 128$ junctions with coupling $\sigma = 0.2$ (full line). We have normalized the average voltage as $V = \bar{v}/g\Omega_{rf}$. The inset is a blowup of the I-V curve in the region of low currents, showing the emergence of a pseudostep with increasing N ($N = 1$, dotted line; $N = 16$, dashed line; $N = 128$, full line). (b) Maximum Liapunov exponent λ as a function of i_{dc}. (c) Number of clusters n_{cl} as a function of i_{dc} for the series array with $N = 128$.

To further characterize these regimes in the JJSA, we analyze their spatial behavior. One important concept in globally coupled maps is "clustering" [10]. A cluster is defined as $\phi_i(t) = \phi_j(t)$ for i, j in the same cluster. An attractor can be characterized by the number of clusters it has, n_{cl}, and the number of elements of each cluster $(M_1, M_2, \ldots, M_{n_{cl}})$. For example, the coherent state is a one-cluster attractor ($n_{cl} = 1, M_1 = N$). In Fig. 1(c) we show n_{cl} as a function of i_{dc}, also for $N = 128$, $\sigma = 0.2$. We find different phases, according to their spatial behavior, which are as follows. (a) First,

we find that the coherent attractor only exists either for currents below the critical current ($i_{dc} < i_c = 0.3$, temporally periodic) or for high currents in the resistive regime ($i_{dc} > 0.514$), corresponding to the temporally quasiperiodic region (iii). (b) In the Shapiro step at $\bar{v} = \frac{1}{2}g\Omega_{rf}$ ($0.2 < i_{dc} < 0.364$) there are few clusters, $n_{cl} \ll N$, a behavior that corresponds to the "ordered" phase of GCM [10]. Here, for most of the currents is $n_{cl} = 2$, and in the places where $n_{cl} > 2$ (but $n_{cl} \ll N$) almost all the junctions oscillate in two big clusters ($M_1 \approx N/2, M_2 \approx N/2, M_3 = 1, \ldots, M_{n_{cl}} = 1$). (c) The temporally chaotic region (ii), $0.03 < i_{dc} < 0.2$, has all the phases different, $n_{cl} \sim N$, a behavior that corresponds to the termed "turbulent" phase of GCM [10]. There is also an "ordered" window with $\bar{v} = \frac{1}{3}g\Omega_{rf}$ in the middle of the turbulent phase ($0.156 < i_{dc} < 0.170$), for which $n_{cl} = 3$. In fact, for the different cases we have studied, the ordered phase of JJSA seems to coincide with the Shapiro steps, with the number of big clusters being equal to the order m of the step. (d) The current range above the step of $\frac{1}{2}g\Omega_{rf}$ that corresponds to the region (iv), $0.364 < i_{dc} < 0.514$, even when it can have some temporally chaotic solutions, is clearly different from the turbulent phase in its spatial behavior. It can have (depending on the initial conditions) either attractors with few clusters, $n_{cl} \ll N$, or attractors with many clusters, $n_{cl} \sim N$, but with almost all the junctions concentrated in one or two of these clusters. This regime corresponds to the "partially ordered" or "glassy" phase of GCM [10]. We also find that while λ and S_0 change smoothly as a function of i_{dc} in the turbulent phase, they change wildly in the partially ordered phase.

How does the behavior of the JJSA depend on a function of N? We find that the turbulent phase is the one that shows the most notable changes with increasing N. In fact, we find a nonstatistical behavior for large N, like the one found by Kaneko in GCM [11] as a breaking of the law of large numbers. First of all, let us note that the voltage per junction $v^{(N)}(t) = \frac{1}{N}\sum_{j=1}^{N} g\dot{\phi}_j$ acts as a "mean field" in Eqs. (1) and (2). Since in the turbulent phase the $\phi_j(t)$, and therefore the $\dot{\phi}_j(t)$, take random values almost independently, one might expect that $v(t)$ will behave as an average noise. The power spectrum of $v(t)$ will be

$$S(\omega) = \frac{1}{N}|v_j(\omega)|^2 + \frac{1}{N^2}\left[\sum_{i\neq j} v_i(\omega)v_j^*(\omega)\right], \qquad (4)$$

with $v_j(\omega)$ the Fourier transform of $v_j(t) = g\dot{\phi}_j(t)$. If the $\dot{\phi}_j(t)$ are completly independent, the second term in (4) will vanish for low frequencies, $\omega \to 0$. Therefore $S_0^{(N)} \sim \frac{1}{N}S_0^{(1)}$, with $S_0^{(N)}$ the low frequency part of the power spectrum of a JJSA with N junctions. This is the equivalent of the law of large numbers for a periodically driven system. Then we might expect that in the large N limit the the broadband noise part of $v^{(N)}(t)$ will tend to vanish ($S_0 \to 0$, for $N \to \infty$), reducing the dynamics of the JJSA to N independent chaotic junctions with an additional time periodic driving $v^{(N\to\infty)}(t)$.

In Fig. 2 we show the calculated values of S_0 as a function of N for different values of σ and for $i_{dc} = 0.124$ (similar behavior is also seen for other values of i_{dc} within the turbulent phase). We see that for some values of σ, S_0 follows a $1/N$ behavior. But for some other values of σ, S_0 saturates for large N, indicating that some "order" has emerged in the turbulent phase. This corresponds to the breaking of the law of large numbers found in GCM [11,12]. This also affects the full power spectrum $S(\omega)$, where broad peaks develop for large N in the GCM [11,12]. We have seen the same behavior in the JJSA for the power spectrum of $v(t)$ [17].

We find that this subtle coherence of the turbulent phase notably affects the I-V characteristics of the JSSA in an unexpected way. We find that novel "pseudosteps" emerge in the I-V curve for large N at the same time that S_0 saturates in the turbulent phase. This is detailed in the inset of Fig. 1(a). There we see that, while for $N = 1$ the I-V curve in this region has a "noisy" aspect, when increasing N some pseudosteps tend to appear. Many pseudosteps are present all along the range of i_{dc} corresponding to the turbulent phase, as we show in Fig. 3(a) for $\sigma = 0.4$, $N = 128$. Note that $N = 128$ is a value before the full saturation of S_0, since it is hard to simulate very large N for the full I-V. However, we see that the pseudosteps emerge and sharpen up with increasing N, always in coexistence with a saturation of S_0. On the other hand, in Fig. 3(b), we show the case for $\sigma = 0.1$, for which we do not see a breaking of the law of large numbers. There is no evidence of any pseudosteps in the

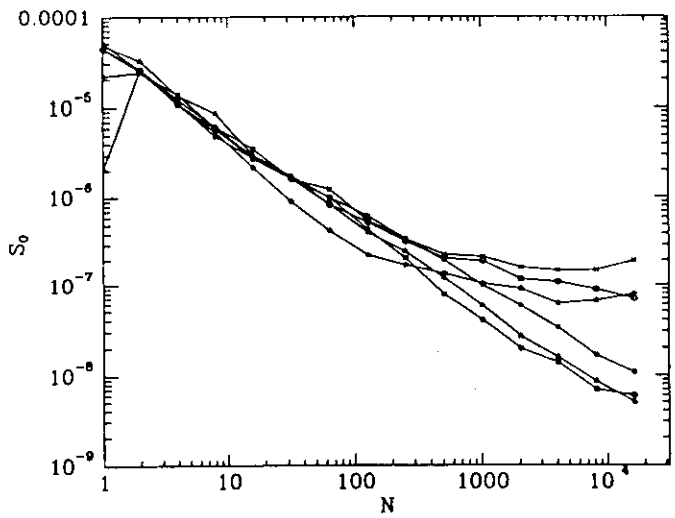

FIG. 2. Low frequency limit of the power spectrum, $S_0 = \lim_{\omega\to 0} S(\omega)$, as a function of the size of the array N, for $\bar{g} = 0.2$, $\Omega_{rf} = 0.8$, $i_{rf} = 0.61$, $i_{dc} = 0.124$ and different values of σ. ($\triangle$, $\sigma = 0.1$; $\square$, $\sigma = 0.15$; $\star$, $\sigma = 0.2$; $\bigcirc$, $\sigma = 0.3$; $\times$, $\sigma = 0.4$; $\blacksquare$, $\sigma = 0.5$.)

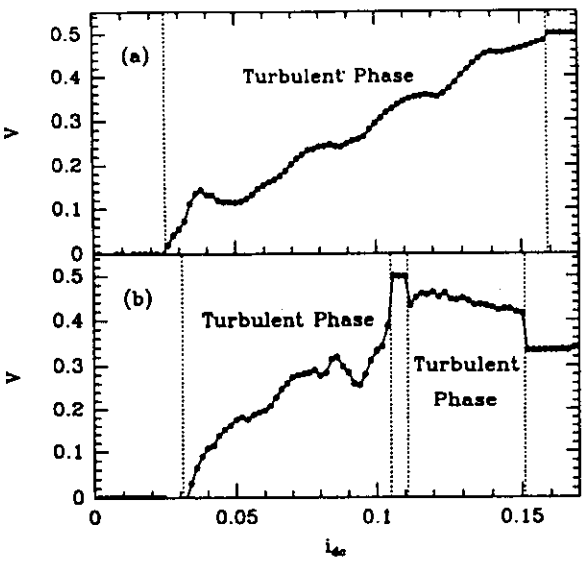

FIG. 3. I-V characteristics for an array with $N = 128$ junctions and with $\tilde{g} = 0.2$, $\Omega_{rf} = 0.8$, $i_{rf} = 0.61$. (a) $\sigma = 0.4$; note the development of pseudosteps; (b) $\sigma = 0.1$. The limits of the turbulent phase ($\lambda > 0$, $n_{cl} \approx N$) are detailed.

I-V either.

The pseudosteps are not true Shapiro steps, since they do not correspond to mode locked periodic states. Instead, they have a positive Liapunov exponent and finite broadband noise emission. This emergence of pseudosteps within the turbulent regime of the JJSA is a new result which one could not have predicted from our previous knowledge of GCM. They seem to arise as an additional effect originated by the fact that we have a system of coupled nonlinear differential equations with a time periodic drive, instead of simply coupled logistic maps.

In conclusion, we find that many phenomena studied in GCM [10–13] can be measured in the laboratory in rf-driven JJSA through their I-V characteristics and power spectra. Charge density waves can be another candidate real system, where there are also many coupled degrees of freedom [18]. Also there, mode locking phenomena and Shapiro steps have been studied in large N systems [18], but so far few studies of chaos have been conducted in this case. Apart from finding an experimental realization of the breaking of the law of large numbers in the turbulent regime of the JJSA, we found that a new collective phenomenon coexists with it. This is the appearance of pseudosteps in the I-V characteristics. They can be experimentally distinguished from the true Shapiro steps since they only exist for large N and have a finite broadband noise S_0. Instead, the true Shapiro steps exist for any N and have $S_0 = 0$.

We acknowledge C. Pando-Lambruschini and J. V. José for useful comments and a critical reading of the manuscript.

* Also at Universidade Estadual de Campinas, Instituto de Fisica, 13081 Campinas, Sao Paulo, Brazil.

[1] S. P. Benz *et al.*, Phys. Rev. Lett. **64**, 693 (1990); H. C. Lee *et al.*, Phys. Rev. B **44**, 921 (1991); S. E. Hebboul and J. C. Garland, *ibid.* **43**, 13703 (1991).

[2] K. H. Lee *et al.*, Phys. Rev. Lett. **64**, 692 (1990); J. U. Free *et al.*, Phys. Rev. B **41**, 7267 (1990); M. Kvale and S. E. Hebboul, *ibid.* **43**, 3720 (1991); H. Eikmans and J. E. van Himbergen, *ibid.* **44**, 6937 (1991); D. Domínguez *et al.*, Phys. Rev. Lett. **67**, 2367 (1991); D. Domínguez and J. V. José, *ibid.* **69**, 414 (1992).

[3] P. Hadley and M. R. Beasley, Appl. Phys. Lett. **50**, 621 (1987); P. Hadley *et al.*, Phys. Rev. B **38**, 8712 (1988); K. Wiesenfeld and P. Hadley, Phys. Rev. Lett. **62**, 1335 (1989); K. Y. Tsang *et al.*, *ibid.* **66**, 1094 (1991); K. Y. Tsang and I. B. Schwartz, *ibid.* **68**, 2265 (1992).

[4] S. E. Strogatz and R. E. Mirollo, Phys. Rev. E **47**, 220 (1993); S. Watanabe and S. E. Strogatz, Phys. Rev. Lett. **70**, 2391 (1993).

[5] F. Falo *et al.*, Phys. Rev. B **41**, 10983 (1990); N. Gronbech-Jensen *et al.*, *ibid.* **46**, 11149 (1992); R. Mehrotra and S. R. Shenoy, Europhys. Lett. **9**, 11 (1989); Phys. Rev. B **46**, 1088 (1992); R. Bhagavatula *et al.*, Phys. Rev. B **45**, 4774 (1992).

[6] A. K. Jain *et al.*, Phys. Rep. **109**, 310 (1984); R. L. Kautz *et al.*, IEEE Trans. Mag. **23**, 883 (1987).

[7] S. P. Benz and C. J. Burroughs, Appl. Phys. Lett. **58**, 2162 (1991).

[8] B. A. Huberman *et al.*, Appl. Phys. Lett. **37**, 750 (1980); E. Ben-Jacob *et al.*, Phys. Rev. Lett. **49**, 1599 (1982); M. H. Jensen *et al.*, Phys. Rev. A **30**, 1960 (1984); **30**, 1970 (1984); M. Octavio and C. Readi Nasser, Phys. Rev. B **30**, 1586 (1984); M. Iansati *et al.*, Phys. Rev. Lett. **55**, 746 (1985).

[9] R. L. Kautz and R. Monaco, J. Appl. Phys. **57**, 875 (1985); M. Levi, Phys. Rev. A **37**, 927 (1988).

[10] K. Kaneko, Phys. Rev. Lett. **63**, 219 (1989); Physica (Amsterdam) **41D**, 137 (1990); Physica (Amsterdam) **54D**, 5 (1992).

[11] K. Kaneko, Phys. Rev. Lett. **65**, 1391 (1991); Physica (Amsterdam) **55D**, 368 (1992).

[12] G. Perez *et al.*, Physica (Amsterdam) **63D**, 341 (1993); G. Perez and H. A. Cerdeira (to be published); G. Perez *et al.*, Phys. Rev. A **45**, 5469 (1992).

[13] S. Sinha *et al.*, Phys. Rev. A **46**, 3193 (1992); **46**, 6242 (1992); S. Sinha, Phys. Rev. Lett. **69**, 3306 (1992).

[14] Recently, in Ref. [4], it has been shown that JJSA with a resistive load, but overdamped ($g = \infty$) and with a dc drive ($I_{rf} = 0$), have $N - 3$ constants of motion.

[15] D. E. McCumber, J. Appl. Phys. **39**, 3113 (1968); W. C. Stewart, Appl. Phys. Lett. **10**, 277 (1968).

[16] S. Shapiro, Phys. Rev. Lett. **11**, 80 (1963).

[17] D. Domínguez and H. A. Cerdeira (to be published).

[18] D. S. Fisher, Phys. Rev. Lett. **50**, 1486 (1983); S. N. Coppersmith and P. B. Littlewood, *ibid.* **57**, 1927 (1986); S. Bhattacharya *et al.*, *ibid.* **59**, 1849 (1987); A. A. Middleton *et al.*, *ibid.* **68**, 1586 (1992).

Spatiotemporal chaos in rf-driven Josephson junction series arrays

Daniel Domínguez
Los Alamos National Laboratory, Theoretical Division, T-11, M.S. B262, Los Alamos, New Mexico 87545

Hilda A. Cerdeira
International Centre for Theoretical Physics, P. O. Box 586, Miramare, 34100 Trieste, Italy
(Received 20 December 1994; revised manuscript received 30 March 1995)

We study underdamped Josephson junction series arrays that are globally coupled through a resistive shunting load and driven by an rf bias current. They can be an experimental realization of many phenomena currently studied in globally coupled logistic maps. We study their spatiotemporal dynamics and we find coherent, ordered, partially ordered, turbulent, and quasiperiodic phases. The ordered phase corresponds to giant Shapiro steps in the IV characteristics. In the turbulent phase there is a saturation of the broad-band noise for a large number of junctions. This corresponds to a breakdown of the law of large numbers as seen in globally coupled maps. Coexisting with this phenomenon, we find an emergence of pseudosteps in the IV characteristics. This effect can be experimentally distinguished from the true Shapiro steps, which do not have broad-band noise emission. We study the stability of the breakdown of the law of large numbers against thermal fluctuations. We find that it is stable below a critical temperature T_{c1}. A measurement of the broad-band noise as a function of temperature T will show three different regimes: below T_{c1} the broad-band noise decreases when increasing T, and there is turbulence and the breakdown of the law of large numbers. Between T_{c1} and a second critical temperature T_{c2} the broad-band noise is constant and the dynamics is dominated by the chaos of the individual junctions. Finally above T_{c2} all the broad-band noise is due to thermal fluctuations, since it increases linearly with T.

I. INTRODUCTION

Josephson junction arrays are mesoscopic devices which can be fabricated with very specific properties and geometries.[1] In the last years they have become a good laboratory for the study of nonlinear dynamical systems with many degrees of freedom.[2–12] Moreover, they have potential applications as high frequency coherent power sources,[13,14] parametric amplifiers, and voltage standards.[13] One of the prototype models of nonlinear systems with many degrees of freedom is coupled logistic maps.[15] In particular, globally coupled maps (GCM's) have been studied as a mean-field-type extension of these models.[16,17] As a consequence of the interplay between temporal chaos and space synchronization, the GCM's exhibit coherent, ordered, partially ordered, and turbulent phases.[16] In the turbulent phase, a surprising result was found by Kaneko:[18] Even when spatial coherence is completely destroyed, a subtle collective behavior emerges. This was seen as a violation of the law of large numbers[18–24] as a function of the number of logistic maps.

We have made contact between these abstract models of GCM's and one-dimensional Josephson junction series arrays (JJSA's).[11,12] In this system, the role of the logistic maps is played by underdamped single Josephson junctions, which are known to show chaotic behavior when they are driven by a rf bias current.[25–28] The global coupling is achieved by connecting this junctions in series but with a common resistive shunting load. Therefore, the two conflicting trends of GCM are present: destruction of coherence due to the chaotic divergences of the individual junctions and synchronization through global averaging of the common shunting load. We have found[11] that the breakdown of the law of large numbers can be observed in rf-driven underdamped JJSA's, and that it is stable for temperatures below a certain T_{c1}.[12] Moreover, we find that whenever the JJSA shows a breakdown of the law of large numbers, pseudo Shapiro steps emerge in the IV characteristics of the JJSA.[11] This last effect is a result which does not result directly from previously known phenomena in GCM's. In this paper we discuss these phenomena in more detail, and we present a thorough analysis of the different dynamical regimes of the JJSA (not only the turbulent phase).

Josephson junction series arrays coupled by an external shunting load have been extensively studied before.[2–5] But in these studies the arrays were driven by a dc current. Since a single Josephson junction with a dc bias never shows chaos, the many interesting chaotic phenomena studied in Refs. 2–5 are a consequence of the high dimensionality of the system. On the other hand, the dynamics of rf-driven two-dimensional Josephson junction arrays has been of great interest in recent years, both experimentally[6] and theoretically.[7,8] Much of the interest has concentrated in the study of giant Shapiro steps and coherent vortex states. Some investigations of chaos and turbulence on two-dimensional Josephson junction arrays have also been done recently.[9,10] In particular Bhagavatula *et al.*[10] have studied chaos in two-dimensional rf-driven Josephson junction arrays. The main difference between the JJSA and the two-dimensional Josephson

0163-1829/95/52(1)/513(14)/$06.00

junction arrays simulated in Ref. 10 is that in the last case there is a locally coupled dynamics instead of the global coupling of the JJSA. Therefore, a breakdown of the law of large numbers is not likely to be found in their case.

The paper is organized as follows. In Sec. II we review the dynamics of chaos in a single Josephson junction, showing simulations for the parameters that will be used for the JJSA in the rest of the paper. In Sec. III we introduce the dynamical equations for the JJSA and compare them with the GCM dynamics. In Sec. IV we present a thorough study of the spatiotemporal dynamics of the JJSA for different coupling strengths and bias currents. In particular we identify the various dynamical phases and their consequences in the *IV* characteristics of the JJSA. In Sec. V we investigate the breakdown of the law of large numbers in the turbulent phase of the JJSA. In Sec. VI we discuss the effect of thermal noise on the turbulent phase of the JJSA. Finally in Sec. VII we present our conclusions and discuss possible experimental consequences of our findings.

II. CHAOS IN SINGLE JOSEPHSON JUNCTIONS

Before considering the JJSA, let us review the dynamics of a single Josephson junction. The supercurrent flowing through a Josephson junction is

$$I_J = I_c \sin\phi \ , \tag{1}$$

where ϕ is the phase difference of the complex order parameters in the two superconductors of the junction, and I_c is the maximum current that can flow through the junction. The voltage drop across the junction is

$$V = \frac{\hbar}{2e}\frac{d\phi}{dt} \ . \tag{2}$$

In real junctions one has to take into account that there is always a source of dissipation and that the junction also works as a capacitor. This is usually described with the resistively shunted junction (RSJ) model.[29] In a current-biased junction, the bias current $I(t)$ flows in parallel with an ideal Josephson junction, a resistor r, and a capacitor C so that the total current is given by

$$I(t) = I_J + \frac{V}{r} + C\frac{dV}{dt} = I_0 \sin\phi + \frac{\hbar}{2er}\frac{d\phi}{dt} + \frac{C\hbar}{2e}\frac{d^2\phi}{dt^2} \ . \tag{3}$$

It can be written in reduced units, with currents normalized by the critical current, $i = I/I_c$, voltages by rI_c, $v = V/rI_c$, and time normalized by the plasma frequency $\omega_p = \sqrt{\frac{2eI_c}{\hbar C}}$, $\omega_p t = \tau$, as

$$\ddot{\phi} + g\dot{\phi} + \sin\phi = i(\tau) \ , \tag{4}$$

where $g = (\frac{\hbar}{2eCr^2I_c})^{1/2} = 1/\beta_c^{1/2}$, with β_c the McCumber parameter.[29]

One of the responses that can be measured experimentally are the *IV* characteristics of the Josephson junctions; which is the time-averaged voltage $\langle v(\tau)\rangle = v$ as a function of the time-averaged bias current $\langle i(\tau)\rangle = i$. When the bias current $I(t)$ is time independent and the junction is overdamped ($C = 0$), Eq. (3) can be solved analytically.[30] In this case, the time-averaged voltage is $v = \sqrt{i^2 - 1}$ for $i > 1$ and $v = 0$ for $i < 1$.

When the junctions are rf biased, with $I(t) = I_{dc} + I_{rf}\sin(\omega_{rf}t)$, they show Shapiro steps.[31,30,25–28] These are plateaus in the *IV* characteristics where the voltages are quantized at

$$V_n = n\frac{\hbar\omega_{rf}}{2e}, \quad n = 1, 2, 3, \dots \ , \tag{5}$$

or in reduced units $v = ng\Omega_{rf}$, with $\Omega_{rf} = \omega_{rf}/\omega_p$. They correspond to phase-locked states, which are periodic solutions in resonance with the rf current, such that $\phi(\tau + 2\pi/\Omega_{rf}) = \phi(\tau) + 2\pi n$. In the underdamped case $g < 1$, there are also subharmonic Shapiro steps for which $v = \frac{n}{m}g\Omega_{rf}$. They correspond to periodic solutions of the type $\phi(\tau + 2\pi m/\Omega_{rf}) = \phi(\tau) + 2\pi n$.

Chaotic behavior can occur in underdamped junctions ($g < 2$) driven by a rf current below the plasma frequency ($\Omega_{rf} < 1$).[28] In these chaotic solutions the junction switches pseudorandomly between unstable, overlapping Shapiro steps.[25–28] It has also been shown that this dynamical system behaves as a circle map in certain cases.[26] Here, we study the chaotic nature of the solutions by computing the maximum Liapunov exponent λ of the dynamical system of Eq. (4). Experimentally,[27] most chaotic modes can be observed as broad-band noise in the power spectrum of the voltage. The power spectrum is computed as $S(\omega) = \frac{2}{t_m}|\int_0^{t_m} v(\tau)e^{i\omega\tau}d\tau|^2$. In the presence of broad-band noise, the low-frequency part of the spectrum approaches a constant, $S_0 = \lim_{\omega\to 0} S(\omega)$.

Let us study one example of Josephson junctions in which there are periodic solutions (Shapiro steps) and chaotic solutions. We choose a case with $g = 0.2$, $\Omega_{rf} = 0.8$, and $i_{rf} = 0.61$. We integrate the dynamical system of Eq. (4) using a fourth-order Runge-Kutta method with fixed step $\Delta\tau = T/160$, with $T = 2\pi/\Omega_{rf}$ the period of the rf drive, and we iterate the dynamics for times as long as $1024T$, after discarding the first 256 periods. For some particular cases, we have checked our results with $\Delta\tau = T/320$ and integration time $2048T$.

In Fig. 1 we show the average voltage $v/g\Omega_{rf}$, the Liapunov exponent λ, and the broad-band noise S_0 as a function of i_{dc}. We distinguish four different regimes as a function of i_{dc}. (i) There are periodic solutions, with $\lambda < 0$ and $S_0 \to 0$. They appear either below the critical current ($i_{dc} < i_c = 0.036$), where there is no average dissipation $v = 0$, or at the Shapiro steps, which in this case are at voltages $\frac{1}{2}g\Omega_{rf}$ ($0.256 < i_{dc} < 0.428$) and $3g\Omega_{rf}$ ($0.476 < i_{dc} < 0.508$). (ii) There are chaotic solutions in the region between i_c and the step at $\frac{1}{2}g\Omega_{rf}$ ($0.036 < i_{dc} < 0.256$), for which $\lambda > 0$, S_0 finite. In this region some periodic "windows" are also seen (notably for voltages $\frac{1}{2}g\Omega_{rf}$ and $\frac{1}{3}g\Omega_{rf}$). (iii) For high currents ($i_{dc} > 0.508$), where there is a linear resistive behavior

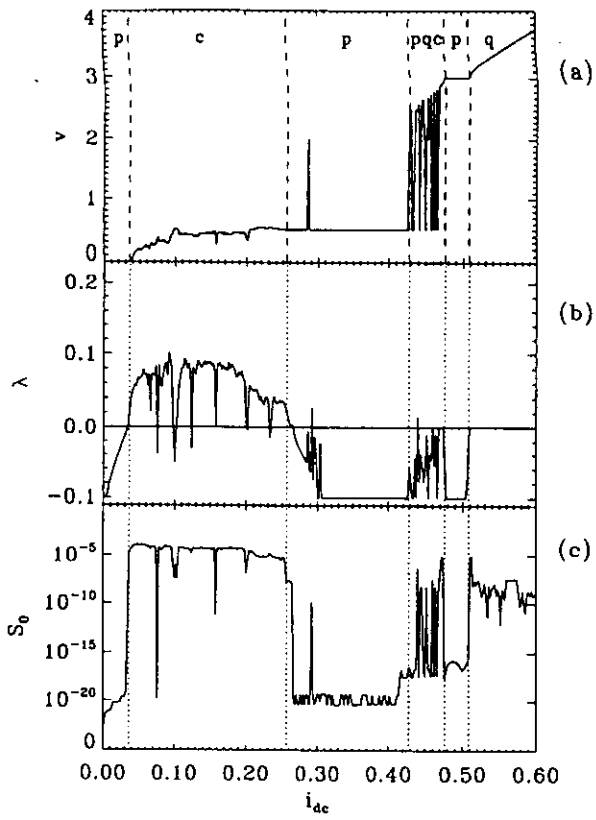

FIG. 1. (a) IV characteristics for one single Josephson junction with $g = 0.2$, $\Omega_{\rm rf} = 0.8$, $i_{\rm rf} = 0.61$. We have normalized the average voltage as $V = v/g\Omega_{\rm rf}$. (b) Maximum Liapunov exponent λ as a function of $i_{\rm dc}$. (c) Low frequency limit of the power spectrum S_0 as a function of $i_{\rm dc}$. Dynamical phases: p, mostly periodic solutions; q, mostly quasiperiodic solutions; c, mostly chaotic solutions.

in the IV characteristics, we find quasiperiodic solutions (also subharmonics with high m are possible here), for which $\lambda \approx 0$, S_0 small. (iv) Finally, between the two steps, there is a region ($0.428 < i_{\rm dc} < 0.476$) where either periodic solutions with $v = \frac{1}{2}g\Omega_{\rm rf}$, quasiperiodic solutions, or chaotic solutions can exist, depending on the initial conditions. In this region the IV characteristics show hysteresis. Note that we have deliberately chosen a case with few stable Shapiro steps. For this set of parameters, most of the Shapiro steps are unstable and overlapping, giving place to a wide region of chaotic states.

III. JOSEPHSON JUNCTION SERIES ARRAYS

A. Dynamical equations

Let us now consider an underdamped JJSA shunted by a resistive load,[2,32] and subjected to a *rf bias current* $I_B(t) = I_{\rm dc} + I_{\rm rf}\sin(\omega_{rf}t)$. This consists of a circuit where there are N junctions connected in series one after another, and there is a common resistive load in parallel to all the junctions (see Fig. 2). The dynamical behavior of each one of the Josephson junctions is described with the RSJ model of Eq. (3),

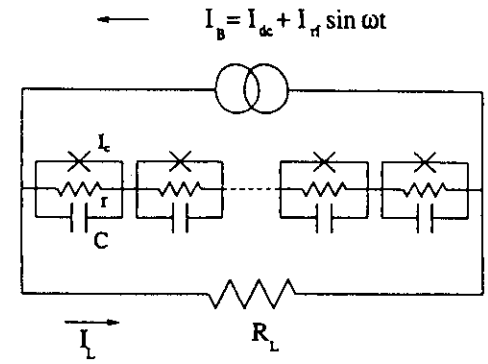

FIG. 2. Schematic circuit of a Josephson junction series array with a resistive load R_L and external current bias I_B. Each Josephson junction, with critical current I_c, is modeled including a shunt resistance r and a capacitance C.

$$I_c\sin\phi_k + \frac{\hbar}{2er}\frac{d\phi_k}{dt} + \frac{C\hbar}{2e}\frac{d^2\phi_k}{dt^2} = I_S \quad k = 1,\ldots,N\,, \tag{6}$$

where I_S is the current flowing through the circuit branch with the junctions in series. On the other hand, the common load satisfies

$$R_L I_L = \sum_{k=1}^{N} V_k = \sum_{k=1}^{N}\frac{\hbar}{2e}\frac{d\phi_k}{dt}\,, \tag{7}$$

where R_L is the resistance of the load and I_L is the current flowing through the load. The bias current divides between the load and the junctions in series,

$$I_B(t) = I_{\rm dc} + I_{\rm rf}\sin(\omega_{rf}t) = I_S + I_L\,. \tag{8}$$

Therefore, the governing equations of the JJSA in reduced units are

$$\ddot{\phi}_k + g\dot{\phi}_k + \sin\phi_k + \frac{\sigma}{N}\sum_{j=1}^{N} g\dot{\phi}_j = i_{\rm dc} + i_{\rm rf}\sin(\Omega_{\rm rf}\tau)\,, \tag{9}$$

where ϕ_k is the superconducting phase difference across the junction k and $k = 1,\ldots,N$. Here $\sigma = \frac{rN}{R_L}$ represents the strength of the global coupling in the array. Note that, when $\sigma = 0$, Eq. (9) reduces to a set of N independent junctions. Here, the voltage per junction $v(t) = \frac{1}{N}\sum_k v_k = \frac{1}{N}\sum_k g\dot{\phi}_k$ acts as a mean field variable.

B. Comparison with globally coupled logistic maps

One of the simplest models among globally coupled dynamical systems are the globally coupled maps (GCM's).[16] They were originally introduced as a mean field extension of coupled map lattices.[15] The GCM's are given by

$$x_{n+1}(i) = (1-\epsilon) f(x_n(i)) + \frac{\epsilon}{N} \sum_{j=1}^{N} f(x_n(j)), \qquad (10)$$

where $x_n(i)$ is a continuous variable $x(i)$ at *discrete* time n, with $i = 1, 2, \ldots, N$ labeling sites in a lattice, and ϵ is a measure of the coupling strength. The mapping function $f(x)$ is chosen such that it shows one-dimensional *chaos*. The simplest attractor of the GCM is the coherent attractor for which $x_n(i) = x_n$ for all i, and the system reduces to the single map $x_{n+1} = f(x_n)$. The most studied case is the well-known logistic map $f(x) = 1 - ax^2$. Also the same phenomena has been studied for the tent map,[16,18] $f(x) = a(\frac{1}{2} - |x - \frac{1}{2}|)$, and for globally coupled circle maps[17,3] as

$$x_{n+1}(i) = x_n + \frac{K}{2\pi} \sin[2\pi x_n(i)] + \Omega + \frac{\epsilon}{2\pi N} \sum_j \sin[2\pi x_n(j)]. \qquad (11)$$

The main ingredients of GCM's are that (i) the individual elements are chaotic and (ii) there is an additive coupling with the same weight for all the elements. The first condition means that the GCM is reduced to a chaotic one-dimensional system either for $N = 1$ (single map) or for $\epsilon = 0$ (ensemble of uncoupled maps), which coincides with the coherent attractor, $x_{n+1} = f(x_n)$. As a consequence, the system has two conflicting tendencies, random behavior and incoherence because of the chaotic instabilities of the single elements, and synchronization because of global averaging by the coupling term.

The JJSA studied here satisfies both conditions. To make the analogy more obvious, the dynamical equations (9) can be rewritten as

$$\ddot{\phi}_k + (\tilde{g} - \epsilon)\dot{\phi}_k + \sin\phi_k + \frac{\epsilon}{N} \sum_{j=1}^{N} \dot{\phi}_j = i_{dc} + i_{rf} \sin(\Omega_{rf}\tau) , \qquad (12)$$

with $\tilde{g} = (1+\sigma)g$ and $\epsilon = \sigma g$. Either in the limit $\epsilon = 0$ or $N = 1$, it reduces to

$$\ddot{\phi}_0 + \tilde{g}\dot{\phi}_0 + \sin\phi_0 = i_{dc} + i_{rf} \sin(\Omega_{rf}\tau) , \qquad (13)$$

which is also the coherent attractor of the JJSA, $\phi_k(t) = \phi_0(t)$. This corresponds to the dynamics of a single Josephson junction as given by Eq. (4). As discussed in Sec. II in the underdamped case and with a rf bias it can have chaotic behavior. Therefore, the only difference with GCM's is that in the JJSA the time is a continuous variable and the dynamics is governed by differential equations instead of maps. Note that previously studied JJSA's (Refs. 2–5) do not follow condition (i). They have been studied only for dc current bias ($i_{rf} = 0$), in which case the single-junction equation does not have chaos. Therefore, their dynamics can not be compared directly with GCM's. In this case the many interesting chaotic phenomena observed arise only from the high dimensionality of the system.

A closely related system is globally coupled oscillators (GCO's).[33,34] They are described by equations like

$$\dot{\phi}_i = \omega + g \frac{1}{N} \sum_{j=1}^{N} \Gamma(\phi_i - \phi_j) , \qquad (14)$$

where ϕ_i is a phase, and the coupling Γ is 2π periodic. These systems have a continuous time and in that sense they are similar to the JJSA. In the absence of coupling, $g = 0$, each unit is moving around its limit cycle at frequency ω. The GCO's are, therefore, similar to the JJSA with a dc current bias only,[2–4] for large currents $I_{dc} \gg I_0$ in the overdamped limit. This is because in that case the single-junction dynamics reduces to the limit cycle $\dot{\phi} = \omega \approx 2erI_{dc}/\hbar$.

An important concept in both GCM's and GCO's is "clustering".[16,33] This means that even when all the elements (i.e., the junctions in the JJSA) are identical, the dynamics can break into different clusters, each of which consists of fully synchronized elements. After the system has fallen in an attractor, we say that i, j are in the same cluster if $x_n(i) = x_n(j)$. An attractor can be characterized by the number of clusters it has, n_{cl}, and the number of elements of each cluster $(M_1, M_2, \ldots, M_{n_{cl}})$. Four types of attractors have been identified in GCM's:[16] (i) the coherent attractor $n_{cl} = 1$; (ii) attractors with few clusters, $n_{cl} \ll N$; (iii) attractors with a large number of clusters, $n_{cl} \sim N$, and large M_1 [for example, $n_{cl} = N/2 + 1, (N/2, 1, 1, \ldots, 1)$]; (iv) attractors with a large number of clusters, $n_{cl} \sim N$ and all M_j small ($M_j \sim 1, 2$). We will use this concept of clustering in the next section in our study of the dynamical regimes of the JJSA.

IV. SPATIOTEMPORAL CHAOS AND *IV* CHARACTERISTICS

Let us study the spatiotemporal behavior of the JJSA for different values of i_{dc} and σ. To compare with the single-junction case presented in Sec. II, we choose $\tilde{g} = 0.2$, $\Omega_{rf} = 0.8$, and $i_{rf} = 0.61$. We work with fixed $\tilde{g}$, instead of g, in order to have in all the cases the same coherent attractor. We integrate the dynamical system of Eq. (9) with the same numerical procedure as in the previous section. For each run we used different sets of random initial conditions $\{\phi_k(0), \dot{\phi}_k(0)\}$.

In Figs. 3, 4, and 5 we show our results for different values of the coupling, $\sigma = 0.05$, $\sigma = 0.2$, and $\sigma = 0.8$, respectively, and fixed size $N = 128$. First, we plot the *IV* characteristics, i.e., the average voltage per junction, $v = \frac{1}{N}\sum_j \langle g\dot{\phi}_j \rangle$, vs the dc bias i_{dc}, in Figs. 3(a), 4(a), and 5(a). Note that v, which is the quantity that can be measured directly in the experiments, is also the time average of the "mean field," $v(\tau) = \frac{1}{N}\sum_j g\dot{\phi}_j$, in the globally coupled dynamical equations. At the same time, we analyze the spatiotemporal behavior of the solutions for each bias i_{dc}. In what regards the temporal behavior, we plot the maximum Liapunov exponent λ of the system in Figs. 3(b), 4(b), and 5(b). In what regards the spatial behavior, we plot the number of clusters, n_{cl} in Figs. 3(c),

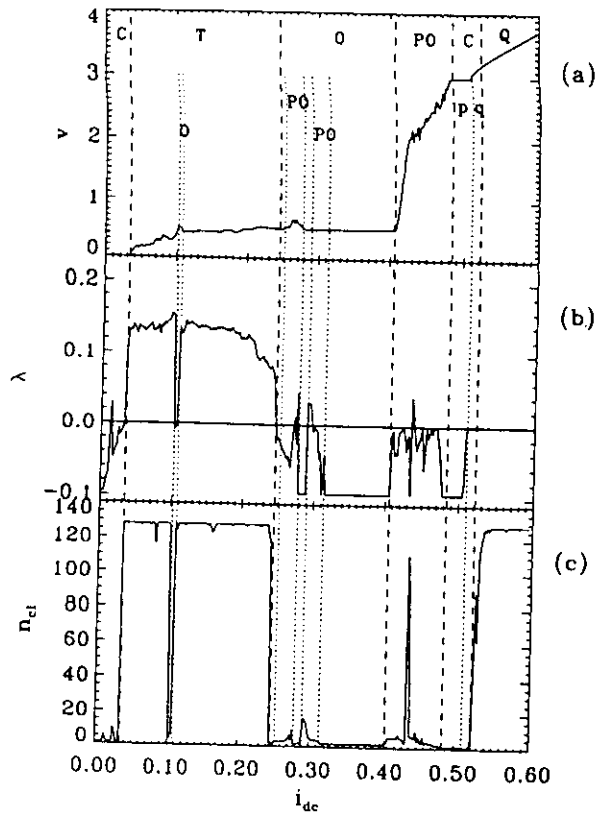

FIG. 3. (a) *IV* characteristics for a Josephson junction series array with $\bar{g} = 0.2$, $\Omega_{rf} = 0.8$, $i_{rf} = 0.61$, $N = 128$ junctions, and coupling $\sigma = 0.05$. The average voltage per junction is normalized as $V = \bar{v}/g\Omega_{rf}$. (b) Maximum Liapunov exponent λ as a function of i_{dc}. (c) Number of clusters n_{cl} as a function of i_{dc}. C, coherent phase, which can have either periodic (p) or quasiperiodic (q) solutions; O, ordered phase; PO, partially ordered phase; T, turbulent phase; Q, quasiperiodic phase.

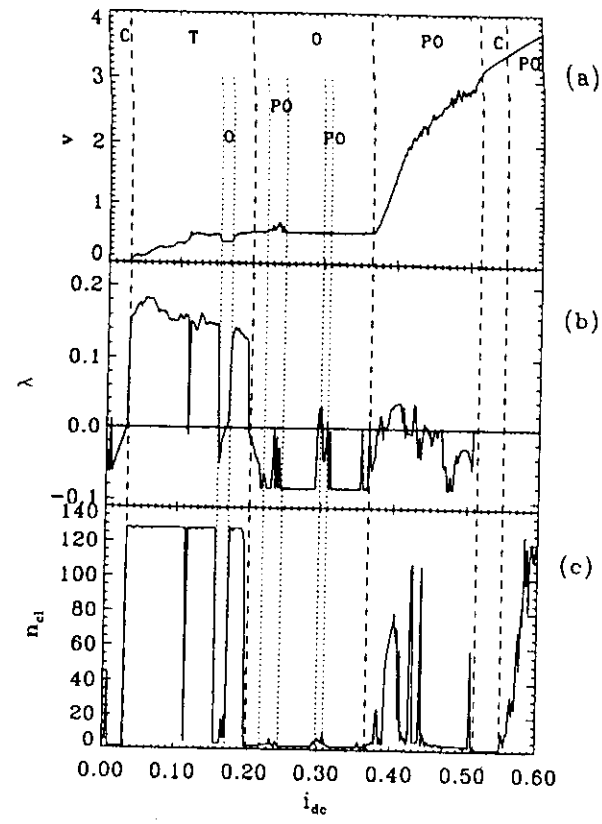

FIG. 4. The same as in Fig. 3 but for coupling $\sigma = 0.2$.

4(c), and 5(c). The criterion for clustering is that two sites i, j belong to the same cluster if $\phi_i = \phi_j + 2\pi n$, with n an integer. We find five different phases.

(a) *Turbulent phase*: all the attractors have many clusters, $n_{cl} \sim N$, and their temporal behavior is chaotic $\lambda > 0$. An example of this case is shown in Fig. 6(a). There we plot the time evolution for each site, showing the points in time where each phase ϕ_j hits $2\pi n$. We see that all the junctions follow a different time evolution, and none of them is periodic. The chaotic behavior is also evident in the power spectrum of the voltage $v(\tau)$ shown in Fig. 7(a). Besides the peaks corresponding to the driving frequency ω_{rf}, the spectrum is broad and tends to a constant at zero frequency. The turbulent phase appears always between the critical current i_c and the 1/2-integer Shapiro step in the *IV* characteristics, for this choice of parameters. Also for high values of σ it can be found at higher bias currents (see Fig. 5).

(b) *Ordered phase*: the attractors have few clusters, and they are periodic in time. This phase corresponds to Shapiro steps in the *IV* characteristics. In Fig. 6(b) we show an example for a 1/3-integer Shapiro step

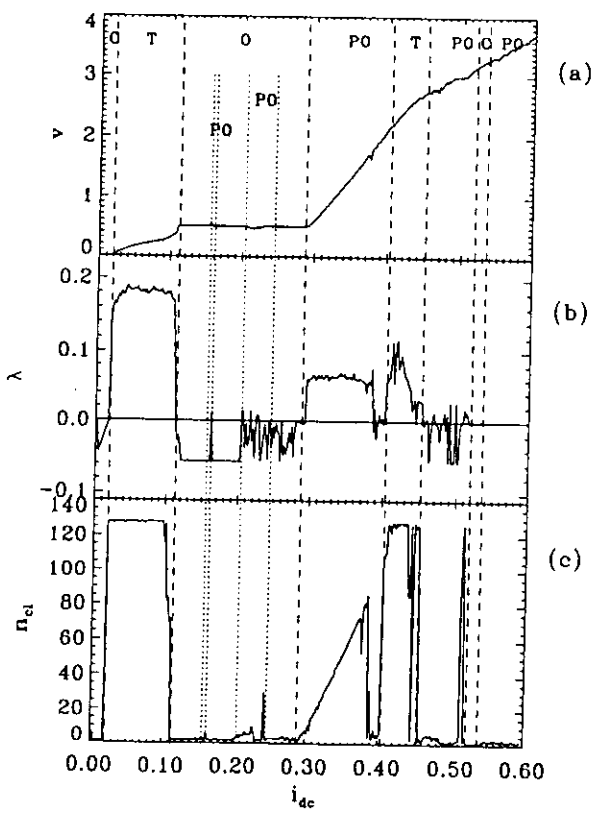

FIG. 5. The same as in Fig. 3 but for coupling $\sigma = 0.8$.

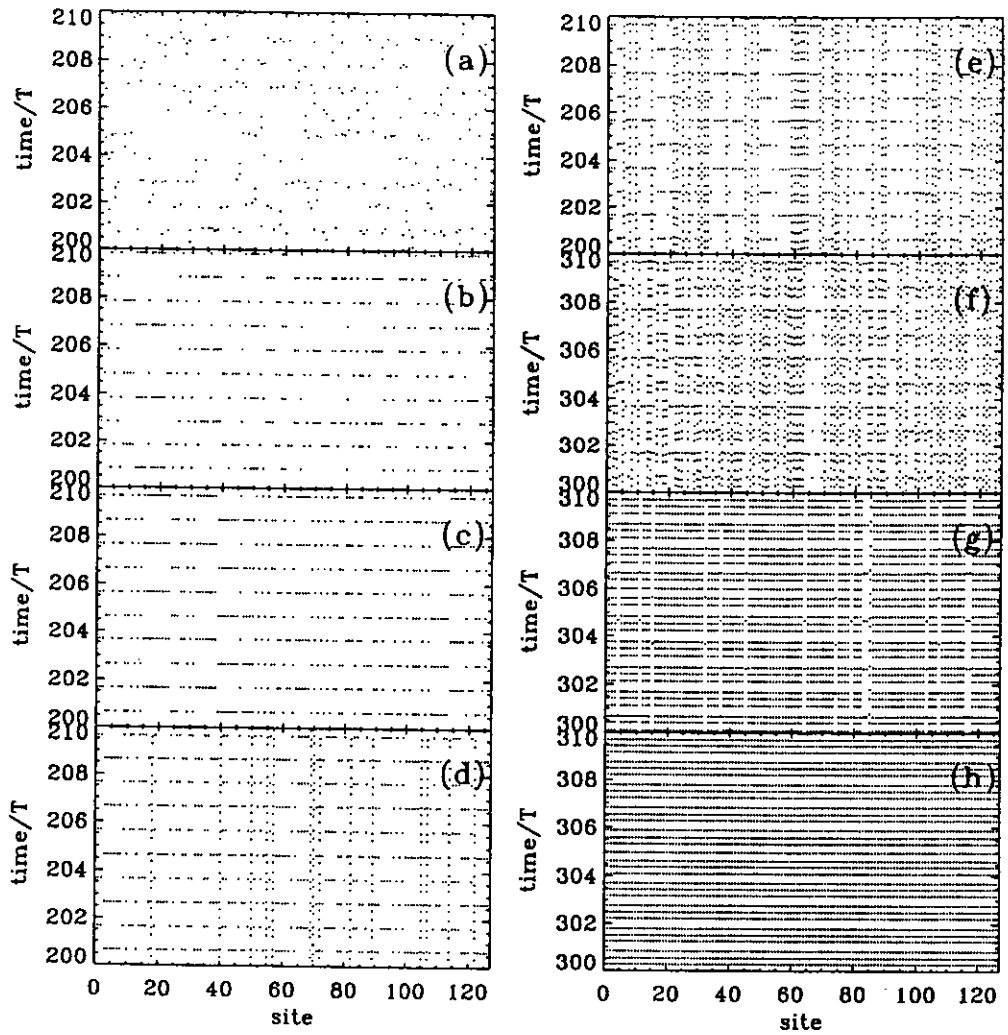

FIG. 6. Spatiotemporal evolution diagrams. For a system with $\tilde{g} = 0.2$, $\Omega_{rf} = 0.8$, $i_{rf} = 0.61$, $N = 128$ junctions, and coupling $\sigma = 0.2$. Each point represents the time when each junction phase ϕ_k hits $2n\pi$. (a) For a turbulent state, $i_{dc} = 0.084$. For ordered states: (b) $i_{dc} = 0.160$, 1/3-integer Shapiro step; (c) $i_{dc} = 0.280$, 1/2-integer Shapiro step. For partially ordered states, (d) $i_{dc} = 0.378$, (e) $i_{dc} = 0.390$, (f) $i_{dc} = 0.404$, (g) $i_{dc} = 0.460$. (h) For a coherent state, $i_{dc} = 0.520$.

$(v/g = \frac{1}{3}\Omega_{rf})$. We see that there are $n_{cl} = 3$ clusters evenly distributed, each cluster oscillating with period $3T$ $(T = 2\pi/\omega_{rf})$. This is also evident in the power spectrum shown in Fig. 7(b), where there are subharmonic peaks at frequencies $\omega = \frac{n}{3}\omega_{rf}$. Another example, corresponding to a 1/2-integer Shapiro step $(v/g = \frac{1}{2}\Omega_{rf})$, is shown in Fig. 6(c) and its corresponding power spectrum in Fig. 7(c). In this case there are $n_{cl} = 2$ clusters, each one of them oscillating with period $2T$. Therefore there are subharmonic peaks in the power spectrum at frequencies $\omega = \frac{n}{2}\omega_{rf}$. We always find that for p/q-integer Shapiro steps $(v/g = \frac{p}{q}\Omega_{rf})$ there are $n_{cl} = q$ clusters with period qT. In particular, for the case of integer steps $(q = 1)$, they fall in a coherent attractor (for example, in Fig. 3 for $\sigma = 0.05$ in the step at $v/g = 3\Omega_{rf}$). We mention that similar periodic attractors with a small number of clusters have also been found in globally coupled oscillator systems.[33,34]

(c) *Partially ordered phase*: depending on the initial conditions, there are attractors with few clusters or with many clusters unevenly distributed [type (iii) attractor in Sec. III(b)]. Let us discuss some examples. In Fig. 6(d) we show a case with $n_{cl} = 4$ clusters and $M_i = (77, 34, 12, 5)$, which is temporally periodic since $\lambda < 0$. Two of the clusters $(M_1 = 77, M_2 = 34)$ are in a periodic state with $v/g = \frac{1}{2}\Omega_{rf}$ and the other two $(M_3 = 12, M_4 = 5)$ in a periodic state with $v/g = 2.5\Omega_{rf}$. The power spectrum in Fig. 7(d) shows subharmonic peaks. Another case is shown in Fig. 6(e), with $n_{cl} = 4$ clusters but temporally chaotic $\lambda > 0$. There are two periodic clusters that correspond to $v/g = \frac{1}{2}\Omega_{rf}$, and the other two are chaotic. The corresponding power spectrum in Fig. 7(e) shows both subharmonic peaks and broad-band noise. In Fig. 6(f) we show a case with $n_{cl} = 80$ clusters $(n_{cl} \sim N = 128)$, which is temporally chaotic $(\lambda > 0)$. The clusters are unevenly distributed $M_i = (26, 24, 1, 1, 1, \ldots, 1)$. The first two large clusters correspond to a periodic solution with $v/g = \frac{1}{2}\Omega_{rf}$, whereas the other 78 single clusters are chaotic, but with average voltage $v/g \approx 2.5\Omega_{rf}$. The last example of this phase is shown in Fig. 6(g). There are $n_{cl} = 4$ clusters unevenly distributed $M_i = (114, 10, 3, 1)$ and the maximum Liapunov exponent is $\lambda \approx 0$. The large cluster $M_1 = 114$ corresponds to a quasiperiodic solution, and the small clusters correspond to periodic solutions with $v/g = \frac{1}{2}\Omega_{rf}$ and with $v/g = 2\Omega_{rf}$. Their power spectrum, shown in Fig. 7(g), has both subharmonic peaks and quasiperiodic peaks at incommensurate frequencies. We found the partially ordered phase with all this different type of solutions mostly at large currents above the big 1/2-integer Shapiro step, for this case.

(d) *Coherent phase*: here all the junctions oscillate

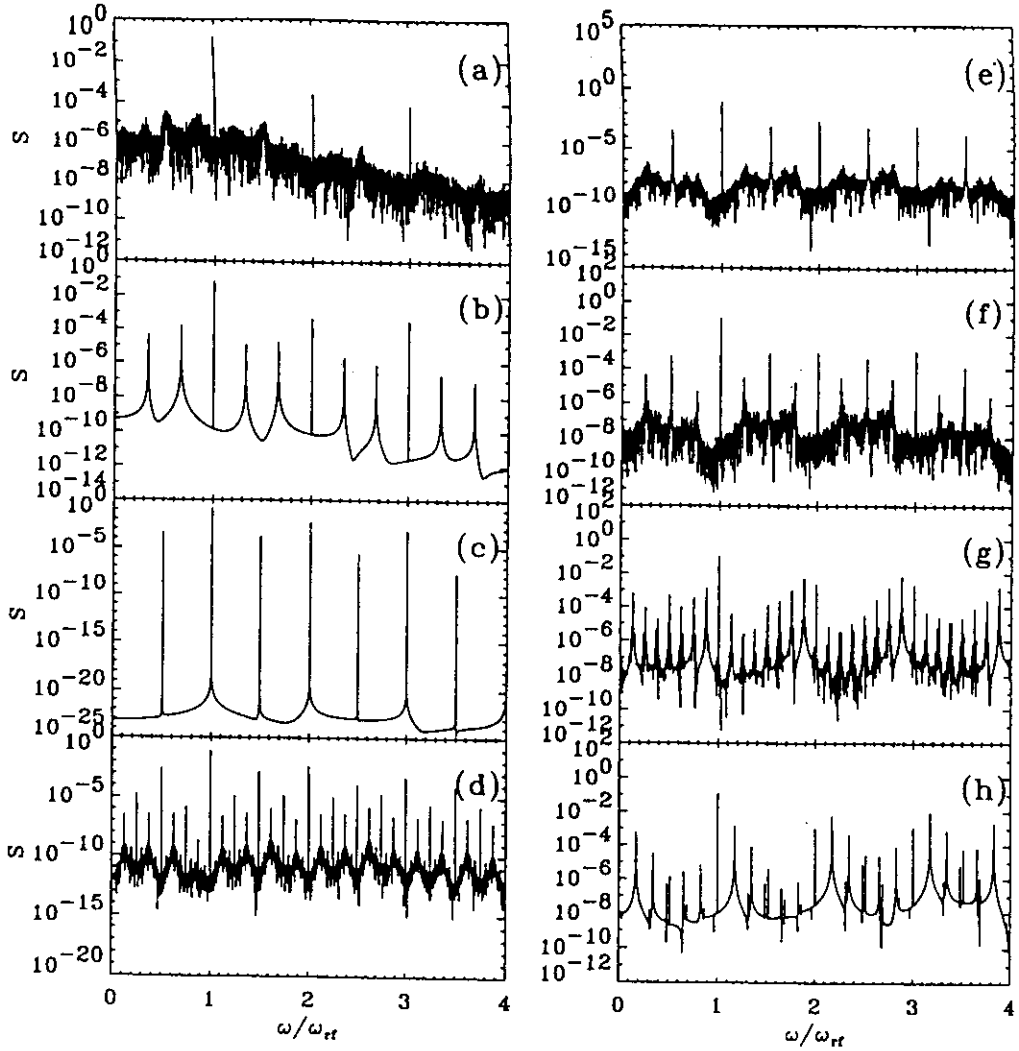

FIG. 7. Power spectra $S(\omega)$ of the voltage $v(\tau)$. For a system with $\bar{g} = 0.2$, $\Omega_{rf} = 0.8$, $i_{rf} = 0.61$, $N = 128$ junctions, and coupling $\sigma = 0.2$. (a) For a turbulent state, $i_{dc} = 0.084$. For ordered states: (b) $i_{dc} = 0.160$, 1/3-integer Shapiro step; (c) $i_{dc} = 0.280$, 1/2-integer Shapiro step. For partially ordered states, (d) $i_{dc} = 0.378$, (e) $i_{dc} = 0.390$, (f) $i_{dc} = 0.404$, (g) $i_{dc} = 0.460$. (h) For a coherent state, $i_{dc} = 0.520$.

with the same phase, $n_{cl} = 1$. It occurs for periodic solutions either below the critical current ($v = 0$) or at integer Shapiro steps ($v/g = n\Omega_{rf}$) and for quasiperiodic solutions at large currents. This last case is shown in Fig. 6(h), and its corresponding power spectrum in Fig. 7(h), where there are peaks at incommensurate frequencies.

(e) *Quasiperiodic phase*: the attractors have a large number of clusters, $n_{cl} \sim N$, but their behavior is quasiperiodic in time ($\lambda \sim 0$). This phase appears at very large currents, when the IV curve is practically linear. A similar phase has been found in globally coupled circle maps[17] (but not in logistic GCM's). It has been suggested[17] to correspond to the phenomena of "attractor crowding".[3]

We have calculated the probability distribution in time of the phases in a fixed site j. This is the probability $P_t(\phi_j^{(n)})$ with $\phi_j^{(n)} = \phi_j(t_0 + nT)$ for fixed j and all the realizations of n. This is shown in Fig. 8(a). Since we calculate the probability only every period of the rf bias, the periodic attractors with period qT show q peaks in P_t, and the chaotic and quasiperiodic states show a broad distribution. Also in Fig. 8(b) we have calculated the probability distribution in space $P_s(\phi_j(t))$ for a given time t. Therefore, a distribution P_s with a few peaks corresponds to an attractor with n_{cl} = number of peaks, whereas a broad distribution corresponds to a turbulent attractor. Both plots correspond to $\sigma = 0.2$ and show the distributions as a function of i_{dc}. We see that the main qualitative difference in the temporal and spatial distributions is in the partially ordered phase. In the ordered phase both have the same peaks (periodicity=number of clusters), and in the turbulent phase both have broad distributions (but they do not coincide).

Finally, in Fig. 9 we show a complete phase diagram in the σ vs i_{dc} plane. We see that in general the tendency for increasing σ is that the turbulent phase reduces in size, the ordered phase (1/2-integer Shapiro step) displaces to lower i_{dc} values, and the partially ordered phase grows in size. For large σ a new turbulent phase develops in the middle of the partially ordered phase. We do not find that, as in GCM's, the coherent phase is the dominant attractor in the large coupling limit. Instead, there is always a rich structure with all the five phases present.

V. BREAKDOWN OF THE LAW OF LARGE NUMBERS AND PSEUDOSTEPS

Let us now study the turbulent phase in detail. As discussed in the previous section, in this phase the time evolution is chaotic ($\lambda > 0$) and practically all the junc-

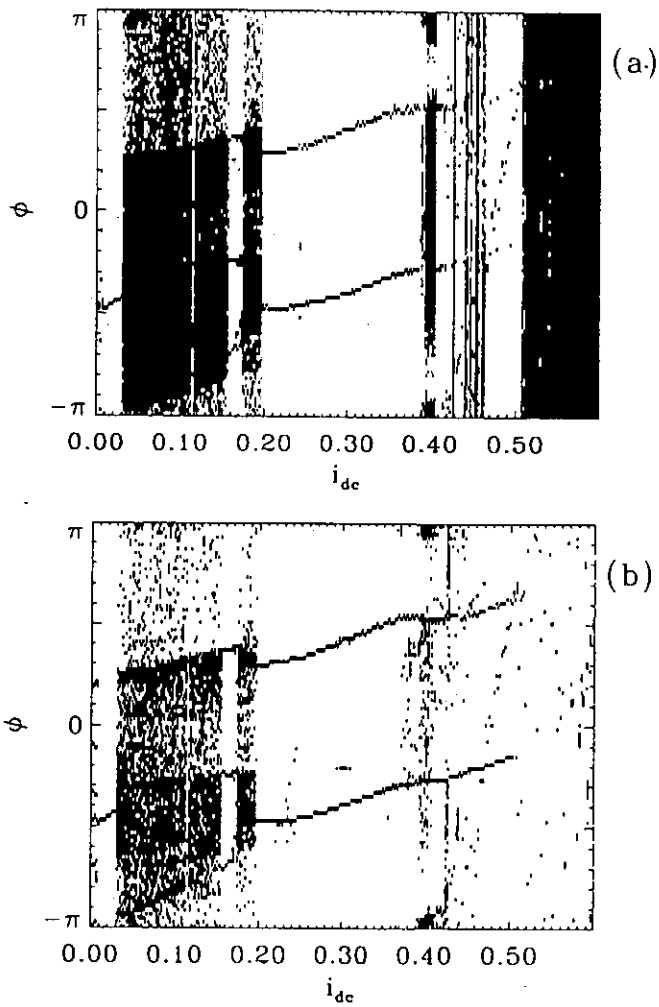

FIG. 8. Probability distribution of phases $\phi_k(t)$ as a function of i_{dc}. For $\tilde{g} = 0.2$, $\Omega_{rf} = 0.8$, $i_{rf} = 0.61$, $N = 128$ junctions, and coupling $\sigma = 0.2$. (a) Temporal behavior: distribution for a given junction k as a function of time. (b) Spatial behavior: distribution of phases at a given time t. Grey scale: white $\equiv P(\phi) = 0$, black $\equiv P(\phi) = 1$.

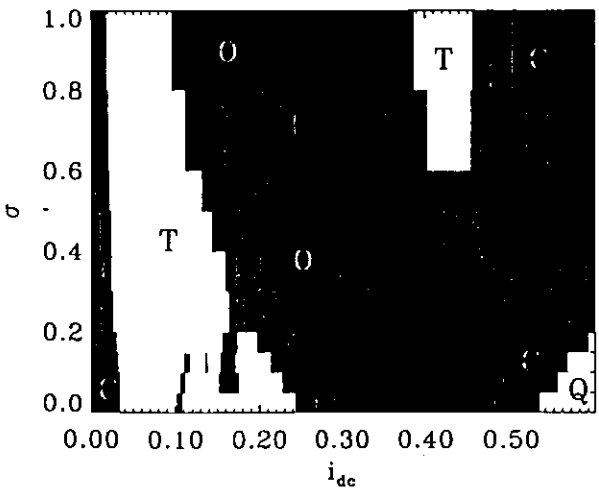

FIG. 9. Phase diagram in the σ vs i_{dc} plane. For a Josephson junction array with $\tilde{g} = 0.2$, $\Omega_{rf} = 0.8$, $i_{rf} = 0.61$, $N = 128$ junctions. C, coherent phase; O, ordered phase; PO, partially ordered phase; T, turbulent phase; Q, quasiperiodic phase.

tions have different phases ($n_{cl} \sim N$). Some interesting properties arise when studying the system as a function of the number of junctions.

First, let us see how the chaos depends on N. In Fig. 10 we plot the maximum Liapunov exponent as a function of N for different values of σ, for a given bias in the turbulent phase ($i_{dc} = 0.124$). We see that λ grows with N and seems to saturate in limit $N \to \infty$. In a system with local coupling, like coupled map lattices, it is always possible to define a characteristic length scale ξ in the behavior of $\lambda(N)$ in the "turbulent" regimes.[15] But in our case there is no characteristic scale in Fig. 10 since, because of the global coupling, all the elements are equally close in distance (i.e., it is equivalent to an infinite-dimensional lattice).

Instead of λ, another quantity that has been studied in GCM's is the fluctuations of the mean field.[18–24] For example, in the GCM of Eq. (10) the mean field is $h_n = (1/N)\sum_i f(x_n(i))$. Kaneko[18] studied the mean square deviations of the mean field $\langle(\delta h)^2\rangle = \langle(h - \langle h\rangle)^2\rangle$, with $\langle\cdots\rangle$ the average over time and initial conditions. In the turbulent phase each element $x(i)$ is chaotic and different for each i. If they can be taken as random uncorrelated numbers, then the mean field fluctuations would follow the law of large numbers, $\langle(\delta h)^2\rangle \propto 1/N$. Thus in the thermodynamic limit $N \to \infty$ the GCM could be reduced to N independent logistic maps. However, Kaneko[18] found that the law of large numbers is broken in GCM's, and $\langle(\delta h)^2\rangle$ tends to a constant for large N. The existence of this size-independent fluctuation suggests that there is a remaining correlation between elements. This means that in the turbulent phase the different variables are not independent even in the thermodynamic limit. This dependence has been quantified by Kaneko by measuring the mutual information between elements.[18] It was found that there remains a finite mutual correlation even in the $N \to \infty$ limit. This question of the relation between synchronization and chaotic be-

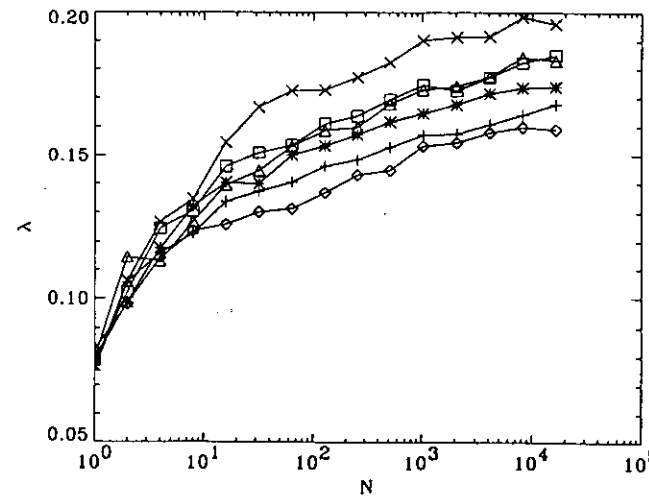

FIG. 10. Maximum Liapunov exponent λ in the turbulent phase as a function of the number N of junctions. For $\tilde{g} = 0.2$, $\Omega_{rf} = 0.8$, $i_{rf} = 0.61$, fixed bias $i_{dc} = 0.124$, and different couplings: +, $\sigma = 0.1$; *, $\sigma = 0.15$; ◇, $\sigma = 0.2$; △, $\sigma = 0.3$; □, $\sigma = 0.4$; ×, $\sigma = 0.5$.

havior has been an important topic in the framework of neuronal modeling; see Ref. 35. In the GCM this mutual correlation has been interpreted as a hidden coherence in the turbulent phase. This coherence shows, for example, in an emergence of broad peaks in the power spectrum of h_n.[18,19] However, an understanding of the origin of this hidden coherence and the frequency dependence of these broad peaks is still lacking in this problem. One of the intriguing questions is that a GCM of tent maps does follow the $1/N$ law.[18,23,24] Since the tent map does not have periodic windows, it is believed that the periodic windows may be relevant in the origin of the breakdown of the law of large number and emergence of peaks in the power spectrum.[18,19,23,24] These and related questions have motivated some discussion in the literature very recently.[21–24]

Regardless of the origin of the breakdown of the law of large numbers in GCM's, we study here this phenomenon in JJSA's, since it may lead to some experimental consequence in this system. First of all, let us note that in this case the voltage per junction, $v^{(N)}(t) = \frac{1}{N}\sum_{j=1}^{N} g\dot{\phi}_j$, acts as the "mean field" in Eq. (9). Since in the turbulent phase the $\phi_j(t)$ and, therefore, the $\dot{\phi}_j(t)$ are chaotic and different for different j, the fluctuations of $v(t)$ are the quantity that interests us here. However, since this is a periodically driven system, $\langle(\delta v)^2\rangle = \langle(v - \langle v\rangle)^2\rangle$ will not only be due to noisy fluctuations but also to the amplitude of the rf-induced oscillations in $v(t)$. [Even in the Shapiro steps it is $\langle(\delta v)^2\rangle \neq 0$.] Instead, we have to study the power spectrum of $v(t)$ which can be written as

$$S(\omega) = \frac{1}{N}|v_j(\omega)|^2 + \frac{1}{N^2}\left[\sum_{i\neq j} v_i(\omega)v_j^*(\omega)\right], \qquad (15)$$

with $v_j(\omega)$ the Fourier transform of $v_j(t) = g\dot{\phi}_j(t)$. If the $\dot{\phi}_j(t)$ are completely independent, the second term in (15) will vanish for low frequencies, $\omega \to 0$. Therefore $S_0^{(N)} \sim \frac{1}{N}S_0^{(1)}$, with $S_0^{(N)}$ the low-frequency part of the power spectrum of a JJSA with N junctions. This is the equivalent of the law of large numbers for a periodically driven system. If it were valid, we could expect that in the large N limit the broad band noise part of $v^{(N)}(t)$ will tend to vanish ($S_0 \to 0$, for $N \to \infty$), reducing the dynamics of the JJSA to N independent chaotic junctions with an additional time-periodic driving $C(t) = v^{(N\to\infty)}(t)$. On the other hand, a finite value in the limit $S_0(N \to \infty)$ will be a measure of the strength of the remaining synchrony between junctions in the turbulent regime, coming from the second term in Eq. (15).

In Fig. 11 we show the calculated values of S_0 as a function of N for different values of σ and for $i_{dc} = 0.124$ (similar behavior is also seen for other values of i_{dc} within the turbulent phase). We see that for some values of the coupling σ, S_0 does not follow the law of large numbers since it saturates for large N. However, for $\sigma > 0.5$ or for

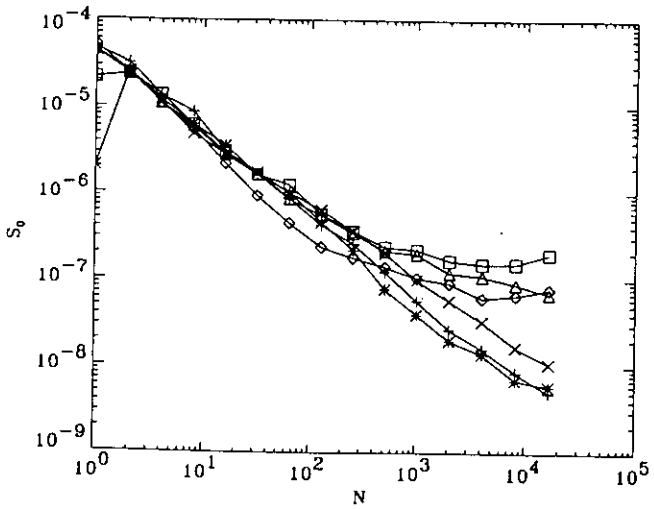

FIG. 11. Low-frequency limit of the power spectrum, $S_0 = \lim_{\omega\to 0} S(\omega)$, as a function of the number N of junctions. For $\tilde{g} = 0.2$, $\Omega_{rf} = 0.8$, $i_{rf} = 0.61$, $i_{dc} = 0.124$, and different values of the coupling: +, $\sigma = 0.1$; *, $\sigma = 0.15$; ◇, $\sigma = 0.2$; △, $\sigma = 0.3$; □, $\sigma = 0.4$; ×, $\sigma = 0.5$.

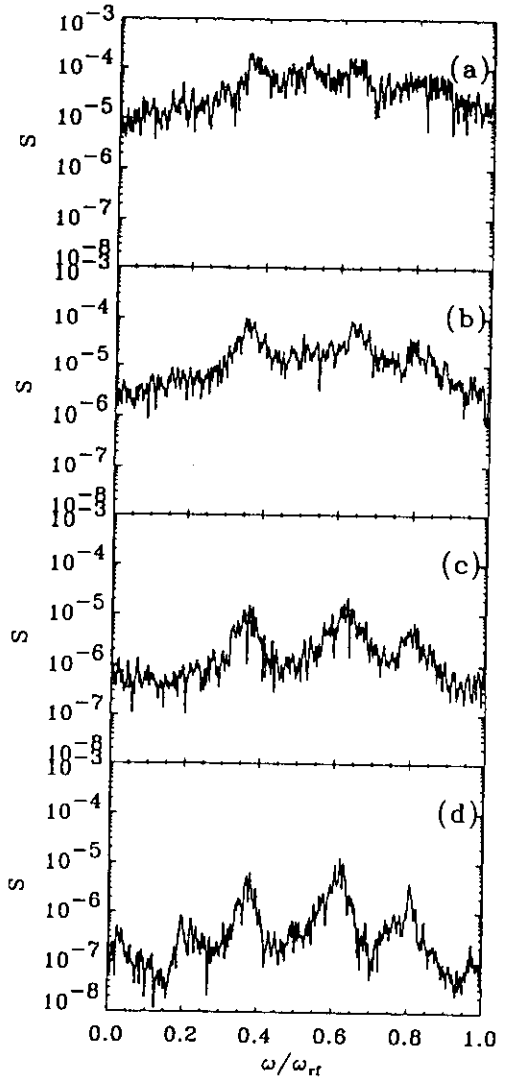

FIG. 12. Power spectrum of $v(\tau)$ for a turbulent state, with increasing N. For $\tilde{g} = 0.2$, $\Omega_{rf} = 0.8$, $i_{rf} = 0.61$, $i_{dc} = 0.124$, and $\sigma = 0.4$. (a) $N = 4$. (b) $N = 16$. (c) $N = 128$. (d) $N = 16\,384$.

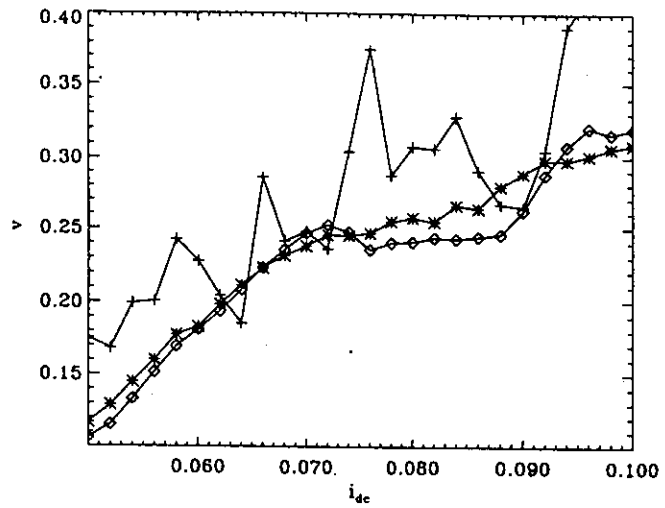

FIG. 13. Detailed IV curve in the turbulent phase, showing the emergence of a pseudostep when increasing N. For $\tilde{g} = 0.2$, $\Omega_{rf} = 0.8$, $i_{rf} = 0.61$, and $\sigma = 0.4$. (+, $N = 1$; *, $N = 16$; ◇, $N = 128$).

$\sigma < 0.1$ we find that it follows the $1/N$ law for the values of N we can simulate. Therefore, this phenomenon seems to happen only for intermediate coupling σ in the JJSA.

We also studied the full power spectrum $S(\omega)$ in the turbulent phase. In Fig. 12 we show the low-frequency part of the spectra, $\omega < \Omega_{rf}$, for increasing number of junctions, for a case that has a breakdown of the law of large numbers. We see that for small N the power spectrum is flat. But when N increases it develops broad peaks. They get sharper with increasing N, up to when S_0 saturates, and then for higher values of N the spectrum remains invariant. This is the same kind of hidden coherence that has been found in GCM's (Refs. 18 and 19) as we mentioned previously.

We find that this subtle coherence of the turbulent phase notably affects the IV characteristics of the JJSA. We find that "pseudosteps" emerge in the IV curve for large N at the same time that S_0 saturates in the turbulent phase. This can be seen in Fig. 13. There we see that, while for $N = 1$ the IV curve in this region has a "noisy" aspect, when increasing N a plateau or pseudostep tends to appear. Many pseudosteps are present all along the range of i_{dc} corresponding to the turbulent phase for the various values of σ for which there is a breakdown of the law of large number, as we show in Fig. 14. Note that $N = 128$ is a value before the full saturation of S_0, since it is hard to simulate very large N for the full IV characteristics. However, we see that the pseudosteps emerge and sharpen up with increasing N, always in coexistence with a saturation of S_0. These pseudosteps are not true Shapiro steps, since they do not correspond to mode-locked periodic states. Instead, they have a positive Liapunov exponent and finite broad-band noise emission. This emergence of pseudosteps within the turbulent regime of the JJSA is a new result which one could not have predicted from our previous knowledge of GCM's. They seem to arise as an additional effect originated by the fact that we have a system of coupled nonlinear differential equations with a time-periodic drive, instead of simply coupled logistic maps.

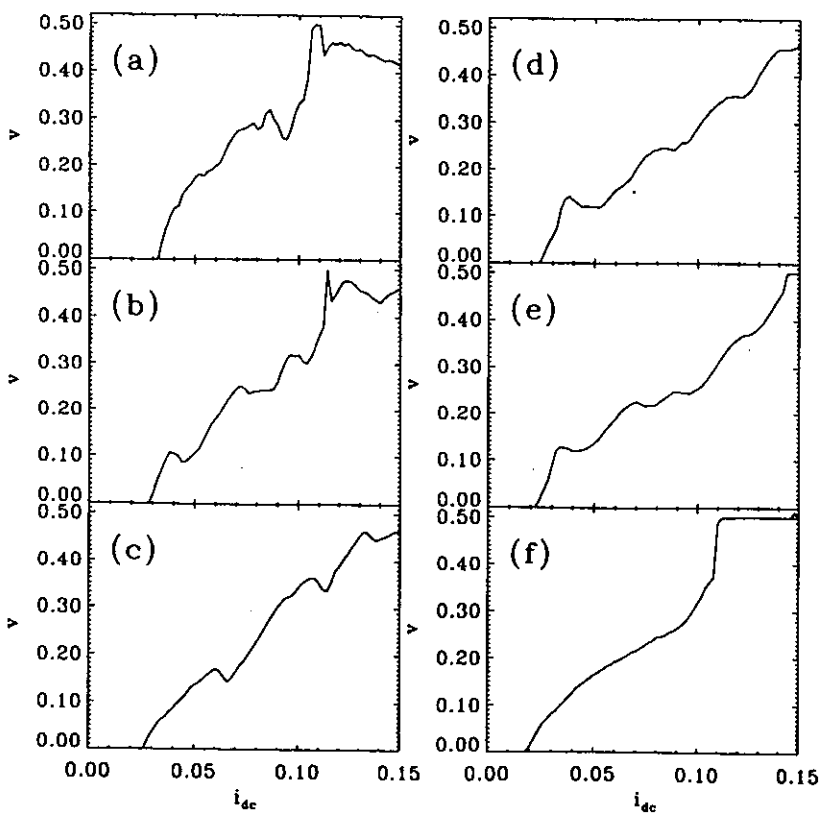

FIG. 14. IV characteristics in the turbulent phase for different couplings σ. For $\tilde{g} = 0.2$, $\Omega_{rf} = 0.8$, $i_{rf} = 0.61$. (a) $\sigma = 0.1$. (b) $\sigma = 0.2$. (c) $\sigma = 0.3$. (d) $\sigma = 0.4$. (e) $\sigma = 0.5$. (f) $\sigma = 0.8$.

VI. THERMAL NOISE EFFECTS

In this section we want to consider the effects of thermal noise on the turbulent phase for two reasons: (a) The thermal effects cannot be ignored in real experiments (then we must know if the phenomena studied in the previous sections are stable at finite temperatures); (b) the addition of noise in the dynamics of GCM's has shown interesting effects in previous studies,[18,19] correlated with the breakdown of the law of large numbers.

We consider the effect of temperature in the dynamical equations of the JJSA by adding the contribution of a Johnson noise in the shunt resistances of each junction, as it is common in the literature.[30] We also add a Johnson noise contribution in the resistive load. Therefore the dynamical equations are now given by

$$\ddot{\phi}_k + g\dot{\phi}_k + \sin\phi_k + (2\tilde{T}g)^{1/2}\eta_k(\tau) + i_L = i_{\rm dc} + i_{\rm rf}\sin(\Omega_{\rm rf}\tau)\ , \quad (16)$$

$$i_L = \frac{\sigma}{N}\sum_{j=1}^{N} g\dot{\phi}_j + \left(\frac{2\tilde{T}g\sigma}{N}\right)^{1/2}\eta_L(\tau)\ . \quad (17)$$

The thermal Johnson noise is given by the white noise terms $\eta_k(\tau), \eta_L(\tau)$, such that $\langle\eta_k(\tau)\rangle = 0$, $\langle\eta_k(\tau)\eta_{k'}(\tau')\rangle = \delta(\tau-\tau')\delta_{k,k'}$. Temperature is normalized such that $\tilde{T} = 2ekT/\hbar I_c$. We have done numerical simulations of these equations using a second-order Runge Kutta method suitable for stochastic differential equations,[36] and the same integration times and time steps as for the previous $\tilde{T} = 0$ calculations.

Let us study the effect of temperature on the breakdown of the law of large numbers. In Fig. 15 we show S_0 as a function of N for $\sigma = 0.4$ and for $i_{\rm dc} = 0.124$ (which corresponds to the turbulent regime) for different temperatures. We see that for $\tilde{T} = 0$, S_0 saturates for large N (breakdown of the law of large numbers). This effect is stable for small temperatures, and only after a critical $\tilde{T}_{c1} \approx 4\times10^{-5}$ is there a crossover to a $1/N$ behavior. Similar phenomena has been found when adding a white noise term to GCM's,[18] where also the $1/N$ behavior is recovered after a critical value of noise intensity.

More interesting, from the experimental point of view, is the behavior of S_0 as a function of temperature for a fixed large number of junctions (if N_* is the typical N for saturation of S_0 at $\tilde{T} = 0$, we consider $N > N_*$). In Fig. 16 we show the results for bias $i_{\rm dc} = 0.124$, $\sigma = 0.4$, and $N = 16384$ junctions. We find three different thermal regimes.

(i) For $\tilde{T} < \tilde{T}_{c1} \approx 4\times10^{-5}$, the broad-band noise *decreases* when increasing the temperature. This counterintuitive behavior is a consequence of the fact that there is a breakdown of the law of large numbers at $\tilde{T} = 0$. The addition of thermal noise reduces in part the subtle coherence that made S_0 saturate for large N. In other words, N_* increases when increasing the temperature. This leads to a decrease of S_0 when increasing $\tilde{T}$ at fixed N. Since there is still a breakdown of the law of large numbers, this is the temperature regime where the *turbulence* and the global coupling of the JJSA's are manifested.

(ii) For $\tilde{T}_{c1} < \tilde{T} < \tilde{T}_{c2}$, with $\tilde{T}_{c2} \approx 5\times10^{-3}$, S_0 remains *constant*. Now the $1/N$ law is fulfilled. Here the ϕ_j act as independent chaotic variables. In this temperature regime, the subtle coherence of the global coupling has been destroyed, and S_0 is mainly due to the *chaos* of the individual junctions.

(iii) For $\tilde{T} > \tilde{T}_{c2}$, S_0 *increases* with temperature. In this part the dynamics of the junctions is dominated by the thermal fluctuations, and therefore the broad-band noise S_0 is a consequence of the *thermal noise*.

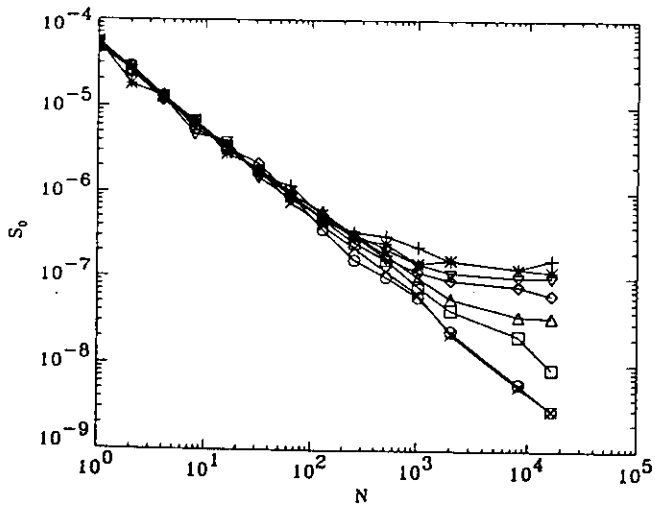

FIG. 15. Low-frequency limit of the power spectrum, $S_0 = \lim_{\omega\to0} S(\omega)$, as a function of the size of the array N. For $\tilde{g} = 0.2$, $\Omega_{\rm rf} = 0.8$, $i_{\rm rf} = 0.61$, $i_{\rm dc} = 0.124$, $\sigma = 0.4$, and different temperatures $\tilde{T}$: +, $\tilde{T} = 0$; *, $\tilde{T} = 1\times10^{-6}$; ∇, $\tilde{T} = 2\times10^{-6}$; $\diamond$, $\tilde{T} = 5\times10^{-6}$; $\triangle$, $\tilde{T} = 1\times10^{-5}$; $\square$, $\tilde{T} = 2\times10^{-5}$; $\times$, $\tilde{T} = 5\times10^{-5}$; $\bigcirc$, $\tilde{T} = 1\times10^{-4}$.

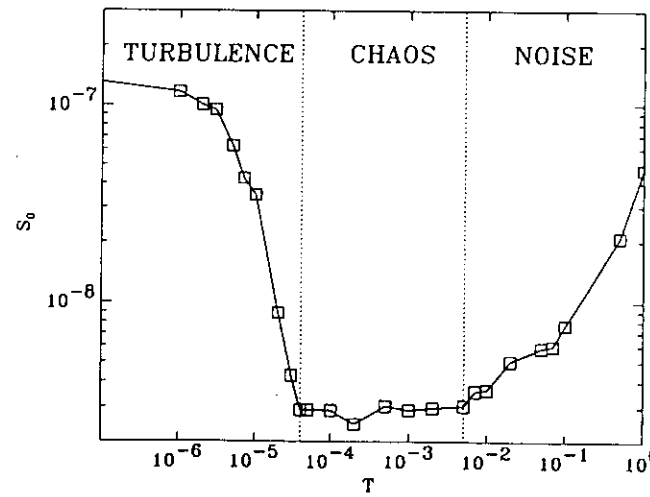

FIG. 16. Low-frequency limit of the power spectrum, $S_0 = \lim_{\omega\to0} S(\omega)$, as a function of the temperature $\tilde{T}$. For $\tilde{g} = 0.2$, $\Omega_{\rm rf} = 0.8$, $i_{\rm rf} = 0.61$, $i_{\rm dc} = 0.124$, $\sigma = 0.4$, for a large array, $N = 16384$.

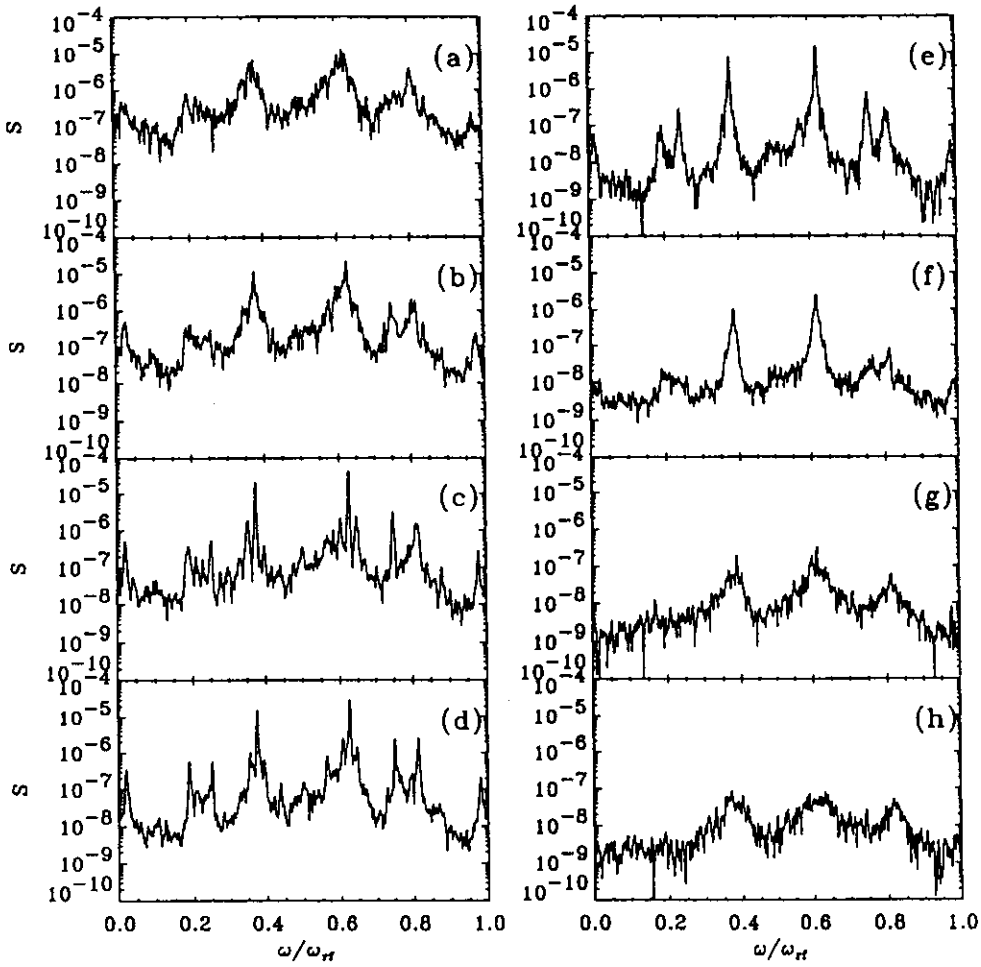

FIG. 17. Power spectrum for different temperatures. For $\tilde{g} = 0.2$, $\Omega_{rf} = 0.8$, $i_{rf} = 0.61$, $i_{dc} = 0.124$, $\sigma = 0.4$, $N = 16384$. (a) $\tilde{T} = 0$. (b) $\tilde{T} = 2\times10^{-6}$. (c) $\tilde{T} = 5\times10^{-6}$. (d) $\tilde{T} = 1\times10^{-5}$. (e) $\tilde{T} = 2\times10^{-5}$. (f) $\tilde{T} = 3\times10^{-5}$. (g) $\tilde{T} = 2\times10^{-4}$. (h) $\tilde{T} = 5\times10^{-4}$.

The thermal noise affects the full power spectrum in a surprising way. Perez *et al.*[19] found that in GCM's the broad peaks in the power spectrum sharpen up when increasing the noise. In Fig. 17 we show the power spectrum for $\sigma = 0.4$, $i_{dc} = 0.124$ as a function of temperature. We see that also in this case the broad peaks, due to the breakdown of the law of large numbers at $\tilde{T} = 0$, get sharper and better defined when increasing temperature [Figs. 17(a)–17(f)]. Only after $\tilde{T} > \tilde{T}_{c1}$ does the power spectrum start to become broadened by the thermal fluctuations [Figs. 17(g), 17(h)]. More quantitatively, following Ref. 19, we have defined the measure of sharpness,

$$W = -\log_{10}\left[\frac{1}{M}\frac{\sum_{l=1}^{M}\sum_{m=1}^{M}S(\omega_{l+m})S(\omega_m)}{\sum_{l=1}^{M}S(\omega_l)^2}\right], \quad (18)$$

where M is the number of discrete points in the spectrum. For a completely flat spectrum $W = 0$, and for a set of δ peaks, $W \to \infty$. We show in Fig. 18 the sharpness W as a function of $\tilde{T}$. We see that W increases with temperature until it reaches $\tilde{T}_{c1}$ where it drops abruptly.

Finally we analyze the effect of temperature in the pseudosteps in the IV characteristics. We show in Fig. 19 the IV curves for $\sigma = 0.4$ in the turbulent phase for different temperatures. We see that the pseudostep structure is stable up to temperatures much larger than $\tilde{T}_{c1}$ and slightly below $\tilde{T}_{c2}$, above which they disappear. Therefore, the pseudosteps seem to be more stable against thermal noise than the breakdown of the law of large numbers. This result suggests that even when both phenomena coexist, they are not completely correlated.

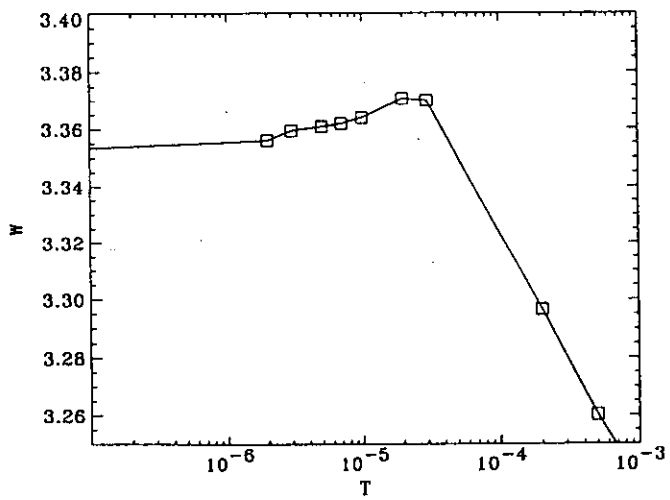

FIG. 18. Measure W of the sharpness of the peaks in the power spectra as a function of the temperature $\tilde{T}$. For $\tilde{g} = 0.2$, $\Omega_{rf} = 0.8$, $i_{rf} = 0.61$, $i_{dc} = 0.124$, $\sigma = 0.4$, and $N = 16384$.

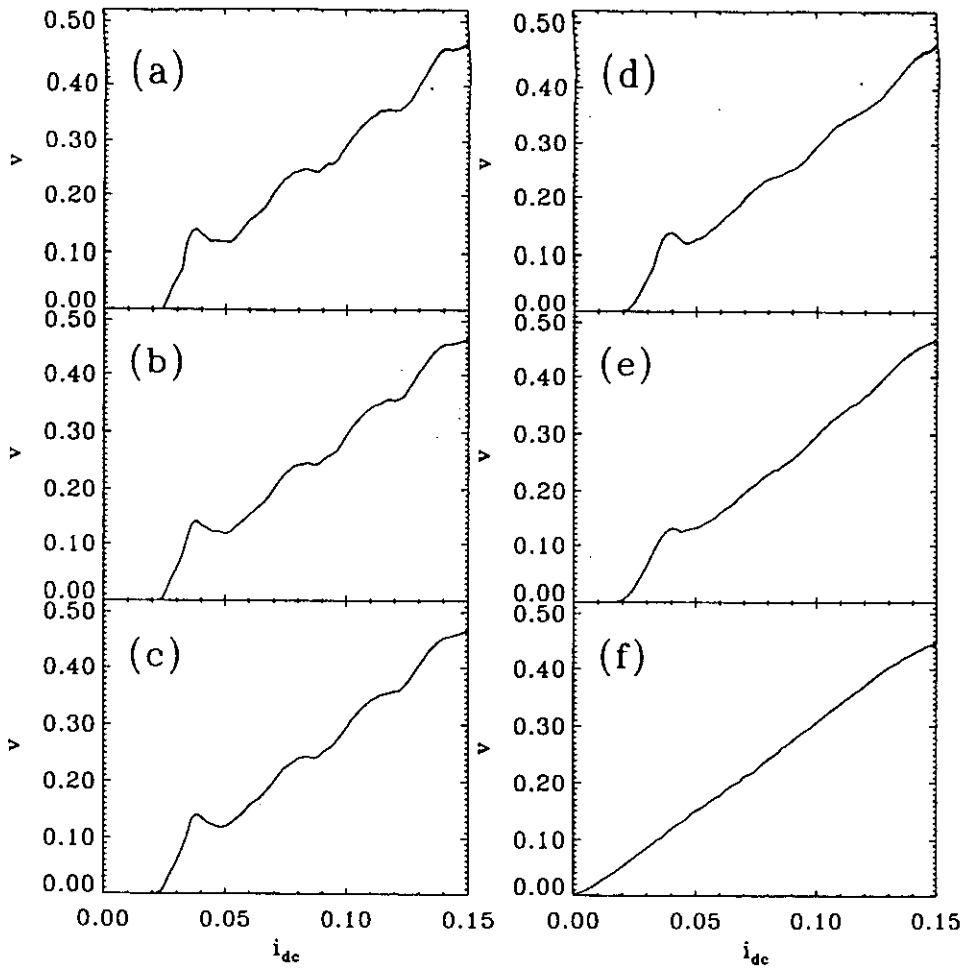

FIG. 19. *IV* characteristics in the turbulent phase for different temperatures $\tilde{T}$ and coupling $\sigma = 0.4$. For $\tilde{g} = 0.2$, $\Omega_{rf} = 0.8$, $i_{rf} = 0.61$. (a) $\tilde{T} = 0$. (b) $\tilde{T} = 1 \times 10^{-4}$. (c) $\tilde{T} = 2 \times 10^{-4}$. (d) $\tilde{T} = 5 \times 10^{-4}$. (e) $\tilde{T} = 1 \times 10^{-3}$. (f) $\tilde{T} = 1 \times 10^{-2}$.

VII. CONCLUSIONS

We have presented a system[11,12] in which many interesting phenomena that are being currently studied in globally coupled logistic maps[16–24] can be measured in concrete experiments. The JJSA's can show coherent, ordered, partially ordered, quasiperiodic, and turbulent phases in their *IV* characteristics. The coherent phase exists for $i_{dc} < i_c$ or for large bias currents. The ordered phase corresponds to the Shapiro steps, for which we have found that the number of big clusters is equal to the order of the step. The turbulent phase of the JJSA shows a breakdown of the law of large numbers. The new feature in this system is that this effect coexists with the appearance of pseudosteps in the *IV* characteristics.

A closely related system is charge density waves. Also in this case there are many coupled degrees of freedom, which have been recently described with a global coupling model.[37] Including a second time derivative term in their equations (due to the displacement current) may lead to the same kind of phenomena studied here.

Josephson junction series arrays like the one discussed in this paper can be fabricated with the present techniques.[13] One possible experiment consists in making an underdamped JJSA with a large number of junctions ($N \sim 10^3$–10^5). At very low temperatures, there will be true Shapiro steps, with no broad-band noise ($S_0 = 0$), and pseudosteps with broad-band noise ($S_0 \neq 0$). A measurement of the broad-band noise S_0 as a function of temperature should show first a plateau below a temperature T_{c2}, and then a sharp increase when decreasing temperature below a critical T_{c1} (for junctions with $I_c = 1$ μA, $T_{c1} \sim 1$ mK, $T_{c2} \sim 0.1$ K). This would be a clear indication of the breakdown of the law of large numbers. Of course, experiments with JJSA's with different number of junctions of the same characteristics will be a more direct verification. A comparison of the different *IV* curves and the different power spectra as a function of N would show clearly the breakdown of the law of large numbers and the emergence of pseudosteps, as described here.

ACKNOWLEDGMENTS

We acknowledge C. Pando-Lambruschini and G. Pérez for useful discussions. H.A.C. also acknowledges support from the Instituto Nazionale di Fisica Nucleare (Italy).

[1] See, for example, *KT Transition and Superconducting Arrays*, Proceedings of the 2nd CTP Workshop on Statistical Physics, edited by D. Kim *et al.* (Min Eum Sa, Seoul, 1993).
[2] P. Hadley and M. R. Beasley, Appl. Phys. Lett. **50**, 621 (1987); P. Hadley, M. R. Beasley, and K. Wiesenfeld, Phys. Rev. B **38**, 8712 (1988).
[3] K. Wiesenfeld and P. Hadley, Phys. Rev. Lett. **62**, 1335 (1989).
[4] K. Y. Tsang, S. H. Strogatz, and K. Wiesenfeld, Phys. Rev. Lett. **66**, 1094 (1991); K. Y. Tsang and I. B. Schwartz, *ibid.* **68**, 2265 (1992).
[5] S. E. Strogatz and R. E. Mirollo, Phys. Rev. E **47**, 220 (1993); S. Watanabe and S. E. Strogatz, Phys. Rev. Lett. **70**, 2391 (1993); Physica D **74**, 197 (1994).
[6] S. P. Benz, M. S. Rzchowski, M. Tinkham, and C. J. Lobb, Phys. Rev. Lett. **64**, 693 (1990); H. C. Lee, R. S. Newrock, D. B. Mast, S. E. Hebboul, J. C. Garland, and C. J. Lobb, Phys. Rev. B **44**, 921 (1991); S. E. Hebboul and J. C. Garland, *ibid.* **43**, 13 703 (1991).
[7] K. H. Lee, D. Stroud, and J. S. Chung, Phys. Rev. Lett. **64**, 692 (1990); J. U. Free, S. P. Benz, M. S. Rzchowski, M. Tinkham, C. J. Lobb, and M. Octavio, Phys. Rev. B **41**, 7267 (1990); M. Kvale and S. E. Hebboul, *ibid.* **43**, 3720 (1991); H. Eikmans and J. E. van Himbergen, *ibid.* **44**, 6937 (1991).
[8] D. Domínguez, J. V. José, A. Karma, and C. Wiecko, Phys. Rev. Lett. **67**, 2367 (1991); D. Domínguez and J. V. José, *ibid.* **69**, 414 (1992); Phys. Rev. B **48**, 13 717 (1993); Int. J. Mod. Phys. B **8**, 3749 (1994).
[9] F. Falo, A. R. Bishop, and P. S. Lomdahl, Phys. Rev. B **41**, 10 983 (1990); N. Gronbech-Jensen, F. Falo, A. R. Bishop, and P. S. Lomdahl, *ibid.* **46**, 11 149 (1992); R. Mehrotra and S. R. Shenoy, Europhys. Lett. **9**, 11 (1989); Phys. Rev. B **46**, 1088 (1992).
[10] R. Bhagavatula, C. Ebner, and C. Jayaprakash, Phys. Rev. B **45**, 4774 (1992).
[11] D. Domínguez and H. A. Cerdeira, Phys. Rev. Lett. **71**, 3359 (1993); in *Chaos in Mesoscopic Systems*, Proceedings of the Adriatico Research Conference, Trieste, 1993, edited by H. A. Cerdeira and G. Casati (World Scientific, Singapore, 1995).
[12] D. Domínguez and H. A. Cerdeira, Phys. Lett. A **200**, 43 (1995); in Proceedings of the ICTP-NATO Workshop, *Quantum Dynamics of Submicron Structures*, Trieste, edited by H. A. Cerdeira, B. Kramer, and G. Schön (Kluwer Academic, Dordrecht, 1995).
[13] A. K. Jain, K. K. Likharev, J. E. Lukens, and J. E. Sauvageau, Phys. Rep. **109**, 310 (1984); R. L. Kautz, C. A. Hamilton, and F. L. Lloyd, IEEE Trans. Magn. **MAG-23**, 883 (1987).
[14] S. P. Benz and C. J. Burroughs, Appl. Phys. Lett. **58**, 2162 (1991).
[15] J. P. Crutchfield and K. Kaneko, in *Directions in Chaos*, edited by Hao Bai-Lin (World Scientific, Singapore, 1987), p. 272.
[16] K. Kaneko, Phys. Rev. Lett. **63**, 219 (1989); Physica D **41**, 137 (1990); J. Phys. A **24**, 2107 (1991).
[17] K. Kaneko, Physica D **54**, 5 (1992).
[18] K. Kaneko, Phys. Rev. Lett. **65**, 1391 (1991); Physica D **55**, 368 (1992).
[19] G. Perez, S. Sinha, and H. A. Cerdeira, Physica D **63**, 341 (1993).
[20] G. Perez and H. A. Cerdeira, Phys. Rev. A **46**, 4792 (1992); G. Perez, C. Pando-Lambruschini, S. Sinha, and H. A. Cerdeira, *ibid.* **45**, 5469 (1992); S. Sinha, D. Biswas, M. Azam, and S. Lawande, *ibid.* **46**, 3193 (1992); **46**, 6242 (1992).
[21] S. Sinha, Phys. Rev. Lett. **69**, 3306 (1992).
[22] M. Ding and L. T. Wille, Phys. Rev. E **48**, R1605 (1993).
[23] A. S. Pinkovsky and J. Kurths, Phys. Rev. Lett. **72**, 1614 (1994).
[24] K. Kaneko (unpublished).
[25] B. A. Huberman, J. P. Crutchfield, and N. H. Packard, Appl. Phys. Lett. **37**, 750 (1980); E. Ben-Jacob, I. Goldhirsh, Y. Imry, and S. Fishman, Phys. Rev. Lett. **49**, 1599 (1982).
[26] M. H. Jensen, P. Bak, and T. Bohr, Phys. Rev. A **30**, 1960 (1984); **30**, 1970 (1984).
[27] M. Octavio and C. Readi Nasser, Phys. Rev. B **30**, 1586 (1984); M. Iansit, Q. Hu, R. M. Westervelt, and M. Tinkham, Phys. Rev. Lett. **55**, 746 (1985).
[28] R. L. Kautz and R. Monaco, J. Appl. Phys. **57**, 875 (1985); M. Levi, Phys. Rev. A **37**, 927 (1988).
[29] D. E. McCumber, J. Appl. Phys. **39**, 3113 (1968); W. C. Stewart, Appl. Phys. Lett. **10**, 277 (1968).
[30] A. Barone and G. Paternó, *Physics and Applications of the Josephson Effect* (Wiley, New York, 1982).
[31] S. Shapiro, Phys. Rev. Lett. **11**, 80 (1963).
[32] Recently, in Ref. 5, it has been shown that JJSA's with a resistive load, but overdamped ($g = \infty$), and with a dc drive ($I_{rf} = 0$), have $N - 3$ constants of motion.
[33] D. Hansel, G. Mato, and C. Meunier, Phys, Rev. E **48**, 3470 (1993).
[34] K. Okuda, Physica D **63**, 424 (1993).
[35] D. Hansel and H. Sompolinsky, Phys. Rev. Lett. **68**, 718 (1992); Softky *et al.*, J. Neurosci. **48**, 1302 (1993); Wei Wang, G. Pérez, and H. A. Cerdeira, Phys. Rev. E **47**, 2893 (1993).
[36] H. S. Greenside and E. Helfand, Bell. Syst. Tech. J. **60**, 1927 (1981).
[37] J. Levy, M. S. Sherwin, F. F. Abraham, and K. Wiesenfeld, Phys. Rev. Lett. **68**, 2968 (1992); M. J. Higgins, A. A. Middleton, and S. Bhattacharya, *ibid.* **70**, 3784 (1993); A. Montakhab, J. M. Carlson, and J. Levy (unpublished).

Coupled maps on trees

Prashant M. Gade and Hilda A. Cerdeira
International Centre for Theoretical Physics, P.O. Box 586, Trieste 34100, Italy

Ramakrishna Ramaswamy
School of Physical Sciences, Jawaharlal Nehru University, New Delhi 110 067, India
(Received 20 September 1994; revised manuscript received 4 April 1995)

We study coupled maps on a Cayley tree, with local (nearest-neighbor) interactions, and with a variety of boundary conditions. The homogeneous state (where every lattice site has the same value) and the node-synchronized state (where sites of a given generation have the same value) are both shown to occur for particular values of the parameters and coupling constants. We study the stability of these states and their domains of attraction. Since the number of sites that become synchronized is much higher compared to that on a regular lattice, control is easier to achieve. A general procedure is given to deduce the eigenvalue spectrum for these states. Perturbations of the synchronized state lead to different spatiotemporal structures. We find that a mean-field-like treatment is valid on this (effectively infinite dimensional) lattice.

PACS number(s): 05.45.+b, 47.20.Ky

I. INTRODUCTION

Coupled map lattices (CML's) have been explored in a variety of contexts in recent years, particularly as prototypes of spatially extended systems. These are simple models wherein both space and time play a role; furthermore, it is anticipated that the insight gained over the past two decades in studying low-dimensional nonlinear dynamical systems can be profitably exploited in providing an understanding of such complex systems [1].

The phenomenology displayed by coupled maps on regular one- and two-dimensional lattices has been extensively studied by Kaneko [2]. In addition, CML's have been used to model a wide variety of complex phenomena, such as the study of the kinetics of phase ordering processes [3], crystal growth [4], neuronal systems [5], optical fibers [6], and pattern formation [7]. Chaté and Manneville have also used CML's to model spatiotemporal intermittency [8]. A route to a spatiotemporally inhomogeneous state through wavelength doubling bifurcations has also been recently identified [9].

In this paper, we study coupled maps on a Cayley tree. This lattice is embedded in infinite dimensions and thus should give some indication of CML phenomenology in higher dimensions [10]. Although the Cayley tree (sometimes termed the Bethe lattice) is an idealized hierarchical lattice with no immediate physical application, it is convenient for study since there are no closed loops. Furthermore, the Bethe lattice is the simplest sort of branching media model encountered in many physical processes.

Previous studies of coupled map systems (except for a study by Cosenza and Kapral [11] of CML's on a Sierpinski gasket) have largely been carried out with local coupling on regular lattices in one and two dimensions or with global coupling, in which case there is no notion of lattice geometry. Our motivation in choosing the Bethe lattice is twofold. Apart from the mathematical convenience, it is worth considering that in many physical situations the medium supporting dynamics could be nonuniform; in cases like chemical reactions in porous media or on diffusion-limited-aggregation clusters, heterogeneity can lead to hierarchical structures [12]. We note that hierarchical structures have long since been studied in spatiotemporal systems like neural nets, also because of their exponentially higher storage capacity [13].

A related question of some current interest is the control of macroscopically cascaded dynamical systems. The synchronization of a large set of oscillators connected in series [14–17] in a given geometry and with particular boundary conditions is directly related to the problem of whether a similar CML can support a synchronized state [18]. We address this problem and show below that the criterion in CML's for a synchronized (but chaotic) state to be stable is that only *one* Lyapunov exponent be positive and all the rest negative. In both cases, i.e., synchronization of the coupled oscillators or of coupled maps, the essence of the problem lies in the nature of the eigenvalues and eigenvectors of the interaction matrix. In the present work we deal with the situation of asymmetric coupling that is easily obtained in experiments [19].

The plan of this paper is as follows. We define our model and the boundary conditions, and show that the stability of synchronized states depends on the spectrum of eigenvalues of the interaction matrix. This is related to the connectivity matrix for the lattice and has a singular-continuous structure. Different patterns can arise from the secondary instabilities. We note that for coupled piecewise linear maps the study of the interaction matrix gives the whole Lyapunov spectrum, which is related to the correlation length.

In several recent studies of globally coupled maps [2,20], a breakdown of the "law of large numbers" has been observed. We find that for this system, even with local coupling, the mean-field description is valid in the

1063-651X/95/52(3)/2478(8)/$06.00

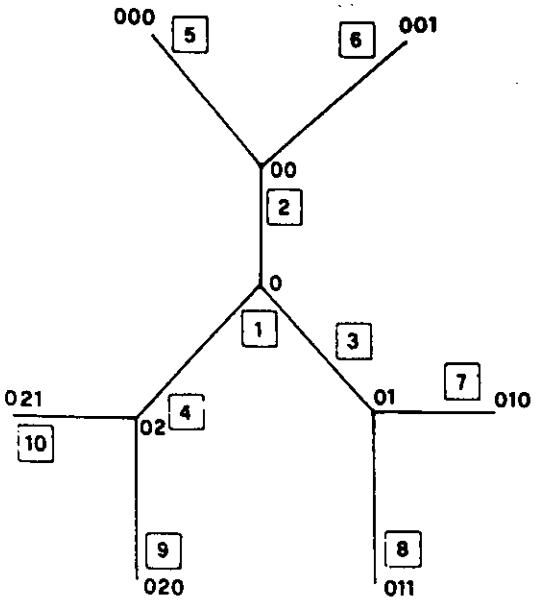

FIG. 1. Cayley tree with three generations and the labeling scheme.

evolution rules and remain synchronized. With parameters

$$o_0 + 3o' = b_0 + b' = h_0 + h_p + 2h_d = 1 \ , \qquad (10)$$

another simple pattern is possible. This is also node-homogeneous, with $z_i = z$ for all i; i.e., all the points on the lattice are synchronized since the evolution is essentially that of a single map f.

These "allowed" patterns can be observed in practice if and only if they are linearly and convectively stable against small perturbations. In the present work, we have mainly dealt with linear stability analysis of this system in the stationary frame, and while we have not analyzed convective stability, numerical experiments suggest that no extra instabilities other than the ones in an equivalent one-dimensional model creep in. This directly evolves from the fact that there are no loops on the lattice; there is only one direction in which instabilities can be enhanced in a moving frame of reference, and these are the same as in the equivalent one-dimensional model.

For the linear stability analysis the eigenvalues and eigenvectors of the matrix $J = \lim_{\tau\to\infty} J(\tau)$, where $J(\tau) = J_\tau \cdots J_2 J_1$, are (asymptotically) relevant. The Jacobian matrix at time t, i.e., J_t, is given by $J_t(i,j) = I(i,j) f'(x_j(t))$ and $x_j(t) = x(t)$ for all j. Thus the Jacobian matrix is $J = \lim_{\tau\to\infty} [I]^\tau f'(x_\tau) f'(x_{\tau-1}) \cdots f'(x_1)$. The eigenvalues of J are $\lim_{\tau\to\infty} \lambda_i^\tau$, where $\lambda_i = v_i \lambda$, where v_i, $i = 1,2,\ldots,g(k)$ are the eigenvalues of the interaction matrix I and $\lambda = \lim_{t\to\infty} |f'(x(t)) f'(x(t-1)) \cdots f'(x(1))|^{1/t}$. The relevant eigenvectors are those of I, and the problem reduces to a study of the eigenvalues and eigenvectors of the interaction matrix.

The fact that coherent patterns are allowed [by the condition in Eq. (10)] implies that a right eigenvector of the interaction matrix is $e_1 = (1,1,\ldots,1)$. This is a characteristic of row stochastic matrices and corresponds to the eigenvalue λ for the product of the J's. From Greshgorin's theorem [22] this is the largest eigenvalue. Consider a small deviation, $\Delta_0 = (\delta_1, \delta_2, \ldots, \delta_{g(k)})$ from the homogeneous pattern $(x,x,\ldots)$. We can reexpress Δ_0 on the basis of eigenvectors $e_1, e_2, \ldots, e_{g(k)}$ as

$$\Delta_0 = a_1 e_1 + a_2 e_2 + \cdots + a_{g(k)} e_{g(k)}. \qquad (11)$$

After t iterations the deviation from the homogeneous condition will be

$$\Delta_t = a_1 \lambda_1^t e_1 + a_2 \lambda_2^t e_2 + \cdots + a_{g(k)} \lambda_{g(k)}^t e_{g(k)}. \qquad (12)$$

If the only eigenvalue with modulus greater than unity is $\lambda_1 = \lambda$ and $|\lambda v_j| < 1$ for $j > 1$, i.e., the rest are less than unity in magnitude, then for large enough t we can write

$$\Delta_t \simeq a_1 \lambda_1^t e_1 \ . \qquad (13)$$

The perturbation grows along the direction $e_1 = (1,1,\ldots,1)$, and any random deviation will eventually be homogenized.

Thus the necessary (though not sufficient) condition for the synchronized pattern to exist (and evolve chaotically in time) is that λ_1 be the only eigenvalue greater than unity and all others be less than unity in magnitude; a linearly stable coherent pattern—in the infinite lattice limit—therefore requires a finite *gap* in the eigenvalue spectrum of the interaction matrix.

The interaction matrix is analogous to the tight-binding Hamiltonian on the Bethe lattice [20], although the eigenvectors are different (since the matrix is not necessarily symmetrical or Hermitian). However, using similar arguments [20], one can see that all the sites at a given generation are equivalent in the sense that, if sites at every generation are synchronized, this pattern will continue to exist in the absence of small perturbations or noise since the evolution rule is the same for all of them. Furthermore, one can see that if any two sites that have the same parent are interchanged along with their subtrees, the system is left unchanged. Using the equivalence of all points at a generation and the permutation symmetries of the lattice, the similarity transformation that will block-diagonalize the interaction matrix can be deduced to be

$$S = \begin{pmatrix} 1 & 0 & 0 & 0 & 0 & 0 & 0 & 0 & 0 & 0 \\ 0 & 1 & 0 & 1 & 0 & 1 & 0 & 0 & 0 & 0 \\ 0 & 1 & 0 & 1 & 0 & -1 & 0 & 0 & 0 & 0 \\ 0 & 1 & 0 & -2 & 0 & 0 & 0 & 0 & 0 & 0 \\ 0 & 0 & 1 & 0 & 1 & 0 & 1 & 1 & 0 & 0 \\ 0 & 0 & 1 & 0 & 1 & 0 & 1 & -1 & 0 & 0 \\ 0 & 0 & 1 & 0 & 1 & 0 & -1 & 0 & 1 & 0 \\ 0 & 0 & 1 & 0 & 1 & 0 & -1 & 0 & -1 & 0 \\ 0 & 0 & 1 & 0 & -2 & 0 & 0 & 0 & 0 & 1 \\ 0 & 0 & 1 & 0 & -2 & 0 & 0 & 0 & 0 & -1 \end{pmatrix}. \qquad (14)$$

(The first three vectors follow from the fact that lattice points at each generation are equivalent. The fourth and sixth vectors simply represent the two linearly independent and mutually orthogonal interchanges possible between points at the second generation [(1,0,−1)

$(0,1,-1)$], while the fifth and seventh vectors are similar interchanges within siblings with the phase derived from the parent site. The last three vectors arise from the interchange among the siblings of the same parent.)

Thus the block-diagonalizing matrix is written using permutation symmetries of the underlying lattice; the blocks are as follows:

$$\begin{pmatrix} o_0 & 3o' & 0 \\ h_p & h_0 & 2h_d \\ 0 & b' & b_0 \end{pmatrix} . \tag{15}$$

The two doubly degenerate eigenvalues are the eigenvalues of the matrix given below. They correspond to the fact that one can have two independent permutations in the three branches at the first node:

$$\begin{pmatrix} h_0 & 2h_d \\ 3b' & b_0 \end{pmatrix} . \tag{16}$$

Finally we have the triply degenerate eigenvalue b_0 (reflecting the fact that one can have permutations among the daughters of any of the three branches at the second node without affecting the matrix). One can see that the consecutive blocks giving eigenvalues are just like earlier blocks except that the first row and column of the matrix are removed. This construction can be trivially extended to a matrix of higher order. The matrix $S^{-1}IS$ is block diagonal.

This scheme can be generalized to higher dimensions and the diagonalizing matrix for the kth stage can be deduced as follows. Specifying the nonzero components of the column vectors [in the notation of Eq. (4) to denote the components] the first k vectors are as follows:

$$\begin{aligned} &v^1_{n(a_1)} = 1, \\ &v^2_{n(a_1,a_2)} = 1, \\ &v^3_{n(a_1,a_2,a_3)} = 1, \end{aligned} \tag{17}$$

..., and

$$v^k_{n(a_1,a_2,a_3,\ldots,a_k)} = 1 \tag{18}$$

[e.g., the first three columns of the matrix defined in Eq. (14)]. Then we have two sets of $k-1$ vectors. One is

$$\begin{aligned} &\{v^{k+1}_{n(0,1)} = v^{k+1}_{n(0,2)} = 1, v^{k+1}_{n(0,3)} = -2\}, \\ &\{v^{k+2}_{n(0,1,a_3)} = v^{k+2}_{n(0,2,a_3)} = 1, v^{k+2}_{n(0,3,a_3)} = -2\}, \end{aligned} \tag{19}$$

..., and

$$\begin{aligned} \{v^{k+(k-1)}_{n(0,1,a_2,\ldots,a_k)} &= v^{k+(k-1)}_{n(0,2,a_2,\ldots,a_k)} \\ &= 1, v^{k+(k-1)}_{n(0,3,a_2,\ldots,a_k)} = -2\}. \end{aligned} \tag{20}$$

[See, e.g., the fourth and fifth columns in Eq. (14).] The other set is

$$\begin{aligned} &\{v^{2k}_{n(0,1)} = 1, v^{2k}_{n(0,2)} = -1\}, \\ &\{v^{2k+1}_{n(0,1,a_2)} = 1, v^{2k+1}_{n(0,2,a_2)} = -1\} , \end{aligned} \tag{21}$$

and

$$\{v^{2k-1+(k-1)}_{n(0,1,a_2,\ldots,a_k)} = 1, v^{2k-1+(k-1)}_{n(0,2,a_2,\ldots,a_k)} = -1\}. \tag{22}$$

[See, e.g., the sixth and seventh columns in Eq. (14).] The next three sets of $k-2$ vectors each are given as follows. The first is of the type

$$\begin{aligned} &\{v^{3k-1}_{n(0,1,1)} = 1, v^{3k-1}_{n(0,1,2)} = -1\}, \\ &\{v^{3k}_{n(0,1,1,a_4)} = 1, v^{3k}_{n(0,1,2,a_4)} = -1\}, \end{aligned} \tag{23}$$

..., and

$$\{v^{3k-2+(k-2)}_{n(0,1,1,a_4,\ldots,a_k)} = 1, v^{3k-2+(k-2)}_{n(0,1,2,a_4,\ldots,a_k)} = -1\}. \tag{24}$$

The second is

$$\begin{aligned} &\{v^{4k-3}_{n(0,2,1)} = 1, v^{4k-3}_{n(0,2,2)} = -1\}, \\ &\{v^{4k-2}_{n(0,2,1,a_4)} = 1, v^{4k-2}_{n(0,2,2,a_4)} = -1\}, \end{aligned} \tag{25}$$

..., and

$$\{v^{4k-4+(k-2)}_{n(0,1,1,a_4,\ldots,a_k)} = 1, v^{4k-4+(k-2)}_{n(0,1,2,a_4,\ldots,a_k)} = -1\}. \tag{26}$$

The last set is

$$\{v^{5k-5}_{n(0,3,1)} = 1, v^{5k-5}_{n(0,3,2)} = -1\} ,$$

and so on. [The last three columns in Eq. (14) are v^{3k-1}, v^{4k-3}, and v^{5k-5}. For $k > 3$ newer sets will appear.] Now we will have sets of vectors that will give blocks of size $k-3$. The next six blocks of $k-3$ vectors arise from permutations between the points on the fourth generation and their descendants and are of the same type as the three sets of $k-2$ vectors mentioned above, which result from the three independent permutations possible between the six points on the third generation. One can continue this scheme until reaching the boundary. The number of points on the boundary is $g(k) - g(k-1) = 3 \times 2^{k-2}$, and $[g(k) - g(k-1)]/2 = 3 \times 2^{k-3}$ permutation vectors are possible [see Eq. (5)], which will give a block of size 1 with the same degeneracy as the number of permutations possible on the boundary.

For boundary conditions in which $o_0 = h_0 + h_p$, $o' = 2h_d/3$, $b_0 = h_0 + 2h_d$, $b' = h_p$, at stage k, the first block of the block-diagonal form is

$$\begin{pmatrix} h_0+h_p & 2h_d & 0 & \cdots & 0 & 0 \\ h_p & h_0 & 2h_d & & 0 & 0 \\ \vdots & & & & & \vdots \\ 0 & 0 & 0 & & h_0 & 2h_d \\ 0 & 0 & 0 & \cdots & h_p & h_0+2h_d \end{pmatrix} , \tag{27}$$

which exploits the equivalence symmetry of all the sites at a given generation. The second block, which exploits the permutation symmetry of the points on the first generation, is

$$\begin{pmatrix} h_0 & 2h_d & 0 & \cdots & 0 & 0 \\ h_p & h_0 & 2h_d & & 0 & 0 \\ \vdots & & & & & \vdots \\ 0 & 0 & 0 & & h_0 & 2h_d \\ 0 & 0 & 0 & \cdots & h_p & h_0+2h_d \end{pmatrix} , \tag{28}$$

and so on. The last two blocks are

$$\begin{pmatrix} h_0 & 2h_d \\ h_p & h_0+2h_d \end{pmatrix}, \quad (h_0+2h_d) . \tag{29}$$

The first block of order k appears once in the block-diagonal form, the second of order $k-1$ appears twice, and next blocks of order $k-n$ ($k-1 \geq n \geq 2$) appears $3 \times 2^{n-2}$ times. The first k eigenvalues are therefore nondegenerate; then $k-1$ eigenvalues are doubly degenerate, $k-n$ eigenvalues have degeneracy $3 \times 2^{n-2}$ for $k-1 \geq n \geq 2$, etc.

From the structure of the matrices and their degeneracies, one sees that for the Cayley tree with one more generation, the $k-1$ degenerate blocks are retained (with, however, the doubly degenerate block becoming triply degenerate and other blocks doubling their degeneracy) with an additional block that has degeneracy 2. The block corresponding to nondegenerate eigenvalues is, however, completely changed. The density of states has to be singular continuous since the new eigenvalues that are created have a lower degeneracy; the eigenvalue spectrum is a sum of δ peaks and is nowhere differentiable, as is common in hierarchical systems [11,21].

In the situation where the synchronized state is linearly stable in the stationary frame, the typical degeneracy structure of eigenvalues is as shown in Fig. 2 for the parameters and boundary conditions as discussed below. The structure is generic if the system is linearly stable, but the width of the gap varies with the parameters. For piecewise linear maps; e.g., $f(x) = rx \bmod y$, the Jacobian is constant in time and the spectrum of eigenvalues of the interaction matrix determines the Lyapunov spectrum of the CML's, and thus (via the Lyapunov dimension) the fractal dimension.

We can see from the degeneracy structure that about a quarter of the eigenstates have their support fully from the boundary. The next layer is approximately half of this number, and so on, with the number of states that have their support up to a length l from the boundary reducing exponentially. This is in keeping with the expectation that the rate must be faster than that in finite-dimensional spaces where the number of modes with wave number $|\kappa| < \kappa$ is proportional to κ^d.

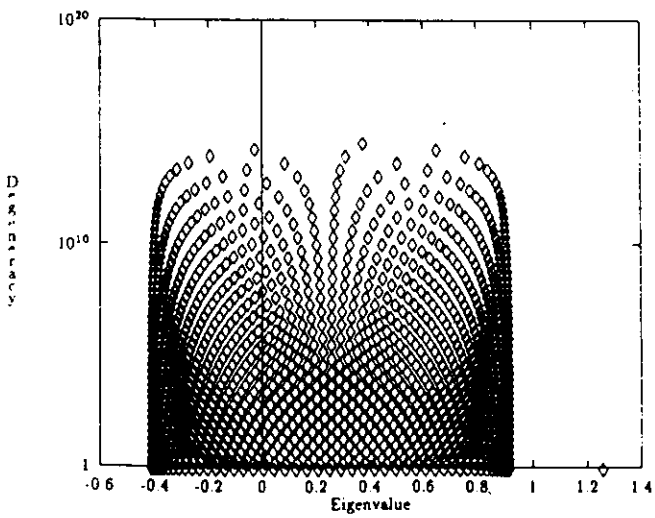

FIG. 2. Eigenvalues and their degeneracies for the synchronized state for $k = 50$ generations. The parameters are $h_p = 0.7$, $h_0 = 0.2$, $h_s = 0.05$, and $\lambda = 1.26$. One can clearly see the gap that separates a nondegenerate eigenvalue greater than unity and all the others below unity. Degeneracies are on a logarithmic scale for clarity.

Note that in the block-diagonal matrix, the blocks are tridiagonal and (for positive couplings) all elements are positive. Such a matrix can be transformed to symmetric form [22] and thus all its eigenvalues are real; there can be no Hopf bifurcation leading to the instability of a synchronized state.

Since the consecutive blocks are the principal (tridiagonal) submatrices of the earlier block, the eigenvalues are interlaced [23]. In other words, the bounds for the eigenvalues of the lower block are contained in the bounds for the eigenvalues for the higher block, and it is enough to consider the first two blocks in order to study the stability of a spatially synchronized state.

For the first block, the nondegenerate eigenvalues are given by $h_0 + h_p + 2h_d$, which is set to 1 by definition, and the other $k-1$ eigenvalues are $h_0 + 2\sqrt{2h_d h_p}\cos(\theta)$, where $\theta = 2\pi i/k$, $i = 1, 2, \ldots, k-1$. The eigenvalues will have a gap if $2h_d \neq h_p$.

Consider the second block of order $m = k-1$, which is tridiagonal and can be symmetrized by using a similarity transformation involving a diagonal matrix with elements $D_{i,i} = [\sqrt{2h_d/h_p}]^{i-1}$. This yields a tridiagonal matrix O such that the diagonal elements remain unchanged and all the elements on upper and lower diagonal are $\sqrt{2h_d h_p}$. Using Greshgorin's theorem [22] again, one can see that the largest eigenvalue cannot exceed $h_0 + 2\sqrt{2h_p h_d}$ if $h_p > 2h_d$. As explained above, the analysis of the first two blocks suffices to explore the stability of the synchronized state and thus the other blocks do not modify the gap in the eigenvalue spectrum of the first block if $h_p > 2h_d$.

Aranson, Golomb, and Sompolinsky [14] consider asymmetrically coupled one-dimensional (1D) chains with open boundary conditions where there is a convective instability of synchronized patterns; perturbations *grow* in the moving frame of reference, destroying macroscopic coherence. As we have shown above, under these conditions macroscopic chaos is linearly stable in a stationary frame also on the Cayley tree. However, the difficulty in synchronizing large systems is less pronounced in this case. Because of the ultrametric topology, much larger systems can be synchronized under the conditions above. With open boundary conditions and asymmetrical coupling, coherence is more easily established in the present case. For example, for $h_1 = 0.7$ in one direction and $h_2 = 0.1$ in the other direction, Aranson, Golumb, and Sompolinsky [14] have a coherence length of around 55 for the choice of map $f(x) = a - x^2$, with a value of a such that the eigenvalue for a single map is 1.26. With $h_p = 0.7$, $2h_d = 0.1$, Fig. 2 shows a plot of eigenvalues as a function of degeneracies at these parameter values for 50 generations. One can clearly see the gap between a single nondegenerate eigenvalue above unity and the others below unity. For the above parameters we can easily obtain a coherent pattern for $k = 20$ with random initial conditions; a CML with $\approx 10^6$ sites is easily synchronized [24] to within 10^{-4}, even under single precision (16 binary digits) evolution. This is in stark

contrast to one-dimensional 1D coupled CML, which has a coherence length of about 55 sites. This example is a good illustration of the dramatic increase in stability with hierarchical connectivity.

To check that no other instabilities than the ones expected from an equivalent one-dimensional model come into the picture, we looked at the function $f(x) = 1.39\,x \bmod 1$ with the same choice of coupling constants as above. Here the coherence is within 10^{-5} for the first six sites on a one-dimensional lattice, and even on the Cayley tree it is maintained for six generations. This is expected since there are no closed loops and the only direction in which the instabilities can *flow and grow* is the one from the center to the boundary. However, we can see that since the number of sites synchronized is exponentially higher on a tree with equivalent generations than on a one-dimensional lattice, an exponentially larger number of sites are synchronized on trees at equivalent parameters. The base of the exponent is related to the number of branches.

Auerbach [15] has shown that one can circumvent the difficulty arising from convective instabilities on a 1D lattice by using system-size dependent feedback control. In essence, we achieve the same ends through a change in geometry, without extra controls. The boundary conditions $o_0 = b_0 = h_0$, $o_p = 3b_d = h_p + 2h_s$ also give the same result, which indicates that some more variants are possible for open boundary conditions and asymmetric coupling.

Now consider the node-homogeneous pattern. The stability matrix is given by

$$J = \prod_{t=1}^{\infty} J_t \,. \tag{30}$$

Thus analysis of the eigenvalues of the product of matrices is reduced to the analysis of the eigenvalues of the product of blocks. This is a great simplification since instead of considering matrices of order 2^k, where k is the number of generations, we only need to consider k matrices of order k and below. The analysis of the Jacobian matrix reduces to analysis of the matrices

$$\prod_{t=1}^{\infty} \begin{pmatrix} o & 3o' & 0 & \cdots & 0 & 0 \\ h_p & h_0 & 2h_d & & 0 & 0 \\ \vdots & & & & & \vdots \\ 0 & 0 & 0 & & h_0 & 2h_d \\ 0 & 0 & 0 & \cdots & b' & b_0 \end{pmatrix} \begin{pmatrix} f'[z_1(t)] \\ f'[z_2(t)] \\ \vdots \\ f'[z_{k-1}(t)] \\ f'[z_k(t)] \end{pmatrix},$$

$$\prod_{t=1}^{\infty} \begin{pmatrix} h_0 & 2h_d & \cdots & 0 & 0 & \\ h_p & h_0 & 2h_d & & 0 & 0 \\ \vdots & & & & & \vdots \\ & 0 & 0 & & h_0 & 2h_d \\ & 0 & 0 & \cdots & b' & b_0 \end{pmatrix} \begin{pmatrix} f'[z_2(t)] \\ f'[z_3(t)] \\ \vdots \\ f'[z_{k-1}(t)] \\ f'[z_k(t)] \end{pmatrix}, \tag{31}$$

and so on.

Again the degeneracy structure is the same as for the interaction matrix; the Lyapunov spectrum is the sum of peaks and is an everywhere discontinuous function as for the fully synchronized state (which is a special case of the node-homogeneous structure). We can similarly argue that the condition for stability of the node-homogeneous state (evolving chaotically in time) is that the first block corresponding to the nondegenerate eigenvectors is the only one with eigenvalues of modulus greater than unity, all other blocks having eigenvalues with modulus less than unity. (This is because the first block corresponds to eigenvectors that have a contribution from all the generations, and the contribution from all the points of the same generation is the same.)

A simple example of such stable patterns can be constructed for $f(x) = rx \bmod 1$, with boundary conditions $o_0 = 0, b_0 = 0, o' = h_d, b' = h_p$ and parameters $r = \sqrt{(3)/2}, h_0 = 0,\ h_d = h_p = \frac{1}{3}$. For the Cayley tree with five generations, i.e., 46 sites, it can be shown that the eigenvalues are higher than unity for the first block alone. Numerically, one can easily get node-homogeneous patterns, starting from random initial conditions. Thus the possible coherent patterns are *characteristically* different from those on regular lattices, and the stability analysis is also distinct [26].

IV. INFINITE DIMENSIONAL CHARACTER

We now study the properties of this model, which should reflect the fact that it is embedded in infinite dimensions, where a mean-field-like treatment can be expected to be valid. A collective variable [2, 20] $h(t)$ is defined as

$$h(t) = \frac{1}{g(k)} \sum_{i=1}^{g(k)} x(i,t). \tag{32}$$

where $g(k)$ is the total number of sites on the Cayley tree with k generations, as noted above; $f(x) = \mu x(1-x)$ with $h_0 = 1-\epsilon$, $h_p = h_d = \epsilon/3$, $b_0 = o_0 = h_0$, $b' = \epsilon$, $o' = \epsilon/3$; while the parameter values are $\epsilon = 0.1$ and $\mu = 4$. The return map of this variable, i.e., $h(t+1)$ vs $h(t)$, is a filled ellipse, whose size decreases rapidly with the number of generations. We conjecture that in the macroscopic limit it tends to a fixed point; i.e., though the evolution is chaotic for the system, the collective variable is invariant in time. The mean square deviation of $h(t)$ decays like $1/N$, where N is the number of sites (see Fig. 3), quite unlike the case of globally coupled maps [27], where some reorganization occurs in such a way that the total number of independent degrees of freedom is not linearly proportional to the number of sites. This is not totally unexpected [28] since the values being summed are not independent random variables. This also means that the mean field is not valid in these systems. However, this expectation is fulfilled for the Bethe lattice, although the variables that are being summed are not only not independent but are also not identically distributed; the boundary evolves differently from the bulk, and boundary effects are not negligible in any limit since half the points reside at the boundary. Figure 4 shows the probability distribution of the central sites and the boundary for the above case, and they are clearly different. However, the sum behaves in a way that is expected from the

Verlag, New York, 1990).
[8] H. Chaté and P. Manneville, Physica D **32**, 409 (1988).
[9] R. E. Amritkar and P. M. Gade, Phys. Rev. Lett. **70**, 3408 (1993); P. M. Gade and R. E. Amritkar, Phys. Rev. E **49**, 2617 (1994).
[10] The number of sites in a d-dimensional lattice with lateral length l scales as l^d in any finite dimensional lattice. On the Cayley tree, this number scales as $\exp(l)$. See for example, R. J. Baxter, *Exactly Solvable Models in Statistical Mechanics* (Academic, New York, 1982).
[11] M. G. Cosenza and R. Kapral, Phys. Rev. A **46**, 1850 (1992).
[12] R. Kopelman, Science **241**, 1620 (1988); and for additional applications, see *The Fractal Approach to Heterogeneous Chemistry*, edited by D. Avnir (Wiley, New York, 1989).
[13] See, e.g., D. Amit, *Modelling Brain Function: The World of Attractor Neural Nets* (Cambridge University Press, Cambridge, 1989).
[14] I. Aranson, D. Golomb, and H. Sompolinsky, Phys. Rev. Lett. **68**, 3495 (1992); see also I. Aranson *et al.*, Nonlinearity **3**, 639 (1990).
[15] D. Auerbach, Phys. Rev. Lett. **72**, 1184 (1994).
[16] J. F. Heagy, T. L. Caroll, and L. M. Pecora, Phys. Rev. E **50**, 1874 (1994).
[17] T. L. Caroll, Phys. Rev. E **50**, 2580 (1994).
[18] In Ref. [16], where the control of cascaded dynamical systems is considered, the case of vector coupling in free-end, symmetrical one-dimensional chains of oscillators is worked out, and the condition for synchronization is a special case of the condition for synchronization in [14]. We would also like to point to G. A. Johnson *et al.*, Phys. Rev. E **51**, 1625 (1995), where the case of convectively unstable open flow is considered in coupled diode resonators.
[19] See, e.g., N. F. Rulkov *et al.*, Phys. Rev. E **51**, 980 (1995).
[20] M. S. Chen *et al.*, J. Chem. Phys. **46**, 1850 (1972).
[21] M. G. Cosenza and R. Kapral, Chaos **1**, 99 (1994).
[22] See, e.g., S. Barnett, *Matrices, Methods and Applications* (Oxford University Press, Oxford, 1990)
[23] A. Ostaszewski, *Advanced Mathematical Methods* (Cambridge University Press, Cambridge, 1990).
[24] The choice of a in [14] gives a larger eigenvalue than that quoted, so we chose $a = 1.5$, corresponding to the eigenvalue ≈ 1.22. The evolution with map $1.26x \bmod 1$ also gives similar results. Note also that the extent of synchronization depends on the noise level in the evolution. Our linear stability analysis merely guarantees the stability of the macroscopic coherent pattern under infinitesimal perturbations in stationary frame.
[25] T. Hogg, B. A. Huberman, and J. M. McGlade, Proc. R. Soc. London, Ser. B **237**, 43 (1989).
[26] Similar coherent structures on regular lattices are discussed in P. M. Gade, Ph.D. thesis, Poona University, 1993 (unpublished).
[27] K. Kaneko, Phys. Rev. Lett. **65**, 1391 (1990).
[28] S. Sinha, Phys. Rev. Lett. **69**, 3306 (1992); M. Grinasty and V. Hakim, Phys. Rev. E **49**, 2661 (1994); A. S. Pikovsky and J. Kurths, Phys. Rev. Lett. **72**, 1644 (1994); G. Perez *et al.*, Physica D **63**, 341 (1993); D. Dominguez and H. Cerdeira, Phys. Rev. Lett. **71**, 3359 (1993).
[29] H. Chaté and P. Manneville, Prog. Theor. Phys. **87**, 1 (1992).
[30] Some of the references are L. Pecora and T. M. Caroll, Phys. Rev. Lett. **64**, 821, (1990); Phys. Rev. A **44**, 2374, (1991); N. Gupte and R. E. Amritkar, Phys. Rev. E **48**, 1620 (1993); K. Pyragas, Phys. Lett. A **181**, 203 (1993). The list is prohibitively long.

Coherent-ordered transition in chaotic globally coupled maps

Fagen Xie[1,2] and Hilda A. Cerdeira[3]
[1]China Center of Advanced Science and Technology (World Laboratory), P.O. Box 8730, Beijing 100080, China
[2]Institute of Theoretical Physics, Academia Sinica, Beijing 100080, China
[3]International Center for Theoretical Physics, P.O. Box 586, 34100 Trieste, Italy
(Received 4 April 1996)

A spatial coherent and temporally chaotic state in globally coupled maps exists in the strong coupling regime. After the coherence loses stability the whole system is attracted to a two-cluster attractor $[M_1, M_2]$. The number of elements in the clusters depends on the initial conditions, which are chosen at random. We find, numerically, that the number of elements in the clusters obeys a power law decay near the onset of the transition. The difference of the two clusters displays a temporal behavior characteristic of on-off intermittency, although the distribution of the laminar phases shows a phase transition as a function of its length, making it essentially different from the latter. [S1063-651X(96)07809-9]

PACS number(s): 05.45.+b

The transition routes to chaos in low-dimensional nonlinear dynamical systems have been well understood. One of them, the intermittency route, was classified into three types by Pomeau and Manneville [1]. The essential feature of intermittency is that a simple periodic orbit is replaced by a chaotic attractor, where the chaotic behavior is randomly interspersed with periodic behavior resembling that before the transition, in an intermittent fashion. Recently, the statistical distribution of a different type of intermittency in some low-dimensional nonlinear dynamical systems, called "on-off" intermittency, has been obtained analytically [2–10]. This intermittency is characterized by a two-state nature. The "off" state, which is nearly constant, and remains so for very long periods of time, is suddenly changed by random bursts, the "on" state, which departs quickly from and returns quickly to the "off" state. A self-organized on-off spatiotemporal intermittency has also been reported in a system of coupled maps via nearest-neighbors interaction [11]. In this paper we focus our attention on some transitions that take place in globally coupled chaotic systems.

Globally coupled systems are ubiquitous in nature. They arise naturally in studies of Josephson junction arrays, multimode laser, charge-density wave, oscillatory neuronal system, and so on [12–14]. As one of the simplest globally coupled system, the globally coupled map (GCM) has been the subject of intensive research in recent years. Some rather surprising and novel results, such as clustering, splay state, collective chaotic behavior, and violation of the law of large numbers in the turbulent regime are revealed in the GCM model [15–18]. In this paper we will study the transition to intermittency in the GCM model, which takes place between the coherent and the ordered phases.

Specifically, we use the following form of GCM:

$$x_{n+1}^i=(1-\epsilon)f(x_n^i)+\frac{\epsilon}{N}\sum_{j=1}^{N} f(x_n^j), \quad i=1,2,\ldots,N, \quad (1)$$

where n, i, and ϵ are the discrete time step, the index of elements, and the coupling coefficient, respectively. The mapping function $f(x)$ is taken as the logistic map $f(x)=ax(1-x)$, and a is the nonlinear parameter. N is the total number of elements or system size.

An important concept in GCM model is "clustering." This means that even when the interactions between all elements are identical, the dynamics can break into different clusters, each of which consists of fully synchronized elements. After the system falls in an attractor, we say that the elements i and j belong to the same cluster if $x_n^i \equiv x_n^j$. Therefore, the behavior of the whole system can be characterized by the number of clusters n_{cl}, and the number of elements of each cluster $(M_1, M_2, \ldots, M_{n_{cl}})$ [15].

As the nonlinearity or coupling strength is varied, the system exhibits successive phase transitions among coherent, order, and turbulent phases [15]. We shall study the transition from the coherent chaotic state to a two-cluster chaotic attractor in the strong coupling regime.

In the coherent chaotic region the system is homogeneous in space, i.e., $x^i \equiv x^j$, $\forall i,j$, and chaotic in time. Thus, it is characterized by only one cluster, i.e., $n_1=1$, $M_1=N$. The motion of each element is equivalent to that of the single logistic map. The stability condition for this coherent state is that modulus of all eigenvalues of the $N\times N$ stability matrix $J=\Pi_{n=1}^{m} f'(x_n) J_0{}^m$ has magnitude less than *one*. Here $f'(x_n)$ is the derivative of the nth iteration of the logistic map; m is taken as the periodic number or infinity for periodic or chaotic motions, respectively. $\mathbf{J_0}$ is a $N\times N$ constant matrix given by

$$\begin{pmatrix} 1-\epsilon+\frac{\epsilon}{N} & \frac{\epsilon}{N} & \cdots & \frac{\epsilon}{N} \\ \frac{\epsilon}{N} & 1-\epsilon+\frac{\epsilon}{N} & \cdots & \frac{\epsilon}{N} \\ \cdots & \cdots & \cdots & \cdots \\ \frac{\epsilon}{N} & \frac{\epsilon}{N} & \cdots & 1-\epsilon+\frac{\epsilon}{N} \end{pmatrix}. \quad (2)$$

The matrix $\mathbf{J_0}$ is a circulant matrix, and can be written as

1063-651X/96/54(4)/3235(4)/$10.00

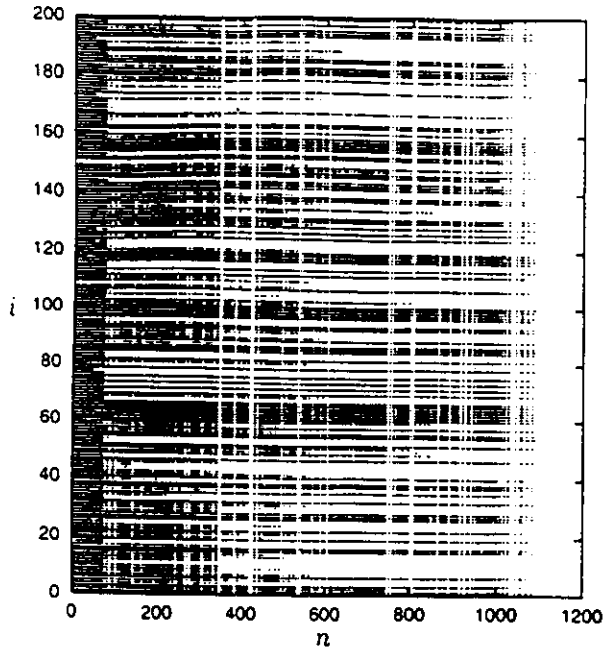

FIG. 1. Space-time evolution of the system at $N=200$, $a=4$, and $\epsilon=0.501$.

$$J_0=M_{\text{circ}}\left(1-\epsilon+\frac{\epsilon}{N},\frac{\epsilon}{N},\ldots,\frac{\epsilon}{N},\frac{\epsilon}{N}\right). \tag{3}$$

The eigenvalues of $\mathbf{J_0}$ are given by

$$\mu_{0,1}=1,$$

$$\mu_{0,r}=1-\epsilon+\frac{\epsilon}{N}\sum_{j=0}^{N-1}e^{i2\pi(r-1)j/N}\equiv 1-\epsilon,$$

$$r=2,3,\ldots,N. \tag{4}$$

Thus the eigenvalues of the stability matrix $\mathbf{J}$ are

$$\mu_1=\prod_{n=1}^{m}f'(x_n),$$

$$\mu_r\equiv(1-\epsilon)^m\prod_{n=1}^{m}f'(x_n),\quad r=2,3,\ldots,N. \tag{5}$$

The eigenvector corresponding to the eigenvalue μ_1 is given by $(1/\sqrt{N})(1,1,\ldots,1)^T$. Thus, the amplification of a disturbance along this eigenvector does not destroy the coherence. Eigenvectors for the other $N-1$ identical eigenvalues are not uniform; the amplification along these eigenvectors destroys the coherent phase. Therefore, the stability condition of the coherent chaotic state is decided by the $N-1$ identical eigenvalues. Their corresponding Lyapunov exponents are

$$\lambda=\lambda_r\equiv\ln(1-\epsilon)+\lambda_0,\quad r=2,3,\ldots,N. \tag{6}$$

where λ_0 is the Lyapunov exponent of the single logistic map. Therefore, the critical stability condition is given by $\lambda=0$, i.e., $\epsilon_c=1-e^{-\lambda_0}$. When ϵ is larger than ϵ_c, all elements quickly evolve to the same motion (the homogeneous state) after a short transient process, since $\lambda<0$. Generally speaking, we are only interested in the parameters where the behavior of the single logistic map is chaotic, $\lambda_0>0$. We have performed calculations for different values of a within the chaotic region. The results that we shall describe hold for all of them, therefore, we fix $a=4$ and $N=200$, where $\lambda_0=\ln 2$, thus, we have $\epsilon_c=\frac{1}{2}$. Figure 1 shows a space-time evolution at $\epsilon=0.501$. The initial condition of each element is randomly chosen in the uniform interval [0,1] throughout this paper. It is very clearly observed that all elements synchronize after almost 1100 iterations. We make the figure according to the rule: if $|x_n(i)-x_n(1)|>10^{-4}$, then the corresponding pixel is black, otherwise, it stays white.

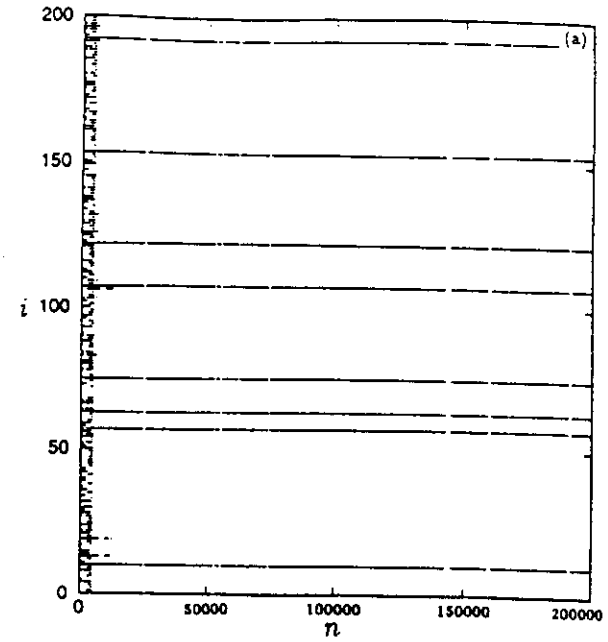

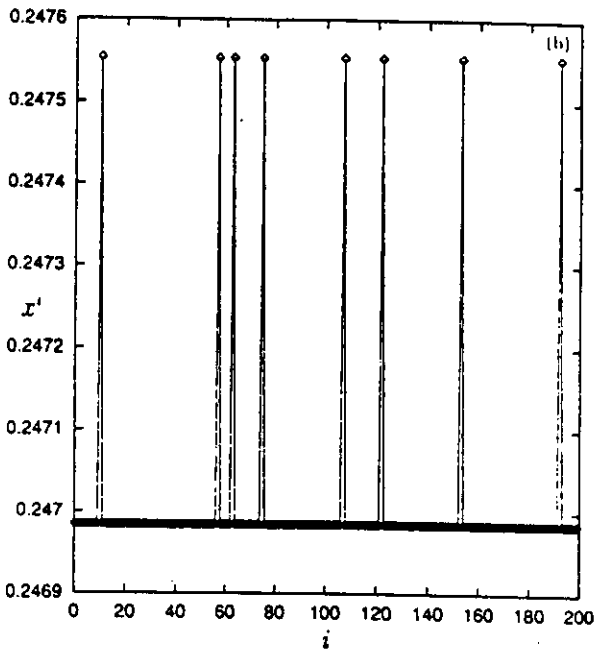

FIG. 2. (a) The same as in Fig. 1 for $\epsilon=0.499$. (b) The space structure of the system after the (3×10^5)th iterations of Eq. (1). Two clusters are clearly observed.

When the coupling ϵ is slightly smaller than the critical

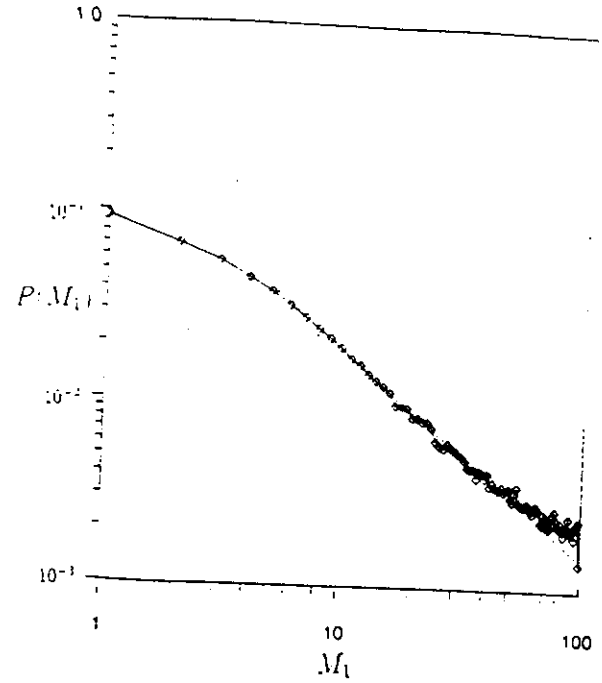

FIG. 3. The distribution of various M_1 (log-log plottings) for $\epsilon=0.499$. The dashed line is the perfect -1.11 power law decay.

value (0.5), the system suddenly evolves to a two-cluster attractor (M_1, M_2) $[M_1+M_2=N=200]$ after the transient process. Figure 2(a) shows a space-time evolution at $\epsilon=0.499$. After some iterations, the system is exactly settled down to a two-cluster chaotic attractor $(M_1, M_2)=(8,192)$. The space structure after the (3×10^5)th iterations is also displayed in Fig. 2(b). Two clusters are clearly observed. M_1 and M_2 depend on the chosen random initial conditions. Since the sum of M_1 and M_2 is always the same (200), only one of the two numbers can be varied freely. Assuming the

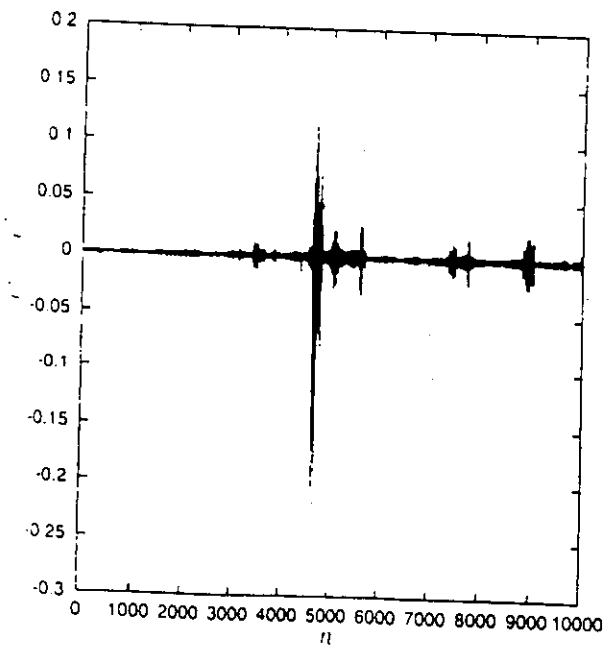

FIG. 4. The evolution of the difference of the two clusters after the transient process at $\epsilon=0.499$.

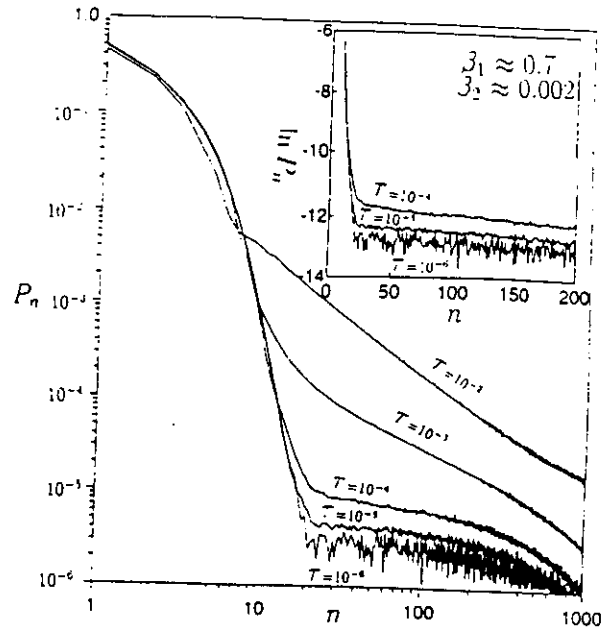

FIG. 5. The relative distribution P_n of the laminar phases of x^1-x^2 plotted against n (log-log plot in the large frame and n-log plot in the upper small frame) for several thresholds at $\epsilon=0.499$.

free variable to be M_1, with $M_1<M_2$, then we have $1\leq M_1\leq 100$. We choose many random initial conditions, and iterate Eq. (1) for each one, then found, numerically, that the distribution of various M_1's obeys an exact power law decay as the control parameter crosses the critical value from above. Figure 3 shows the distribution of M_1 for $\epsilon=0.499$. A total of 10^5 different random initial conditions to iterate Eq. (1) were computed to obtain this curve. Except for the first several points, this distribution is a bonafide power law decay with an approximate exponent -1.11.

When the system falls in a two-cluster attractor, the dynamics can be replaced by

$$x^i_{n+1}=(1-\epsilon)f(x^i_n)+\frac{\epsilon}{N}\sum_{j=1}^{2} M_j f(x^j_n), \quad i=1,2. \tag{7}$$

Although the behavior of each cluster is chaotic, the difference of the two clusters (x^1-x^2) shows some very interesting and complex features. Figure 4 shows a time evolution of x^1-x^2 for the same parameter as those of Fig. 2. It is easily observed that x^1-x^2 remains a long time near zero, and suddenly departs from it and quickly returns after some random bursts. As the deviation from ϵ_c becomes large, more and more random bursts frequently occur.

In order to better characterize the intermittent behavior, we have calculated numerically the statistical distribution of the duration of the laminar phase x^1-x^2 shown in Fig. 5 for several thresholds of the difference τ at $\epsilon=0.499$. These thresholds for the laminar phase are defined by $|x^1-x^2|<\tau$, with τ ranging from 10^{-2} to 10^{-6}. For each threshold a total of 2×10^9 iterations of Eq. (1) were computed to obtain these curves. P_n represents the probability of the laminar phase of length n, namely, $P_n=M_n/M$, where M is the total number of segments of the laminar phase, M_n the number of

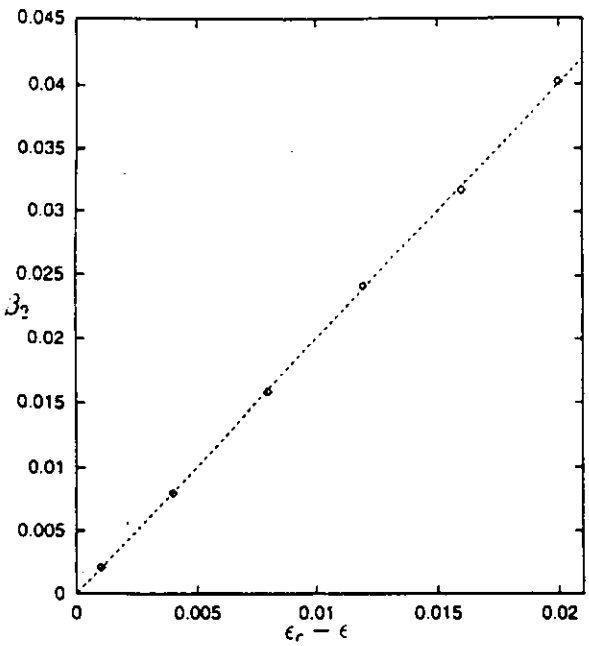

FIG. 6. β_2 vs $\epsilon_c - \epsilon$ at $\epsilon_c = 0.5$. The diamonds are numerical results. The slope of the dashed line is 2.

those of length n. The distribution has the following remarkable property. For small segments of the laminar phase ($n < 15$) the distribution quickly tends to the same exponential law decay with an asymptotic exponent -0.7 as the threshold τ decreases (see Fig. 5). We found numerically that this exponent is independent of the control parameters for small values of n, while for large segments of the laminar phase the distribution seems to depend on the threshold of the laminar phase. For large values of τ it obeys an asymptotic power law decay (see $\tau = 10^{-2}$). As the threshold decreases, this power law is gradually replaced by another one. The new exponent ($-\beta_2$) depends on the deviation of the parameter ϵ from the critical value ϵ_c. Figure 6 shows the relation of β_2 and the coupling deviation $\epsilon_c - \epsilon$. It can be best fitted by

$$\beta_2 = 2(\epsilon_c - \epsilon). \tag{8}$$

Actually, this statistical distribution should be independent of the threshold chosen for the laminar phase. In order to get the invariant distribution, we take smaller values of τ (10^{-5} is enough). The invariant distribution can be approximately formulated as

$$P_n \propto \begin{cases} e^{-\beta_1 n}, & n < n_s, \\ e^{-2(\epsilon_c - \epsilon)n}, & n > n_s. \end{cases} \tag{9}$$

where $\beta_1 \approx 0.7$ and $n_s \approx 15$. Thus, the distribution of the laminar phase described in this work shows a transition at n_s. Although this type of intermittency has similar characteristics to those of the conventional on-off intermittency (see Fig. 4), this transition does not exist in the latter, since its distribution obeys an asymptotic power law near the onset, with exponent $-\frac{3}{2}$.

In conclusion we have investigated the intermittency transition from a coherent chaotic state to a two-cluster chaotic attractor in globally coupled systems. We have found a new intermittency transition for globally coupled maps. We found that the numbers of elements in the clusters obey a power law decay near the onset of the transition. We have seen that this type of intermittency is essentially different from the types of intermittency known before, showing a phase transition as a function of the length of the laminar phase. The features of this type of intermittency are rather generic for globally coupled chaotic systems and are independent of the local mapping function, which we have taken as the logistic map to illustrate the phenomenon. Both spatially global uniform coupling and chaotic motion of the individual elements are of crucial importance.

[1] Y. Pomeau and P. Manneville, Commun. Math. Phys. **74**, 189 (1980).
[2] H. Fujisaka and T. Yamada, Prog. Theor. Phys. **69**, 32 (1983); **74**, 919 (1985).
[3] L. Yu, E. Ott, and Q. Chen, Phys. Rev. Lett. **65**, 2935 (1990).
[4] N. Platt, E. A. Spiegel, and C. Tresser, Phys. Rev. Lett. **70**, 279 (1993).
[5] J. F. Heagy, N. Platt, and S. M. Hammel, Phys. Rev. E **49**, 1140 (1994).
[6] P. W. Hammer, N. Platt, S. M. Hammel, J. F. Heagy, and B. D. Lee, Phys. Rev. Lett. **73**, 1095 (1994).
[7] E. Ott and J. C. Sommerer, Phys. Lett. A **188**, 39 (1994).
[8] S. C. Venkataramani, T. M. Antonsen Jr., E. Ott, and J. C. Sommerer, Phys. Lett. A **207**, 173 (1995).
[9] Y. C. Lai and C. Grebogi, Phys. Rev. E **52**, R3313 (1995).
[10] A. S. Pikovsky and J. Kurths, Phys. Rev. Lett. **72**, 1644 (1994).
[11] J. Redondo, E. Roldán, and G. J. de Valcárcel, Phys. Lett. A **210**, 301 (1996).
[12] Fagen Xie, Gang Hu, and Zhilin Qu, Phys. Rev. E **52**, R1265 (1995).
[13] K. Wiesenfeld, and P. Hadley, Phys. Rev. Lett. **62**, 1335 (1989).
[14] D. Domínguez, and H. A. Cerdeira, Phys. Rev. Lett. **71**, 3359 (1993); Phys. Rev. B **52**, 513 (1995).
[15] H. G. Winful and L. Rahman, Phys. Rev. Lett. **65**, 1575 (1990).
[16] K. Kaneko, Phys. Rev. Lett. **63**, 219 (1989); **65**, 1391 (1990); Physica D **41**, 137 (1990); D **55**, 368 (1992).
[17] G. Perez and H. A. Cerdeira, Phys. Rev. A **46**, 7492 (1992); Phys. Rev. E **49**, R15 (1994).
[18] G. Perez, S. Sinha, and H. A. Cerdeira, Physica D **63**, 341 (1993).

Clustering bifurcation and spatiotemporal intermittency in rf-driven Josephson junction series arrays

Fagen Xie[1] and Hilda A. Cerdeira[2]

1 *Institute of Theoretical Physics, Academia Sinica, Beijing 100080, China*

2 *International center for Theoretical Physics, P.O. Box 586, 34100 Trieste, Italy*

(July 23, 1997)

Abstract

We study the spatiotemporal dynamics of the underdamped Josephson junction series arrays (JJSA) which are globally coupled through a resistive shunting load and driven by an rf bias current. Clustering bifurcations are shown to appear. In particular, cluster-doubling induced period-doubling bifurcations and clustering induced spatiotemporal chaos are found. Furthermore, an interesting spatiotemporal intermittency is also found. These phenomena are closely related to the dynamics of the single cell.

The dynamics of globally chaotic systems has been of great interest in recent years. They arise naturally in studies of Josephson junctions arrays, multimode laser, charge-density wave, oscillatory neuronal system, and so on. Some rather surprising and novel features, such as clustering, splay state, collective behavior, and violation of the law of large numbers are revealed in these continuous and discrete globally coupled models [Benz et al.; 1990, Bhattacharya et al., 1987; Chernikov & Schmidt, 1995; Domínguez et al., 1991; Domínguez & Cerdeira, 1995; Eikmans & van Himbergen, 1991; Fisher, 1983; Free et al., 1990; Hadley & Beasley, 1987; Hadley et al., 1988; Hebboul & Garland, 1991; Kaneko, 1989; Kvale & Hebboul, 1991; Lee et al., 1992; Middleton et al., 1992; Strogatz & Mirollo, 1993; Tchiastiakov, 1996; Tsang et al., 1991; Tsang & Schwartz, 1992; Watanabe and Strogatz, 1993; Wiesenfeld et al., 1996].

Being a paradigm for the study of nonlinear dynamical systems with many degrees of freedom, Josephson junction series arrays (JJSA) have been a subject of active research. After scaling the parameters [Domínguez et al., 1991], the dynamical equations of an underdamped JJSA shunted by a resistive load, and subject to a rf-bias current $I(t) = I_{dc} + I_{rf}\sin(\omega_{rf}t)$,[Hadley & Beasley, 1987; Hadley et al., 1988; Tsang et al., 1991; Tsang & Schwartz, 1992] are

$$\begin{aligned} &\ddot{\phi}_i + g\dot{\phi}_i + \sin\phi_i + i_L = i_{dc} + i_{rf}\sin(\Omega_{rf}\tau), \\ &i_L = \sigma v(\tau) = \frac{\sigma}{N}\sum_{j=1}^{N} g\dot{\phi}_j, \quad i = 1,\ldots,N, \end{aligned} \tag{1}$$

where ϕ_i is the superconducting phase difference across the junction k. N is the total number of Josephson junctions or system size. Here, we use reduced units, with currents normalized by the critical current, $i = I/I_c$; time normalized by the plasma frequency $\omega_p t = \tau$, with $\omega_p = (\frac{2eI_c}{\hbar C})^{\frac{1}{2}}$ and C the capacitance of the junctions; and voltages by rI_c, with r the shunt resistance of the junctions. i_L is the current flowing through the resistive load; $g = (\frac{\hbar}{2eCr^2I_c})^{\frac{1}{2}} = \beta_c^{-\frac{1}{2}}$, with β_c the McCumber parameter [McCumber, 1968; Stewart, 1968]; $v = \frac{V_{total}}{N}$ is the total voltage across the array per junction; $\sigma = \frac{rN}{R}$, with R the resistance of the shunting load, represents the strength of the global coupling in the array;

and the normalized rf frequency is $\Omega_{rf} = \frac{\omega_{rf}}{\omega_p}$. Eq. (1) exhibits rich spatiotemporal behavior, including phase locking, bifurcations, chaos, solitonic excitation, and pattern formation, breaking the law of large numbers and novel pseudo-Shapiro steps emerge in turbulence [Benz et al., 1990; Domínguez et al., 1991; Domínguez & Cerdeira, 1995; Eikmans & van Himbergen, 1991; Free et al., 1990; Hebboul & Garland, 1991; Kvale & Hebboul, 1991; Lee et al., 1992]. However, to the best of our knowledge, the mechanism of the transitions among these dynamical phases, specially the transition from coherence to turbulence, has never been discussed. In this paper we study the interesting spatiotemporal intermittency, clustering bifurcation and clustering induced spatiotemporal chaos in the system (1).

For a single cell (i.e., $N = 1$), the dynamical equation reduces to

$$\ddot{\phi} + \bar{g}\dot{\phi} + \sin\phi = i_{dc} + i_{rf}\sin(\Omega_{rf}\tau), \tag{2}$$

with $\bar{g} = (1 + \sigma)g$. It is well known that Eq. (2) can exhibit chaotic behavior in the underdamped regime, i.e., $\bar{g} < 1$ and $\Omega_{rf} < 1$ [Ben-Jacob et al., 1982; Bhagavatula et al., 1992; Huberman et al., 1980; Iansiti et al., 1984; Jensen et al., 1984; Kautz & Monaco, 1985; Octavio & Raedi Nasser, 1984]. In Figs. 1(a) and 1(b) we show the bifurcation diagrams, for $\bar{g} = 0.2, \Omega_{rf} = 0.8$, as a function of i_{rf} and i_{dc} respectively. In Fig. 1(a) with $i_{dc} = 0.03$, the following points are to be remarked: as i_{rf} increases, the system undergoes a series of continuous period-doubling bifurcation leading to a small scale region of chaos. At $i_{rf} \approx 0.832$, this chaotic attractor suddenly expands, and is replaced by a large scale chaotic motion. After the expanding transition the system acquires a rotating motion, and the time-averaged voltage becomes nonzero. The bifurcation diagram as a function of i_{dc}, with $i_{rf} = 0.61$, is shown in Fig. 1(b). The bifurcation behavior is essentially different from that of Fig. 1(a). As i_{dc} increases, the period-1 orbit first loses its stability, then a new period-2 solution arises via period-doubling bifurcation. The most interesting and surprising point is that this period-doubling solution meets with an unstable period-2 orbit (the dashed lines), and they suddenly disappear via inverse tangent (saddle-node) bifurcation as i_{dc} reaches a critical value $i_{dc} \approx 0.035076$. Beyond this *threshold*, the behavior of the system

is rotating and the motion is chaotic in a large scale region, and have the characteristic of type-I intermittency [Pomeau & Manneville, 1980]. In Fig. 1(b), it is clear that another period-2 orbit appears via tangent bifurcation for i_{dc} near zero. Increasing i_{dc}, this period-2 solution first bifurcates into a small region of chaos through a series of continuous period-doubling bifurcations, then this chaotic motion coincides with the unstable period-2 orbit, and suddenly disappears due to a boundary crises [Grebpgi et al., 1983]. The two attractors form an interesting hysteresis phenomenon. In the following we investigate the complicated spatiotemporal dynamics in JJSA and how it originates from that of a single Josephson junction.

An important concept in a model for globally coupled systems is "clustering." This means that even when the interaction between all elements is identical, the dynamics can break into different clusters, each of which consists of fully synchronized elements. After the system falls in an attractor, we say that the elements i and j belong to the same cluster if $\phi_i \equiv \phi_j$ for all time. Therefore, the behavior of the whole system can be characterized by the number of clusters n_{cl}, and the number of elements of each cluster $(M_1, M_2, \cdots, M_{n_{cl}})$ [Domínguez Cerdeira, 1995; Kaneko, 1989].

The simplest attractor of the system (1) is the spatially homogeneous configuration, so called *coherent* state, i.e., $\phi_i(\tau) \equiv \phi(\tau)$, $n_{cl} = 1, M_1 = N$. Linearizing Eq. (1) around the $\phi(\tau)$ state

$$\delta\ddot{\phi}_i + g\delta\dot{\phi}_i + \cos\phi\delta\phi_i + \frac{\sigma}{N}\sum_{j=1}^{N} g\delta\dot{\phi}_j = 0, \quad i = 1, \ldots, N. \tag{3}$$

Introducing the difference coordinates defined by

$$Y_k = \delta\phi_k - \delta\phi_{k+1}, \quad k = 1, \ldots, N-1 \tag{4}$$

After simple algebra, the critical stability boundaries of this coherent state are determined by the *zero* Lyapunov exponent of the following set of equations:

$$\begin{aligned} &\ddot{\phi} + \bar{g}\dot{\phi} + \sin\phi = i_{dc} + i_{rf}\sin(\Omega_{rf}\tau), \\ &\ddot{Y}_k + g\dot{Y}_k + \cos\phi Y_k = 0. \end{aligned} \tag{5}$$

The critical boundaries of the coherent state in the σ vs. i_{rf} parameter plane are shown in Fig. 2(a) with $\bar{g} = 0.2$, and $i_{dc} = 0.03$. In the white region, the coherent state is *locally* stable, while in the shaded region, the coherent state loses its stability, and bifurcates to a multi-cluster state. As the coupling strength σ decreases to zero, the instability regions collapse to the discrete bifurcation points for a single cell ($\sigma = 0$). After the coherent state loses the stability, lots of multi-clusters are created in the JJSA. A class of interesting states are multi-clusters with a uniform distribution of junctions per cluster (i.e., $M_1 = \cdots = M_{n_{cl}}$, with M_i, being the number of elements in the ith cluster), and each cluster may have the same motion except for uniformly distributed phase shifts. We focus on this kind of states, a period-m state with k clusters will be called TmCk state. It often happens that $m = k$, then the dynamics of the TkCk state is reduced to

$$\ddot{\phi}(\tau) + g\dot{\phi}(\tau) + \sin\phi(\tau) + \frac{\sigma}{k}\sum_{j=1}^{k} g\dot{\phi}(\tau + \frac{2\pi}{\Omega_{rf}}j) = i_{dc} + i_{rf}\sin(\Omega_{rf}\tau). \tag{6}$$

To investigate the clustering bifurcations in JJSA with nonzero coupling, we show the asymptotic state of the system (1) in Fig. 2(b) as a function of i_{rf} with $\sigma = 0.1$ and the other parameters equal to those of Fig. 1(a). However, the bifurcation diagram is essentially different from that of Fig. 1(a). The T1C1 state first undergoes a cluster-period-doubling bifurcation at $i_{rf} \approx 0.662$ to create a stable T2C2 state. By increasing i_{rf}, the state undergoes further cluster-period-doubling bifurcations leading to spatiotemporal chaos. Fig. 2(b) is interesting due to the following novel features. First, we find a cluster-doubling induced period-doubling. The bifurcation point value is below the period-doubling condition for a single Josephson junction. Global coupling leads to cluster doubling at this parameter, which induces period doubling in time. Second, we find a cluster-doubling sequence 1-2-4 (and the induced period-doubling sequence). Nevertheless, the tendency of cluster doubling bifurcations leading to spatiotemporal chaos can still be seen in Fig. 2(c), where we plot number of clusters vs. i_{rf} for the state described in Fig. 2(b). Therefore, we conclude that spatiotemporal chaos is made possible by clusterization, and call it "clustering induced spatiotemporal chaos". Moreover, these cluster-doubling sequences grow from the period-

doubling sequences of the single cell due to the nonzero global coupling. As σ decreases to zero, the clustering-doubling sequences is identified as the period-doubling sequence of the single cell. If the period-doubling sequence of the single cell is broken off, then the character of the clustering bifurcation in JJSA also changes suddenly. This can be clearly seen in Fig. 3(a) which shows the asymptotic state of the system (1) along the i_{dc} axis, with $\sigma = 0.6$ and the other parameters are the same as those of Fig. 1(b). The T1C1 state first undergoes a cluster-period-doubling bifurcation at $i_{dc} \approx 0.02087$ to create a stable T2C2 state. However, since the period-doubling period-2 solution in the single cell (see Fig. 1(b)) is destroyed by the inverse saddle-node bifurcation by increasing i_{dc}, the T2C2 state in the JJSA is suddenly destroyed by the spatiotemporal intermittency transition near $i_{dc} = 0.02143$. In Figs. 2(b) and 3(a), first we run Eqs. (1) to get the coherent state from random initial conditions, then we compute Eqs. (1) by gradually increasing the parameter value (i_{dc} or i_{rf}) and by using the final state for the previous parameter value as the initial state for the new parameter value, in this way we can surely get clusters with a uniform distribution of cells for all cluster-doubling cascade. Fig. 3(b) shows the phase diagram among T1C1 state, T2C2 state and the turbulent phase in the σ vs i_{dc} plane. The two critical transition curves in Fig. 3(b) are obtained by the numerical simulation of the system (1). It is clear that the regime of the T2C2 state is very narrow. Figs. 4 show the snapshots of ϕ for the T1C1 state and T2C2 state after a long transient process. The features of coherence and two-cluster are clearly observed in Fig4. (a), and (b)-(c), respectively. The most interesting phenomenon is that the system suddenly evolves to a very complicated rotating motion as i_{dc} is increased beyond a critical value ($i_{dc} \approx 0.02143$ for $\sigma = 0.6$). The system falls in a large $n_{cl} \sim N$ clusters motion with all M_j small. Fig. 5 shows the space-time evolution after a very long and complicated transient process for $i_{dc} = 0.0215$ and $\sigma = 0.6$. The turbulent character of the motion is very clear. The evolution of ϕ_1 (the first junction) is displayed in Figs. 6(a) at the same parameters values as those of Fig. 5. The motion displays periodic behavior (2P) for a long time, is suddenly interrupted by large bursts and quickly resumes the periodic fashion. The similar features of the difference $\phi_1 - \phi_2$ are also

displayed in Fig. 6(b). As i_{dc} is far from the critical value, more and more random large bursts take place more frequently. Although this behavior is similar to the characteristic of well-known intermittency, which were investigated in the low-dimensional systems [Pomeau Manneville, 1980], it is an essential type of spatiotemporal intermittency, which has not been found before in the rf-driven JJSA or other high dimensional globally chaotic systems. The spatial variable, the dynamics of a single cell and the global coupling are of crucial importance for this interesting phenomenon.

In conclusion we analyzed the complex spatiotemporal dynamics of the rf-driven JJSA. Clustering bifurcation, clustering induced spatiotemporal chaos and spatiotemporal intermittency are shown to appear in these systems. The spatial variable, the dynamics of a single cell and the global coupling are of crucial importance for the existence of these interesting spatiotemporal phenomena.

REFERENCES

Ben-Jacob E., Goldhirsh I., Imry Y., and Fishman S. (1982) "Intermittent chaos in Josephson junctions", Phys. Rev. Lett. **49**, 1599.

Benz S.P., Rzchowski M.S., Tinkham M. and Lobb C.J. (1990), "Fractional giant Shapiro steps and spatially correlated phase motion in 2D Josephson arrays", Phys. Rev. Lett. **64**, 693.

Bhagavatula R., Ebner C. and Jayaprakash C.(1992), "Dynamics of capacitive Josephson junction arrays subjected to electromagnetic radiation", Phys. Rev.B **45**, 4774.

Bhattacharya S., Stokes J.P., Higgins M.J. and Klemm R.A. (1987), "Temporal coherence in the sliding charge-density wave condensate", Phys. Rev. Lett.**59**, 1849.

Chernikov A.A. and Schmidt G. (1995), "Conditions for synchronization in Josephson-junction arrays", Phys. Rev. E **52**, 3415.

Domínguez D., Jose J.V., Karma A. and Wiecko C. (1991), "Novel axisymmetric coherent vortex state in arrays of Josephson junction far from equilibrium", Phys. Rev. Lett. **67**, 2367.

Domínguez D.and Cerdeira H.A. (1995), "Spatiotemporal chaos in rf-driven Josephson-junction series arrays", Phys. Rev. B **52**, 513.

Eikmans H. and van Himbergen J.E. (1991), "Stability analysis of Shapiro steps in Josephson-junction arrays",, Phys. Rev. B **44**, 6937.

Fisher D.S. (1983), "Threshold behavior of charge-density waves pinned by impurities", Phys. Rev. Lett. **50**, 1486.

Free J.U., Benz S.P., Rzchowski M.S., Tinkham M., Lobb C.J. and Octavio M. (1990), "Dynamical simulations of fractional giant Shapiro steps in two-dimensional Josephson arrays", Phys. Rev. B **41**, 7267.

Grebogi C., Ott E. and Yorke J.A. (1983), "Crises, sudden changes in chaotic attractors and transient chaos", Physica **7D**, 181.

Hadley P. and Beasley M.R. (1987), "Dynamical states and stability of linear arrays of Josephson junctions", Appl. Phys. Lett. **50**, 621.

Hadley P.*et al.* (1988), "Phase locking of Josephson-junction series arrays", Phys. Rev. B **38**, 8712.

Hebboul S.E. and Garland J.C. (1991), "Radiofrequency spectral response of two-dimensional Josephson-junction arrays", Phys. Rev. B **43**, 13703.

Huberman B.A., Crutchfield J.P. and Packard N.H. (1980), "Noise phenomena in Josephson junctions", Appl. Phys. Lett. **37**, 750.

Iansiti M., Hu Q., Westervelt R.M. and Tinkham M. (1985), "Noise and chaos in a fractal basin boundary regime of a Josephson junction", Phys. Rev. Lett. **55**, 746.

Jensen M.H., Bak P. and Bohr T. (1984), "Transition to chaos by interaction of resonances in dissipative systems. II. Josephson junctions, charged density waves and standard maps", Phys. Rev. A **30**, 1970.

Kaneko K. (1989), "Chaotic but regular Posi-Nega switch among coded attractors by cluster-size variation", Phys. Rev. Lett. **63**, 219.

Kautz R.L. and Monaco R. (1985), "Survey of chaos in the rf-biased Josephson junc-

tion", J. Appl. Phys. **57**, 875.

Kvale M. and Hebboul S.E. (1991), "Theory of Shapiro steps in Josephson junction arrays and their topology", Phys. Rev. B **43**, 3720.

Lee H.C., Newrock R.S., Mast D.B., Hebboul S.E., Garland J.C. and Loff C.J. (1991), "Subharmonics Shapiro steps in Josephson junction arrays", Phys. Rev. B **44**, 921.

McCumber D.E. (1968), "Effect of ac-impedance on dc voltage-current characteristics of superconductor weak-link junctions", J. Appl. Phys. **39**, 3113.

Middleton A.A., Biham O., Littlewood P.B. and Sibam P. (1992), "Complete mode locking in models of charge-density waves", Phys. Rev. Lett. **68**, 1586.

Octavio M. and Readi Nasser C. (1984), "Chaos in a dc-bias Josephson junction in the presence of microwave radiation", Phys. Rev. B **30**, 1586.

Pomeau Y. and Manneville P. (1980), "Intermittent transition to turbulence in dissipative dynamical systems", Commun. Math. Phys. **74**,189.

Stewart W.C. (1968), Current-voltage characteristics of Josephson junctions", Appl. Phys. Lett. **12**, 277.

Strogatz S.E. and Mirollo R.E. (1993), "Splay states in globally coupled Josephson arrays: Analytical prediction of Floquet multipliers", Phys. Rev. E **47**, 220.

Tchistiakov V. (1996), "Detecting symmetry breaking bifurcations in the system describing the dynamics of coupled arrays of Josephson junctions", Physica D **91**, 67.

Tsang K.Y., Strogatz S.H. and Wiesenfeld K.H. (1991), "Reversibility and noise sensitivity of Josephson arrays", Phys. Rev. Lett. **66**, 1094.

Tsang K.Y. and Schwartz I.B. (1992), Interhyperhedral diffusion in Josephson-junction arrays", Phys. Rev. Lett. **68**, 2265.

Watanabe S. and Strogatz S.E. (1993), "Integrability of a globally couled oscillation array", Phys. Rev. Lett. **70**, 2391.

Wiesenfeld K., Colet P. and Strogatz S.H. (1996), "Attractor crowding in oscillator

arrays", Phys. Rev. Lett. **76**, 404.

FIGURE CAPTIONS

Fig. 1 Plots of ϕ at $t = nT(T = \frac{2\pi}{\Omega_{rf}})$, with n being large enough to exclude the transient process.

Fig. 2 (a) Bifurcation diagram for the homogeneous or coherent state in σ vs. i_{rf} plane. In the shaded region the coherent state is unstable due to the clustering bifurcation. (b) bifurcation sequences plotted versus i_{rf} for $\bar{g} = 0.2$, $\Omega_{rf} = 0.8$, $i_{dc} = 0.03$ and $\sigma = 0.1$. (c) The number of cluster, n_{cl}, vs. i_{rf} for the state of Fig. 2(b).

Fig. 3 (a) Bifurcation sequences plotted versus i_{dc} for $\bar{g} = 0.2$, $\Omega_{rf} = 0.8$, $i_{rf} = 0.61$ and $\sigma = 0.6$. (b) The critical boundaries among the T1C1 state, the T2C2 state and the turbulent phase in $i_{dc} - \sigma$ plane with the parameters of (a).

Fig. 4 Snapshot of the asymptotic solution of the system (1) after the transient process for $\bar{g} = 0.2$, $i_{rf} = 0.61$, $\Omega_{rf} = 0.8$, $\sigma = 0.6$, and $N = 100$. (a) $i_{dc} = 0.0206$. (b) and (c) are two successive snapshots for $i_{dc} = 0.0210$.

Fig. 5 The time-space evolution of the system (1) for $i_{dc} = 0.0215$ and the other parameters the same as those of Fig. 4. The plots are at $t = nT$ after some transient process, where T is the same as in Fig. 1. The features of turbulence are clearly observed.

Fig. 6 The evolution of ϕ_1 and $\phi_1 - \phi_2$ with the same parameters as those of Fig. 5. The features of spatiotemporal intermittency are clear.

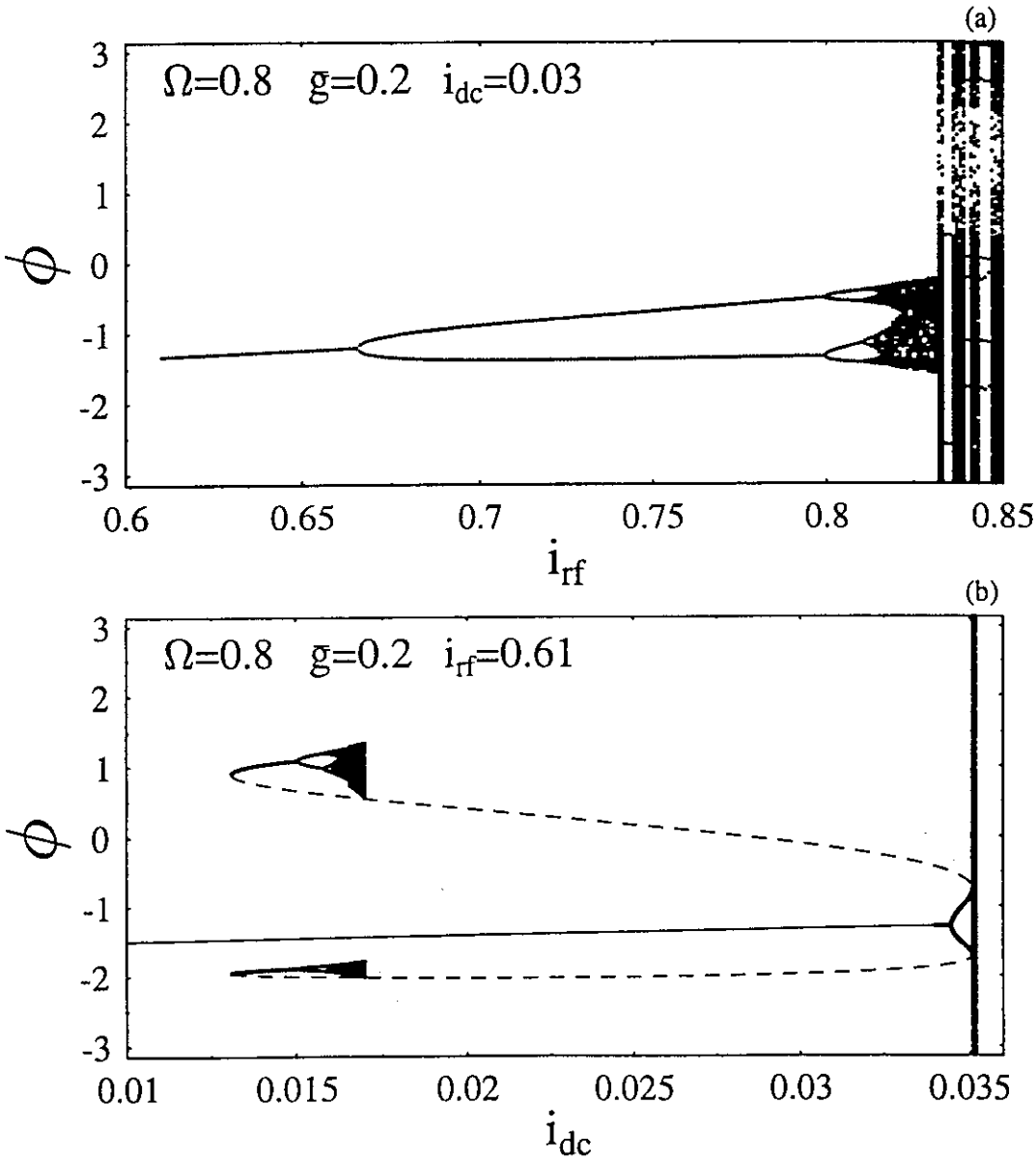
(a)
Ω=0.8 g=0.2 i_{dc}=0.03
3
2
1
0
-1
-2
-3
ϕ
0.6
0.65
0.7
0.75
0.8
0.85
i_{rf}
(b)
Ω=0.8 g=0.2 i_{rf}=0.61
3
2
1
0
-1
-2
-3
ϕ
0.01
0.015
0.02
0.025
0.03
0.035
i_{dc}

Fig 1

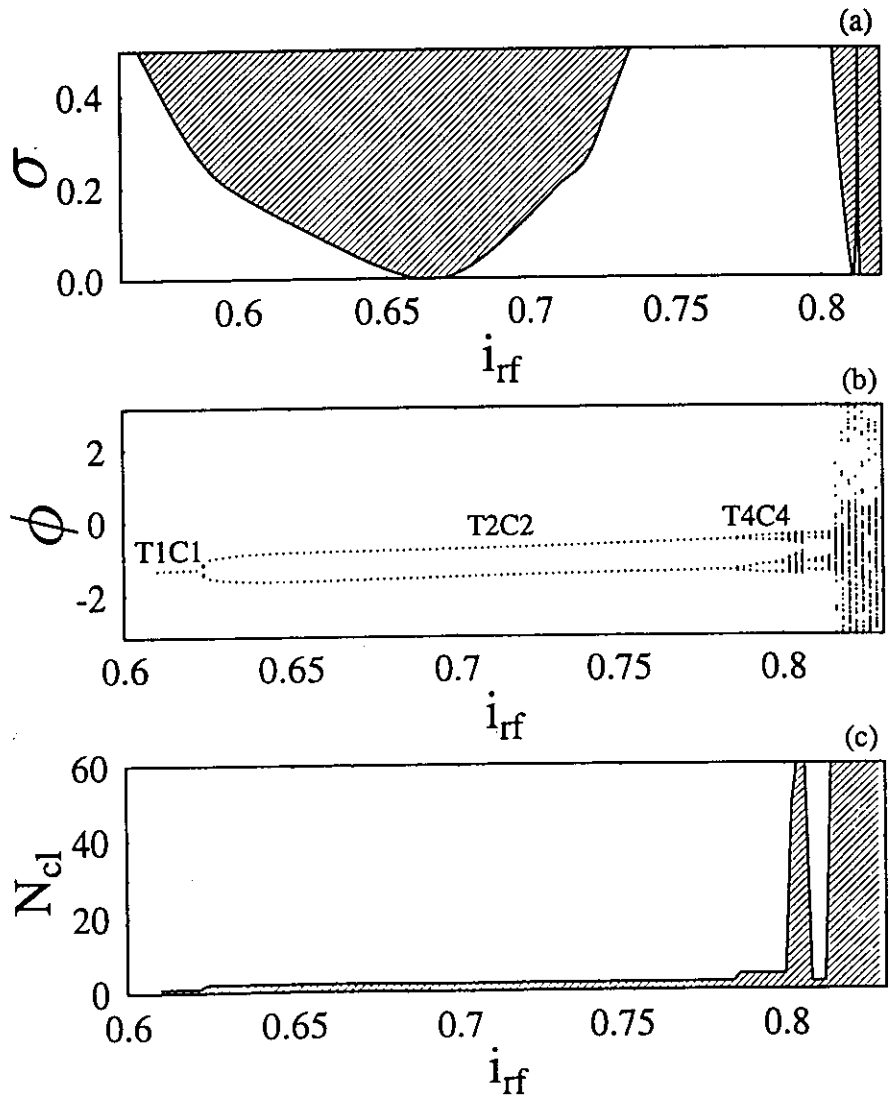
(a)
0.4
0.2
0.0
σ
0.6
0.65
0.7
0.75
0.8
i_{rf}
(b)
2
0
-2
ϕ
T1C1
T2C2
T4C4
0.6
0.65
0.7
0.75
0.8
i_{rf}
(c)
60
40
20
0
N_{cl}
0.6
0.65
0.7
0.75
0.8
i_{rf}

Fig 2

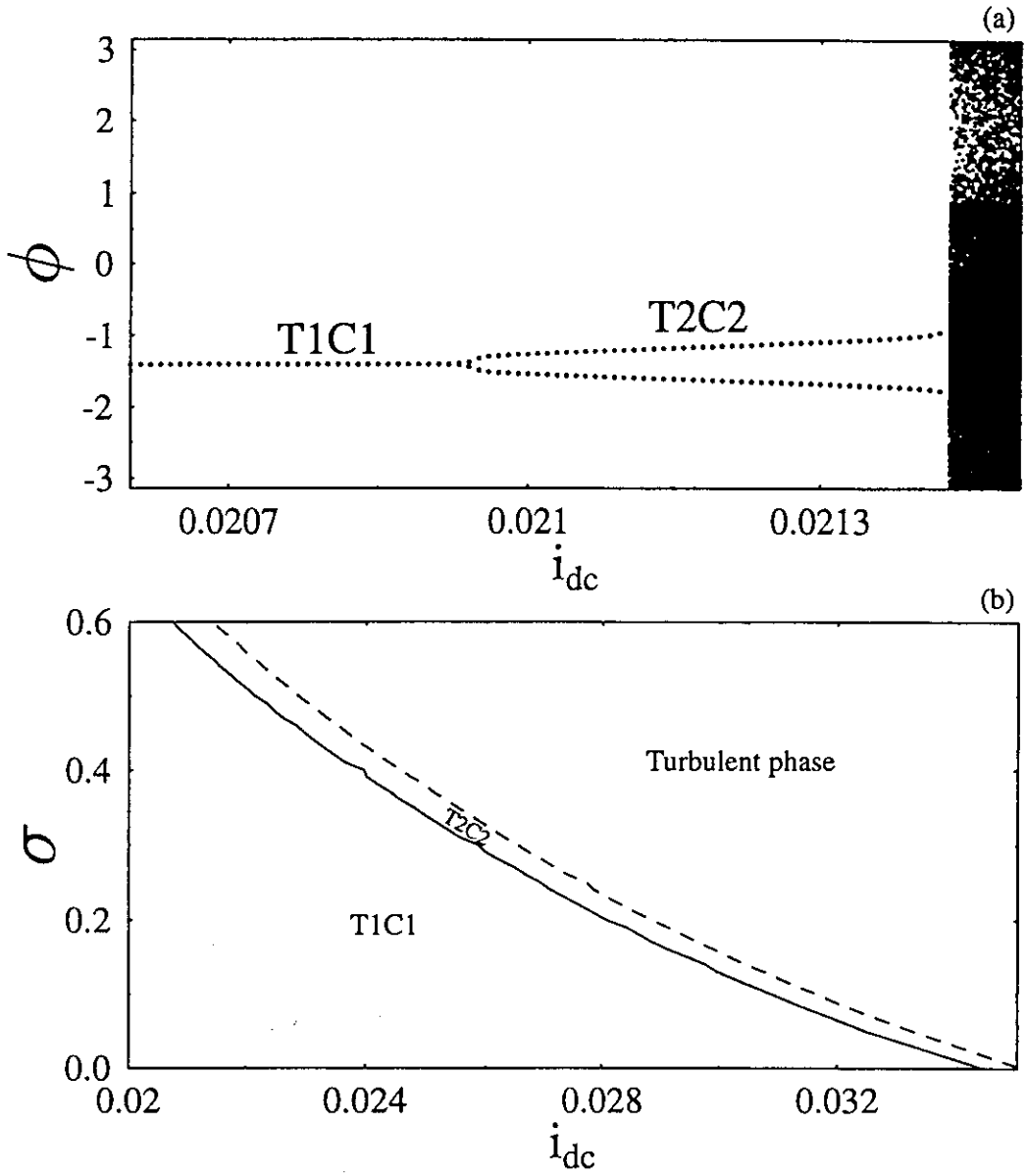
(a)
3
2
1
0
-1
-2
-3
ϕ
T1C1
T2C2
0.0207
0.021
0.0213
i_{dc}
(b)
0.6
0.4
0.2
0.0
σ
Turbulent phase
T2C2
T1C1
0.02
0.024
0.028
0.032
i_{dc}

Fig 3

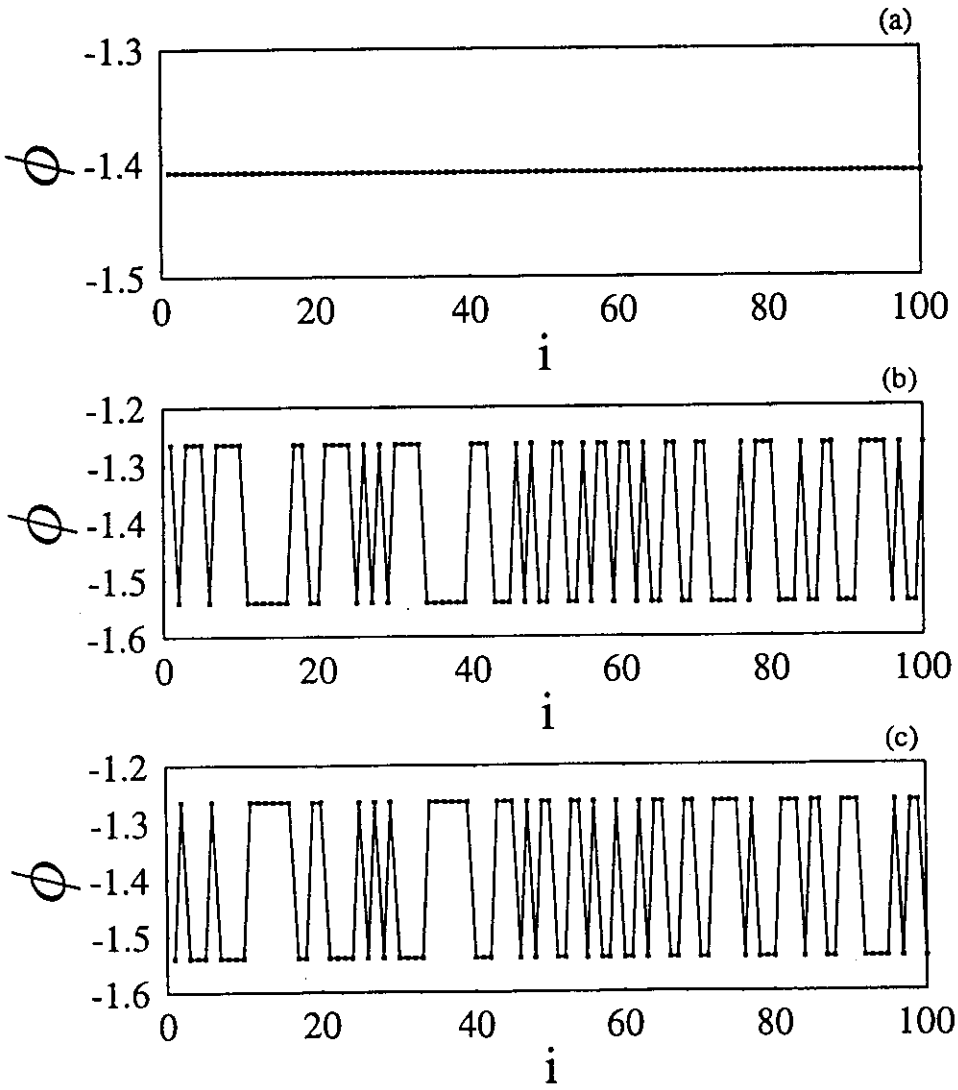
(a)
-1.3
-1.4
-1.5
0
20
40
60
80
100
i
(b)
-1.2
-1.3
-1.4
-1.5
-1.6
0
20
40
60
80
100
i
(c)
-1.2
-1.3
-1.4
-1.5
-1.6
0
20
40
60
80
100
i

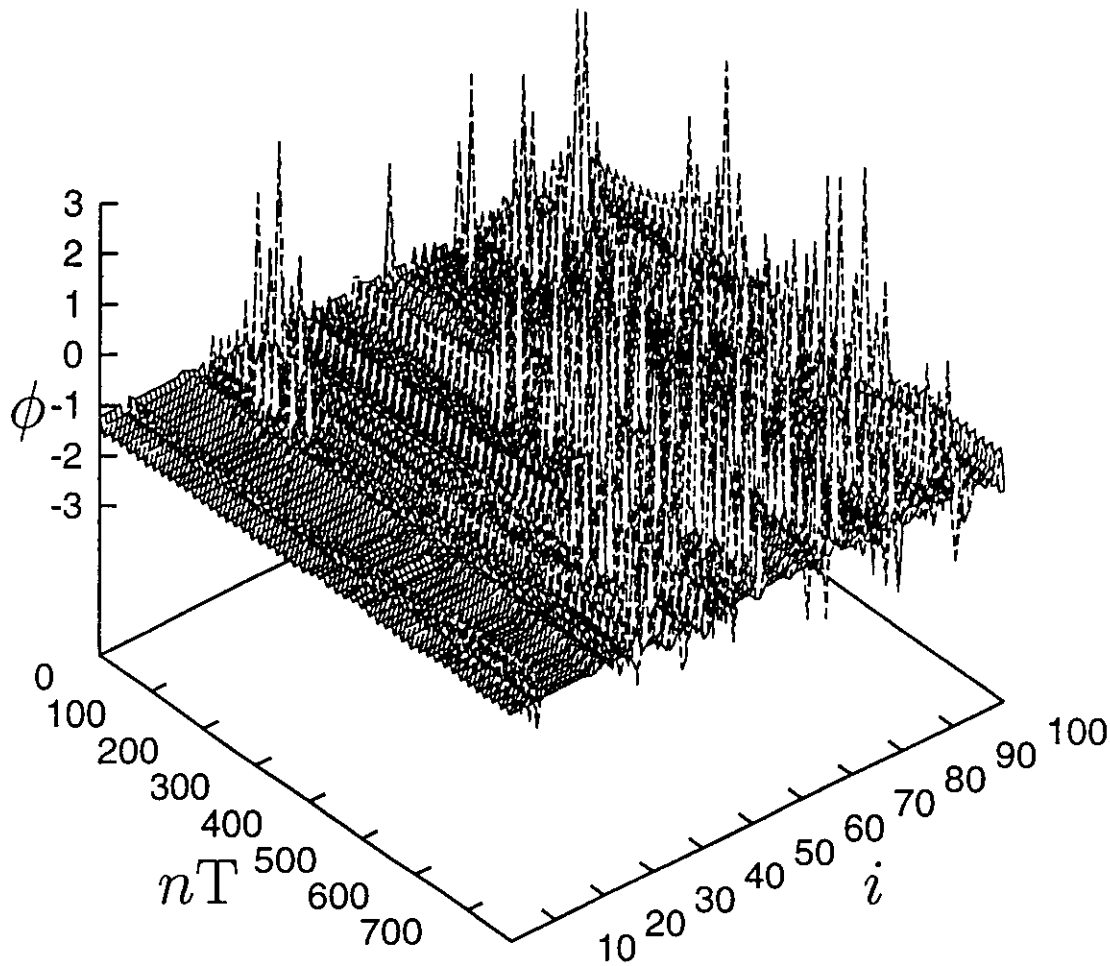
3
2
1
0
ϕ -1
-2
-3
0
100
200
300
400
nT 500
600
700
10 20 30 40 50 60 70 80 90 100
i

Fig 5

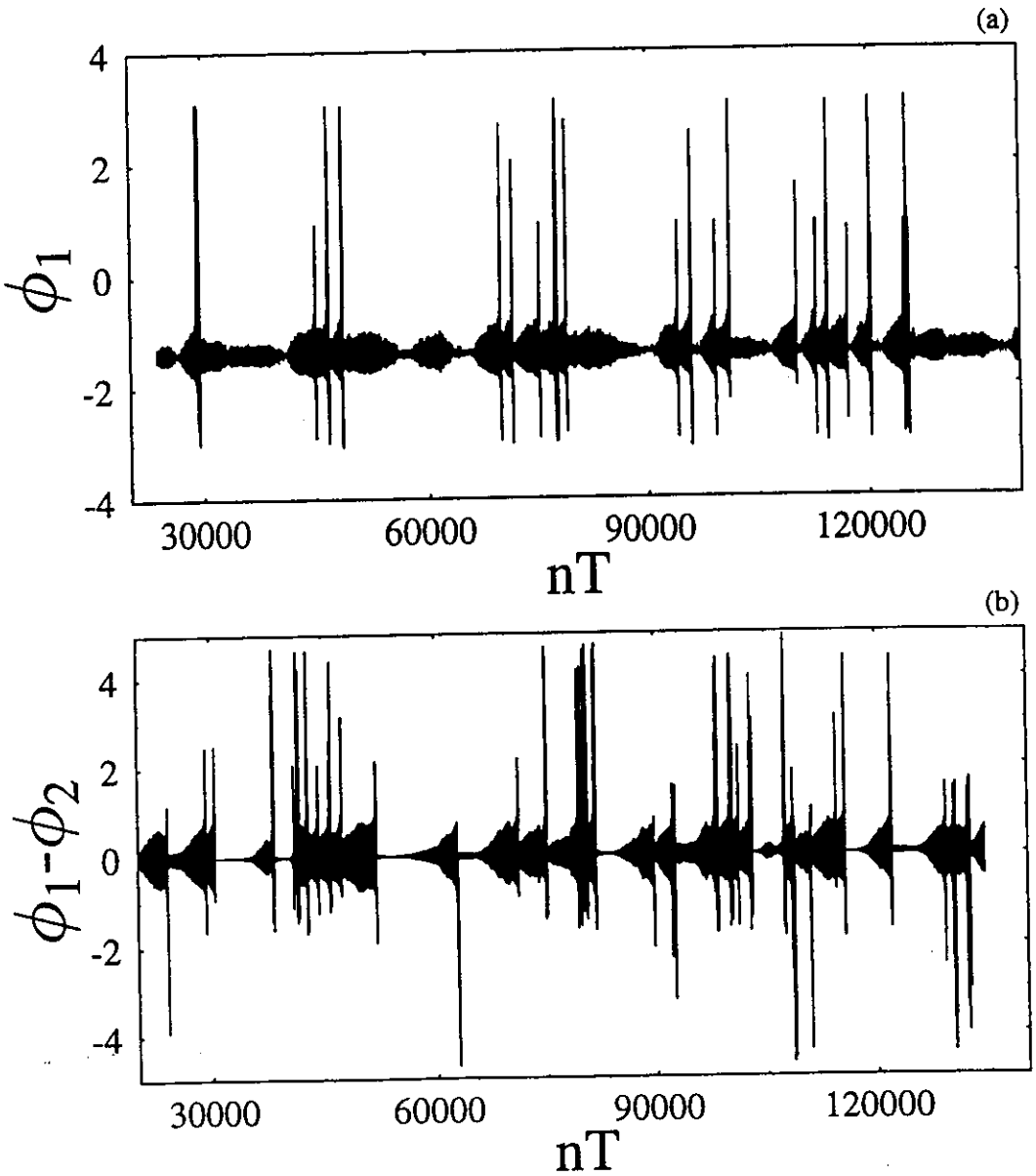
(a)
4
2
0
-2
-4
ϕ_1
30000
60000
90000
120000
nT
(b)
4
2
0
-2
-4
ϕ_1-ϕ_2
30000
60000
90000
120000
nT

Fig 6